Development of model systems to investigate transdermal transport by advanced optical microscopy

Ing. Roberta Liuzzi

PhD in Industrial Product and Process Engineering - XXIX Cycle

Dipartimento di Ingegneria Chimica, dei Materiali e
della Produzione Industriale
Università Federico II di Napoli

Tutor

Prof. Stefano Guido

May 2017

...The journey of a thousand miles begins
with a single step...

Contents

List of figures

Abbreviations

TDD	Transdermal drug delivery
BEG	Bicontinuous emulsion gel
CLSM	Confocal laser scanning microscopy
NMR	Nuclear magnetic resonance
O/W	Oil-in-water
SB	*Stratum basale*
SS	*Stratum spinosum*
SG	*Stratum granulosum*
SC	*Stratum corneum*
PC	L-α-phosphatidylcholine
ME	Microemulsion
NE	Nanoemulsion
W/O	Water-in-oil
OECD	Organisation for Economic Co-operation and Development
SCCS	Scientific Committee on Consumer Safety
TPM	Two-photon microscopy
RS	Raman spectroscopy
BIJEL	Bicontinuous interfacially jammed emulsion gel
FDA	Food and Drug Administration
SEM	Scanning Electron Microscopy
PE	Phosphatidylethanolamine
PS	Phosphatidylserine
PBS	Phosphate buffer saline
ELP	Egg lipid powder
PMP	Protein lipid powder
RT	Room Temperature
MGL	Mean Green Level
SPAN 80	Sorbitane monooleate
TWEEN 20	Polyethylene glycol sorbitan monolaurate
PGPR	Polyglycerol polyricinoleate
SR	Swelling ratio

Abstract

Several applications, ranging from standard cosmetic to advanced drug delivery, involve the interaction of different formulations, generally creams or lotions based on emulsions, with biological systems, for example skin. Drug release through the skin, usually referred to as Transdermal Drug Delivery (TDD), requires penetration through the skin barrier, which is a highly organized system composed of several layers with different properties and morphology. TDD can be considered as good alternative to traditional oral or parenteral delivery, which are more painful for the patients. However, standard methods for transdermal studies, such as microscopy, spectroscopy and the well-established Franz cell diffusion chamber, can only capture few aspects of the drug penetration process and do not allow a complete view of the interactions between single components. For the same reasons, although many works have been aimed at improving drug transport by optimization of the carriers (vesicles, nanoparticles, and emulsion droplets), a full understanding of possible enhancer effects is currently lacking. Dimensions, shape or amount of the ingredients in the formulation are considered possible parameters involved in this improvement.

Here, an innovative methodology to investigate penetration of different compounds through the skin, by time-lapse confocal microscopy and images analysis is presented. In particular, diffusion of fluorescent molecules in solutions or emulsions is investigated and the corresponding diffusion coefficients are estimated. Based on the formulations properties and their affinity with the medium in which they diffuse, a different behavior is observed. In particular, emulsion microstructure seems to play an important role, enhancing the penetration compared to pure solutions. In addition, the possibility to use soft materials, such as Bicontinuous Emulsion Gels (BEGs), tunable as desired to mimic skin morphology and/or properties are presented as a valid alternative to skin biopsies in penetration studies. The easy preparation and low cost of these materials are some of the main advantages of the proposed approach. To this aim, gelatin is used to mimic hydrophilic properties of skin cells, while cross-linked oil is used for the lipid matrix. A

complete characterization of the gelatin gel and its structure-related mechanisms are investigated by Confocal Laser Scanning Microscopy (CLSM), Nuclear Magnetic Resonance (NMR) and birefringence imaging.

More in detail, the present work is organized as follow: in Chapter 1, a general background about TDD, BEGs formulation and gelatin gel characterization is presented together with a description of the current problems to specifically localize and quantify molecules in a colloidal systems, such as emulsions. Motivations of the study are also stated. In Chapter 2, the possibility to appropriately staining one or more components of an emulsion is investigated. In particular, immunofluorescence techniques, commonly used in the biological field, are proposed as an innovative method to localize specific molecules in oil-in-water (O/W) emulsion. To this aim a specific antibody, TEPC-15, is exploited against choline-based phospholipids, used as natural surfactants in many cosmetic and pharmaceutical products. In Chapter 3, the experimental set-up based on CLSM and images analysis is described and used for testing diffusion of different fluorescent molecules in solutions or emulsions in a system based on an agarose gel. The latter is used only for the validation of the set-up. Preliminary diffusion experiments in skin biopsies are also reported. Data obtained from images analysis are processed and fitted in order to estimate the diffusion coefficients. In Chapter 4, the use of BEGs obtained from an emulsification process is proposed as an alternative for penetration studies by mimicking skin structure and/or properties. Gelatin gel and sunflower oil are used as main components to mimic hydrophilicity of skin cells and hydrophobicity of lipid matrix. The addition of surfactants or cross-linkers will be needed in order to guarantee a higher stability of the system and a gel-like consistency. In Chapter 5, an experimental campaign on gelatin gels is carried out by estimating swelling ratio (SR) and molecular dynamic of water molecules of gelatin at increasing polymer concentrations and during swelling for 72 h. Pores dimension is estimated for all gelatin concentrations and at different swelling times. Finally, a qualitative distribution of the tension in the gelatin network during swelling is also reported. Conclusions and future works are described in Chapter 6. Lastly, Appendix A reports in detail the Matlab script

used for the comparison of diffusion equations, and the choice of the equations for data fitting.

1 Introduction

TDD is one of the most commonly used methods for the administration of active ingredients in the organism, from cosmetic products to pharmaceuticals. In this chapter, TDD is presented as a viable alternative to standard drug administration routes. Structure of the skin and typical transdermal carriers contained in emulsion-based formulations are described in detail in order to better understand the mechanisms behind penetration through the skin. Deeper aspects on transport efficiency in TDD have been covered in a review article, published in 2016 in Colloid and Surfaces B: Biointerfaces [1]. The mathematical approach of the penetration process is also reported. In addition, a general overview about soft materials as possible model systems to mimic skin structure and properties is presented. Particular focus is on gelatin gel structure and its structure-related mechanisms. Finally, an innovative multidisciplinary approach to localize specific molecules in colloidal systems is presented as helpful method to investigate the interaction of single formulation components with skin.

1.1 Transdermal Drug Delivery

Drug delivery refers to methodologies and approaches for transporting drugs into the body, to achieve a therapeutic effect. Over the past 30 years, great interest has been addressed in the pharmaceutical field to the development of formulations able to release drugs in the body in a controlled manner [2]. However, it is important to take into account several problems related to the drug assumption such as the insolubility in water, the non-absorption by the stomach acids or from the blood, the stability of the formulation (shelf-life) and its half-life once introduced into the organism, the low bioavailability and possible side effects. The physical and chemical properties of drugs, must therefore be suitably characterized [3].

The TDD is nowadays considered as valid alternative to traditional administration routes, able to release an active principle to the target site in a sustained manner, reducing side effects due to first-pass metabolisms and gastric enzymes [4, 5]. Moreover, the

administration may be carried out directly by the patient, without the need of a specialized staff, also for long times. The specificity for the target site is increased thanks to a localized application. By this way any side effects are localized to the application site and it is possible to stop the treatment simply removing the formulation. All these aspects represent advantages also compared to parenteral administration, where the use of needles for intravenous or hypodermic injections is certainly much more invasive for the patients [6]. Despite the great potential of TDD, it also present some limits, for example, due to the high complex structure of the skin, described in the following paragraph, only low-molecular weight molecules can spontaneously pass the skin barrier, while larger molecules require the use of further techniques such as electroporation, dermabrasion, microneedles[7] and ultrasounds, which temporally and reversibly alter the skin structure allowing molecules passage, or the addition of additives (solvent, surfactant ect.) which act as promoter for the penetration [3, 5].

1.1.1 Skin structure: *stratum corneum*

Skin is one of the most extensive organs of the human body and covers a surface of about 2 m^2. Its main functions include thermoregulation, gas and liquids exchange and protection against the entry of toxic substances and UV radiations. Given the complex organization of its constituents, it has a very low permeability to the penetration of external molecules. Skin thickness is of few millimeters and presents a complex multilayer structure composed of three main parts, the epidermis, the dermis and the fat tissue (Figure 1.1). In the inner part, adipose cells help to store energy in form of lipids acting as link with the above tissues. Dermis is the only vascular layer of the skin rich in fibroblasts cells embedded in a collagen and elastin matrix. The outer epidermal layer can be further divided in four distinct strata according to the corresponding cell differentiation: *stratum basale* (SB), *stratum spinosum* (SS), *stratum granulosum* (SG), and the outer *stratum corneum* (SC). Starting from SB, cells appear the more elongated and keratinized, the more external they are, up to lose their nuclei and differentiate in flattened corneocytes. These non-living cells are rich in proteins and are embedded in a matrix of lipid bilayers. This structure represents the main barrier to the penetration of molecules in the skin [8, 9] and it is often schematized as a “bricks and mortar model”

(even if in a simplistic way) where cells are the bricks and lipids represent the mortar (Figure 1.1). A comparison with a histological skin section is also reported in Figure 1.1.

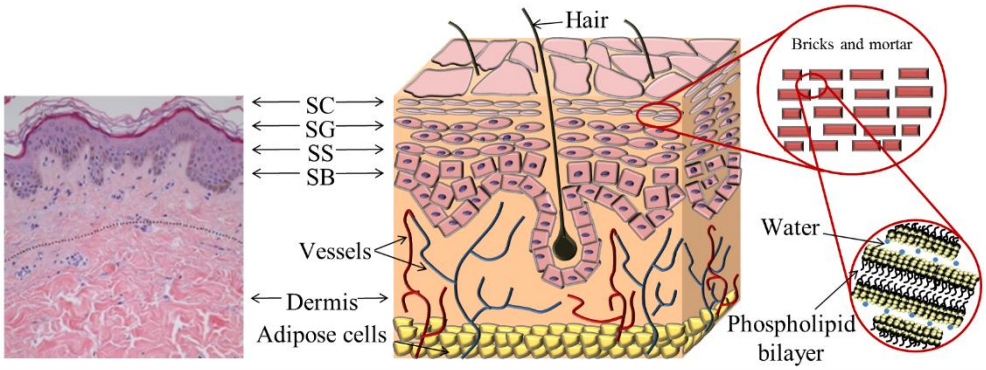

Figure 1.1 – Schematization of skin structure. Comparison with an histological skin section (left) [10]. Bricks and mortar model and lipid organization of the SC (right). Taken from [1]

The SC has essentially lipophilic characteristics and a very low water content (approximately 13%). The hydrophilic properties of the skin, instead, gradually increase passing from the SC to the deeper layers until reaching the dermis, where the water content rises to about 70%, favoring the absorption of hydrophilic drugs. Transdermal absorption requires the violation of this barrier in order to drive molecules down to dermis, and includes three different steps. Initially, the molecules enter in the outer skin *stratum* (penetration). Molecules then pass from a layer to another and from a *stratum* to the following (permeation). Finally, molecules reach the dermis and the vascular system (resorption). Depending on the properties and affinity with the skin components, the drug may behave differently, for example, it can remain on the surface or it can pass through one or more layers of the skin, following different ways of penetration: the intercellular route (Figure 1.2a), the follicular route (Figure 1.2b) and the intracellular path (Figure 1.2c) [11].

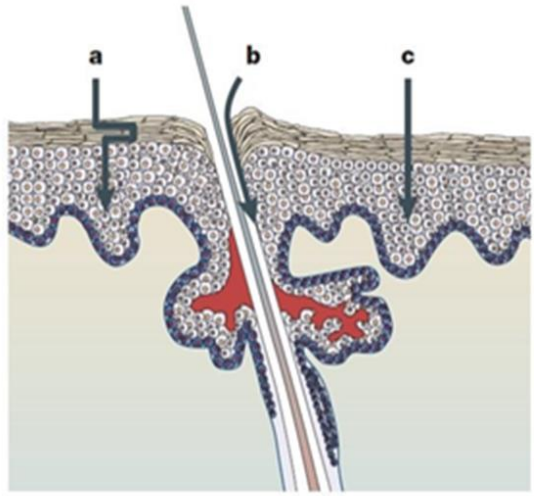

Figure 1.2 – Penetration pathways through the skin: intercellular (a), follicular (b) and intracellular (c) [12]

In the intercellular route (Figure 1.2a) the drug follows a tortuous path around cells, exploiting the lipid matrix to reach deeper *strata*. In the follicular path (Figure 1.2b) drug exploits the pores present on the skin surface. This route has been generally neglected in past as only the 0.1% of the body surface is covered by pores and sebaceous glands, but in recent years it has been demonstrated its important role in the penetration, in particular for nanoparticles used as carriers, which can accumulate in the pores and then spread deeper. In the intracellular path (Figure 1.2c) the drug, instead, passes inside the corneocytes pushing towards the deeper layers. It is the most direct route, but at the same time, it requires a transport through the densely compact lipids interspaces which makes the whole absorption process more complex. A drug that uses this path meets an additional resistance to permeation. For all these reasons, so far, the intercellular route seems to be the predominant route of penetration [11].

1.1.2 Transdermal carriers

The most common formulations for transdermal applications include lotions, mousses, gels, creams, ointments. However, within these formulations, the active ingredient is not free, but is encapsulated in specific vehicles, or carriers, which protect it from the early degradation. The efficacy of the topical applications depends on the vehicle used for the

transport, the morphological, biophysical and physico-chemical properties of the skin, as well as the properties of the specific drug. Widely used vehicles are vesicles, nanocarriers, and emulsions (Figure 1.3a-c).

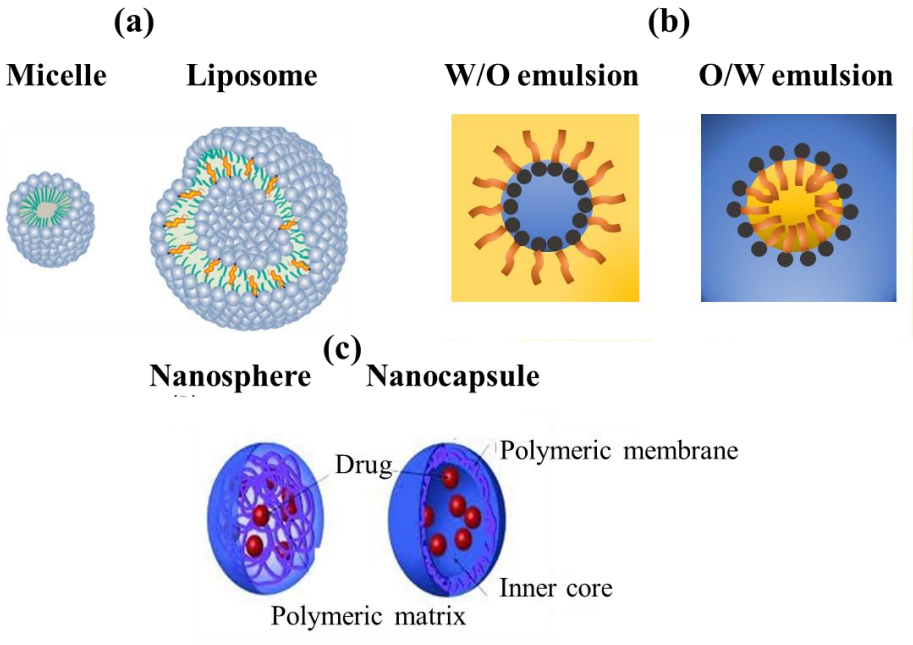

Figure 1.3 – Examples of vehicles for TDD: vesicles (a) [13], emulsions (b) and nanocarriers (c) [14]

Vesicles, which typically refer to liposomes or their variants (ethosomes, niosomes, etc.) [15-17], are colloidal particles, generally constituted by phospholipids, principally phosphatidylcholine and cholesterol combined with other ingredients. The addition of surfactants can further improve the deformability of the vesicles and their properties. Such carriers are able to encapsulate mainly hydrophilic drugs by protecting them from degradation, and minimizing side effects. At the same time, their efficiency of encapsulation is still very low, together with a poor storage stability.

A valid alternative are polymeric nanoparticles [18], whose production can be designed specifically for the application. Moreover, they help to improve stability of the drug and the controlled release to the target site due to their size (5-10 nm), smaller than skin pores, where they can easily accumulate, thus endorsing the follicular route [19, 20]. However, the choice of the right polymer, its production, investigation of required

properties, first of all the biocompatibility, and final costs, are just some of the main aspects to consider.

Finally, emulsions, in particular those with a fine dimensions of droplets, are considered optimal transdermal vehicles due to their ability to solubilize both hydrophilic and hydrophobic molecules [3, 21]. A major insight in this kind of formulation is reported in the following paragraph. Penetration of an active ingredient can be improved by setting the properties of the two phases and of the interfacial agents. Active molecules can be embedded in the droplets or even at the interface. The possibility to obtain different emulsions microstructures is another advantage to improve and optimize the penetration process. It is known, in fact, from literature that microemulsions (MEs) [3, 22] or nanoemulsions (NEs) [23, 24], which present a dimension of the inclusions in the range of few nanometers act as penetration enhancers [25] by changing, disrupting and fluidizing the lipid structure of the SC or increasing the partition coefficient between vehicle and skin [26]. However, the real causes of this improvement are still a challenge. Type, shape and dimensions of the inclusions as well as the type and the amount of each ingredient are so far the main factors considered.

1.1.2.1 Emulsions-based formulations

Most of the cosmetic or pharmaceutical formulations are based on emulsions. The latter are heterogeneous systems composed of two immiscible liquids, one of which is dispersed in form of droplets or inclusions. Typically, emulsions can be O/W or water-in-oil (W/O) systems, but multiple emulsions such as W/O/W or O/W/O are also possible. These systems are thermodynamically unstable due to several phenomena that tend to separate the two phases, including coalescence (small droplets join aggregate to form bigger droplets), flocculation (droplets aggregate to give 3D clusters), creaming and sedimentation (different density of the two phases drives the separation). In order to avoid separation phenomena one or more emulsifiers (or surfactants) can be added to the formulation. Due to their amphiphilic nature, they tend to localize at the droplet interface reducing the interfacial tension, which involve adhesive forces between the two phases in contact. Regarding the use of surfactants in emulsions for TDD applications, it is worth mentioning to consider that some emulsifiers, for example the polyethylene

glycol sorbitan monolaurate (Tween), fatty acids/esters (oleic acid) [27] or solvents (ethanol) are able to act as penetration enhancer improving penetration of active components [5, 28]. Although more surfactants are often used for their ability to alter the SC in a reversible manner facilitating the penetration [29], it is difficult to discriminate the real contribution of each component. Moreover, the concentrations necessary to achieve useful levels of penetration must be controlled, being potentially irritant for the skin. The most popular surfactants commonly used in transdermal formulations are isopropyl myristate, isopropyl palmitate and medium chain triglycerides [27]. Other surfactants, generally suggested for their biocompatibility are phospholipids, in particular L-α-phosphatidylcholine (PC) from egg yolk, or from soybean whose enhancer effect has been validated.

1.1.3 Investigation of penetration through the skin

Investigating the penetration process through the skin is rather complex. Generally, studies are carried out on skin samples, whose availability (but also maintenance and storage) requires considerable attention. Furthermore, the possibility of any damage to the sample during treatments is a further difficulty. Pig skin is suggested as good alternative by the Organisation for Economic Co-operation and Development's (OECD) guidelines [30, 31]. However, the European Commission is working to obtain animal free testing in cosmetic and pharmaceutical industries. 3D reconstructed-skin, commercially available or produced in laboratory, are also used as good substitutes to skin biopsies even if at high cost. Typical examples are Episkin®, Epiderm®, SkinEthic® [32, 33]. Synthetic membrane, such as Strat-M® membrane (Figure 1.4) [34-36], composed of multi-layers of polyethersulfone and polyolefin and with a thickness of 300 µm, is able to create a flux similar to that through the human skin [34]. The organization of the polymeric layers are compared with a histological skin section in Figure 1.4.

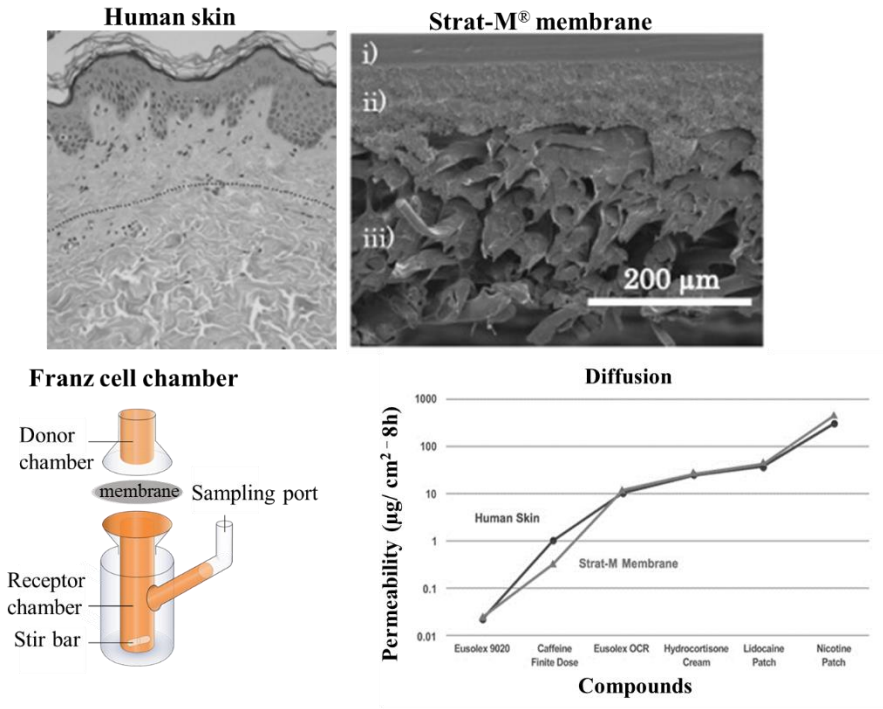

Figure 1.4 – Upper: comparison between human skin histological section [10] and synthetic Strat-M® membrane. Letters indicate the three different organization of membrane strata [34]. Below: a schematization of a standard Franz cell diffusion chamber. Plot on the right shows a comparison between permeability of different compounds in human skin and Strat-M® membrane (http://www.merckmillipore.com/IT/)

The three layers of Strat-M® well mimic SC hydrophobicity on the top layer, while a larger organization of polyolefin is visible immediately below (Figure 1.4). The obtained porous structure creates a gradient across the membrane in terms of pore size and diffusivity. As visible from the plot, permeability of different compounds through human skin and Strat-M® membrane in 8h are in good agreement [37]. However, as already mentioned, the cost for the production of these membranes is still very high.

The main objectives of literature research on TDD focused on the use of different techniques and methods whom allow one to investigate morphology of the skin and to follow penetration of external molecules through the different skin layers. Franz cell diffusion chamber (Figure 1.4), recognized as a standard method by the Scientific Committee on Consumer Safety (SCCS) and guidelines (OECD) for in vitro testing of skin penetration process is generally used for quantitative experiments. Briefly, it is

composed of a donor chamber (Figure 1.4), which contains the test formulation and a receptor chamber containing a buffer solution. The skin sample (human, animal or synthetic membranes) is placed between the two compartments and acts as a membrane through which the diffusion takes place. The determination of the amount of permeated substance over time is carried out by suitable analytical techniques as result of successive withdrawals from the receptor buffer. Unfortunately, this method does not allow the identification of the penetration pathways of single components of the formulation [38]. Moreover, phenomenon such as swelling of the corneocytes, which occur when formulation is water-based, is not considered [39, 40]. However, regarding this last point, SC can increase 3-4 times in thickness and few microns in area and length due to the swelling. Although this changes in structure are quite uniform, they should be considered due to the increase of molecules paths.

For the study of skin morphology and its molecular composition as well as for penetration studies, microscopy techniques such as CLSM, Two-Photon microscopy (TPM) and Raman spectroscopy (RS) are widely used. Each of these techniques has been used for *in vitro*, *ex vivo* or *in vivo* investigations. CLSM, as well as TPM allow high-resolution images even up to 30-40 μm depth, and dynamic visualization of the penetration process by using time-lapse imaging and appropriate staining of formulation components, such as one phase of the emulsion or the active principle. By this way, it is possible to observe eventual changes in skin structure and the penetration pathway of the labeled components. Some exhaustive results obtained with CLSM are reported in Figure 1.5.

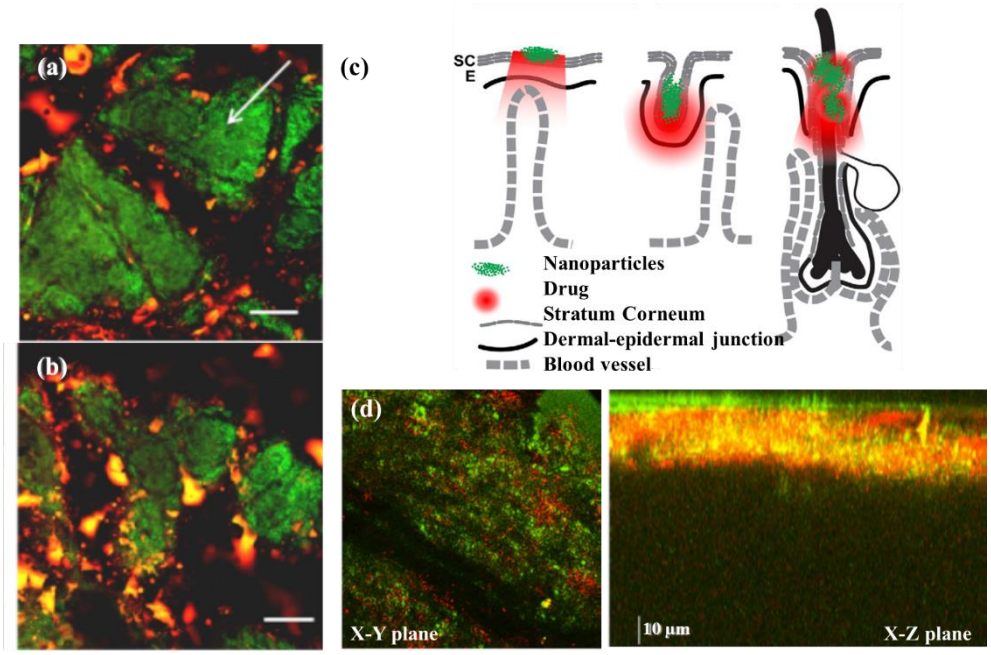

Figure 1.5 – Distribution of polymeric vesicles (red stained) into cadaveric skin (green stained) after 2 h (a) and 4 h (b) diffusion [41]. Routes of penetration of nanoparticles (c) [42]. X-Y and X-Z images of nanocapsules penetration through the skin. Nanocapsule shell is red stained while drug core is stained in green. A uniform distribution suggests that nanoparticles do not penetrate the skin releasing the drug, which alone reaches deeper layers [43]

CLSM images in Figure 1.5a-b show a time-dependence distribution of polymeric vesicles (red stained) in a cadaver skin (green stained) at different times, specifically at 2h and 4h of penetration. As visible, red vesicles tend to initially accumulate between cells on the top skin layer and then tend to reach deeper layers exploiting intercellular and follicular route [41].

Concerning penetration of nanoparticles, CLSM allowed to demonstrate that possible routes for their penetration on skin surface are furrows and hair follicles (Figure 1.5c) [42]. Nanocapsule shell (red stained) and drug-core (green stained) on the surface, are unable to penetrate, as visible in Figure 1.5d., but then the presence of the drug in the deeper layers suggests that the release occurs on the top of the skin while active principle diffuse freely. As previously mentioned, intercellular route seems to be the preferential path [43].

Another CLSM example is reported in Figure 1.6 [44], in order to show the higher transdermal efficiency by using MEs as carriers.

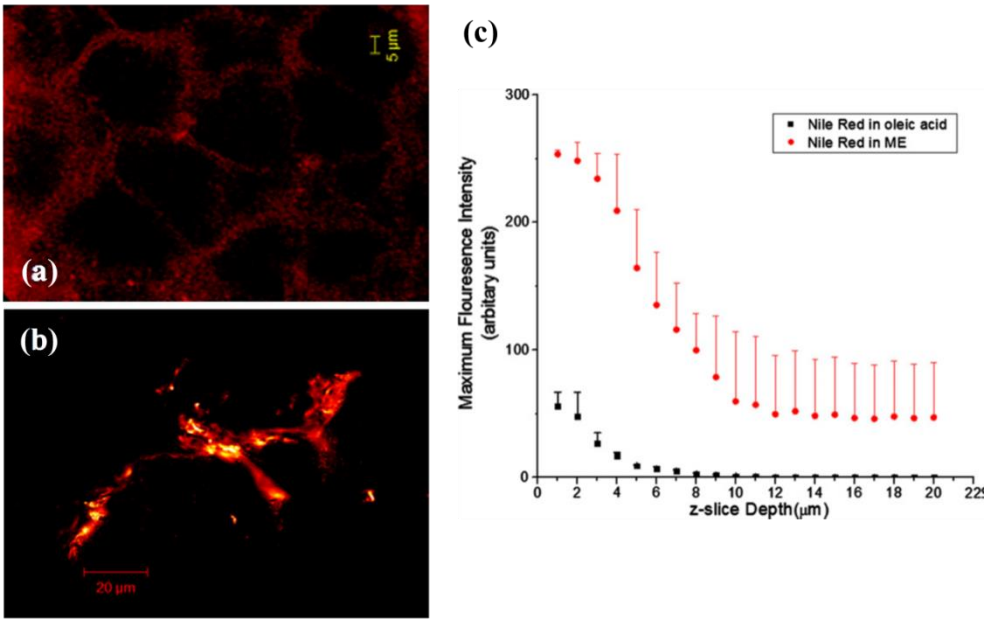

Figure 1.6 – (a-b) CLSM images of ME diffusion into the SC. Fluorescence intensity of ME, stained with Nile red is visible in the interspaces between cells. (c) A comparison between ME and pure oleic acid diffusion as a function of SC depth [44]

Here, O/W ME with droplets diameter in the range 10-13 nm, is stained with Nile red, in the oil phase, in order to mimic lipophilic drugs. After 2h of penetration, corneocytes are well visible in dark, while oil fluorescent phase is intercalated in the interspaces between cells (Figure 1.6a-b). Plot in Figure 1.6c reports the maximum fluorescence intensity of the ME and of a pure oil phase, both stained with Nile red, where it is clear the enhancer effect of ME compared to the oil solution. Moreover, at the end of the 2h the ME fluorescence signal is still evident at about 20 µm depth, suggesting the reach of the SG. The exponential decreasing profile of fluorescence intensity could be indicative of a classic Fickian diffusion of the compounds through the SC or may indicate only the "off" of the fluorophore through the examined skin sample. It is worth mentioning that the use of the CLSM could allow the visualization of more than one component at the same time, and to understand the real behavior of the penetrating system. Other examples of MEs are reported in [45-49], where it has been demonstrated that penetration efficiency increases with increasing water content, showing a better performance of O/W emulsions compared to W/O or double emulsions. This result is not always confirmed,

depending on the type and properties of each component of the formulations. Recently, Mahrhauser et al. [50] demonstrated the essential role of the shape of the emulsions droplets, showing an enhancer effect if the shape is more elongated than spherical. Drop shape can be dependent on the water content, or can be driven by external viscous stress due to an imposed flow [51]. Often, formulators produce emulsions without a clear knowledge of the internal microstructure [52], which can be highly modified by flow process (at industrial level), but also by the simple spreading and rubbing of the product during its application. Studies on the behaviour of the simplest components of the formulation, the droplet, in flow conditions, could be helpful for a deeper comprehension of the process. Studies of single droplets under flow have been widely carried out [51, 53-55].

However, CLSM analysis does not allow to have enough information about the penetration process, due to some limitations such as the high turbidity of the sample, the autofluorescence of some skin components (keratin, collagen and elastin) or the strong laser intensity which could damage the sample. For this reasons, a combination of CLSM with other techniques such as the RS [56], which provide precise information on the molecular composition of a certain layer in the sample and therefore the presence or not of the molecule of interest, could be favourable for a more complete understanding of the process.

1.1.4 Diffusion through the skin

Generally, the distribution of the drug within the skin is described by means of a simple diffusion mechanism [57]. Mathematically this phenomenon is described by Fick's law, characteristic equation of the diffusive transport. In fact, first Fick's law

$$J = -D\frac{\partial C}{\partial z} \qquad \textit{Equation 1}$$

relates the flow, *J*, of a substance per unit area at a given instant of time and at a given position to the concentration gradient ∂C with respect to the position according to a

diffusion coefficient *D*, specific for each molecule. The first Fick's law does not take into account what happens over time, which is rather considered in the second Fick's law:

$$\frac{\partial C}{\partial t} = D\frac{\partial C^2}{\partial z^2} \qquad \textit{Equation 2}$$

valid for a one-dimensional space with constant *D*. The time required to reach a certain concentration at a given distance from the source of the diffusion, goes with squared distance. General solution of the Equation 2 is [57]

$$C = \frac{A}{t^{1/2}}\exp(-\frac{z^2}{4Dt}) \qquad \textit{Equation 3}$$

where A is a constant, related to the total amount of the diffusing material. Result from Equation 3 is symmetric with respect to zero. Concentration trend approaches to zero for $t > 0$ and is null everywhere for $t = 0$ except at $z = 0$ where becomes infinite. The simplest approximation considers diffusing substance confined in an infinite reservoir and the interface as a semi-infinite slab (or membrane). Considering these hypothesis it is possible to assume that at $z = 0$, concentration is in equilibrium with the reservoir and equal to C_0 while it approaches to zero far from the interface. It is hence possible to write boundary conditions as follow:

$$C(z, 0) = 0 \qquad \textit{Equation 4}$$

$$C(0, t) = C_0 \qquad \textit{Equation 5}$$

$$C(z \to \infty, t) \to 0 \qquad \textit{Equation 6}$$

The resulting concentration profile is:

$$C(x,t) = \frac{1}{2} C_0 erfc\left(\frac{z}{\sqrt{4Dt}}\right) \qquad \textit{Equation 7}$$

where *erfc(z)* is the complementary function of the error function:

$$erf(z) = \frac{2}{\pi^{\frac{1}{2}}} \int_0^z \exp(-\eta^2) d\eta \qquad \textit{Equation 8}$$

where $\eta = \frac{\xi}{\sqrt{4Dt}}$.

It is worth mentioning that for the transdermal delivery case, this description results quite simplistic, not considering very complex interactions, which can occur during penetration of external molecules. More detailed definition could be necessary in order to describe more realistically the diffusion process through the skin.

1.2 Model systems: Bicontinuous Emulsions Gel

To overcome the above mentioned problems related to the low availability of skin biopsies and high costs of synthetic membranes, BEGs [58] can represent a good reference model of soft material to mimic SC structure and/or properties. Unlike simple emulsions, where one phase is dispersed into another in presence of surface agents, in BEGs a thermal treatment is able to produce a "partial coalescence" of the oil droplets, which creates a sort of rigid bridges between each other giving to the sample a gel-like consistency [59]. The obtained interpenetrating network form a bicontinuous structure which can be tuned as desired, since such a structure cannot be obtained mechanically. Stability of these systems can be achieved by addition of surfactants, reducing surface tension, or by using one or more layers of colloidal particles at the interface. In the latter case, the system is known as "bijel" (bicontinuous interfacially jammed emulsion gel) [60-62]. The interesting aspect of these tunable systems is that the two phases can be composed of different materials, from liquids, to gels or polymer mixtures [63]. Moreover, the final properties of the obtained system are completely different from the

properties of each single component and can represent an advantage in the optimization of the morphology.

The creation of BEGs or bijels in the laboratory presents several drawbacks. For example a deep gap remains between the experimental system and the simulated one. An example of BEG and bijel is reported in Figure 1.7a-b. The BEG is formed by a biopolymer mixture of gelatin-maltodextrin (7.3%) at 20°C, used to alter the internal microstructure in an oil phase [63]. The bijel, instead, is composed of a binary mixture consisting of an aromatic organic compound (2,6-lutidines) and water. The particles are silica-based, and their volume concentration is 2% [60].

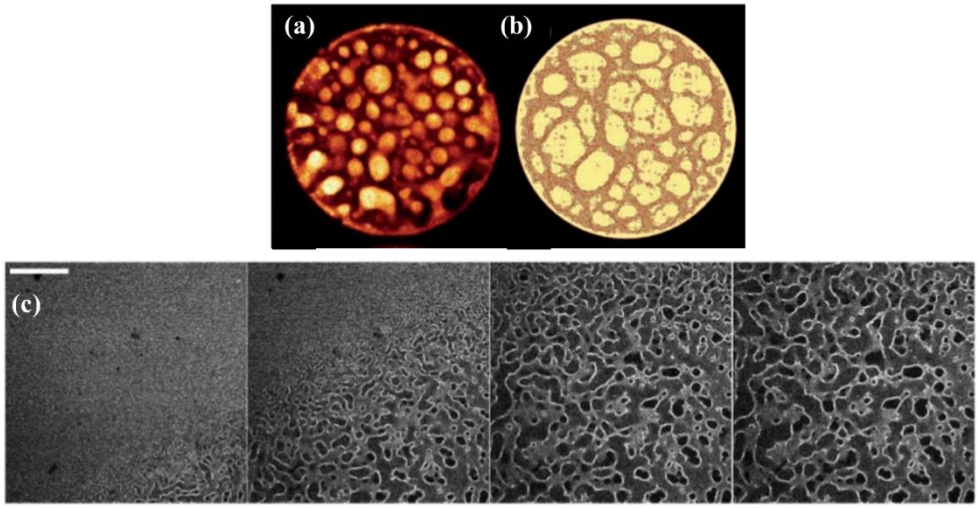

Figure 1.7 – CLSM image (a) and simulated structure (b) of a BEG composed of biopolymer mixture in oil at 20°C [63]. (c) Bijel formation over time. Scale bar is 100 µm [60]

In Figure 1.7a gelatin-maltodextrin, which are labeled with Rodhamine B, are visible as large red inclusions surrounded by the black oil phase. In the elastic Lennard-Jones simulated model (Figure 1.7b), structure of gelatin-maltodextrin rich areas correspond to the regions at lower density of particles. By changing concentration of the maltodextrin, internal microstructure is quickly altered. In the case of bijel (Figure 1.7c), initially it is visible a phase separation at the interface while colloidal particles remain blocked, generating a structure defined as "cross-sectional pattern".

Despite all these aspects, the use of these systems to mimic SC morphology and/or properties cannot be excluded.

1.3 Gelatin gel: characterization and applications

Gelatin is a high molecular weight polypeptide derived from a partial hydrolysis of collagen, which is plentiful in bones, skin, connective tissues and extracellular matrix. Different types of gelatin (type A and B) can be obtained by choosing an acid, rather than alkalin, pre-treatment of initial collagen [64]. Gelatin is provided commercially in form of powder, granules, sheets or flakes which are added to hot water (about 40-50°C) to form an aqueous solution, the latter generally yellow-colored, odorless and transparent. By lowering temperature below 30°C, initial random macromolecules undergo a partial re-naturation, approaching each other and resulting in a gel state (Figure 1.8). Interspace between macromolecules are filled with remaining water molecules.

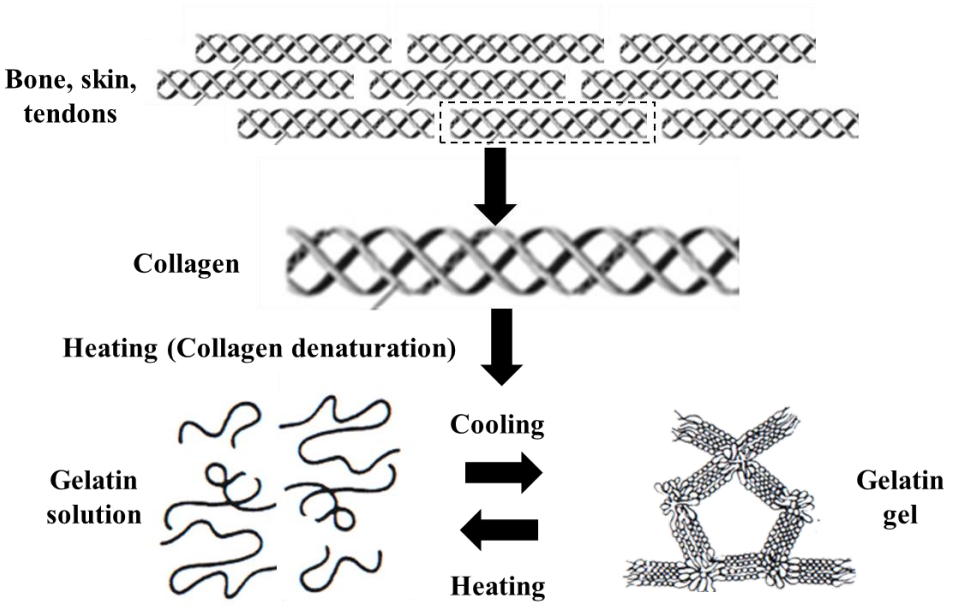

Figure 1.8 – Gelatin derivation from collagen in bone, skin or tendons. Thermal treatment allows to pass from gelatin solution in which macromolecules are randomly distributed, to a gel state where they reorganize in triple helices

Although these macromolecules are in form of triple helices, such as in the case of collagen, their arrangement and organization can vary due to the manufacturing [54, 65, 66]. Moreover, gelation process is thermoreversible [67] and it is strongly dependent on gelatin concentration and temperature.

The final structure of gelatin gel is not easy to determine *a-priori*. It is strictly related to several factors including polymer concentration, humidity, temperature [68] and possible addition of other stabilizing agents (cross-linkers) [69]. Tunable properties of the gelatin together with its cost efficiency and high biocompatibility guarantee a wide use in many different industrial applications including food industry [70, 71] photographic and pharmaceutical fields. For example, it has often used in topical products, in syrups, tablets and in parenteral formualtions. Moreover, it has recognized by the Food and Drug Administration (FDA) as inactive ingredient. [72] Recently, an increasing use of the gelatin gel has been also introduced in the medical field [73] where production of capsules [69, 74-76] and in particular the development of scaffolds for tissues regeneration [77] are the main applications. As example, by varying gelatin and cross-linker (i.e. gluteraldehyde) concentrations (Figure 1.9), and the manufacturing process, a wide variety of gel structure and porosity can be obtained. Surfactants also play a role in the regulation of gel porosity [78]. Scanning Electron Microscopy (SEM) images in Figure 1.9 show that in gelatin scaffold, obtained from a freezing process, pore shape passes from polygonal to round by increasing gelatin concentration from 1% to 5% thus reducing their diameters [79].

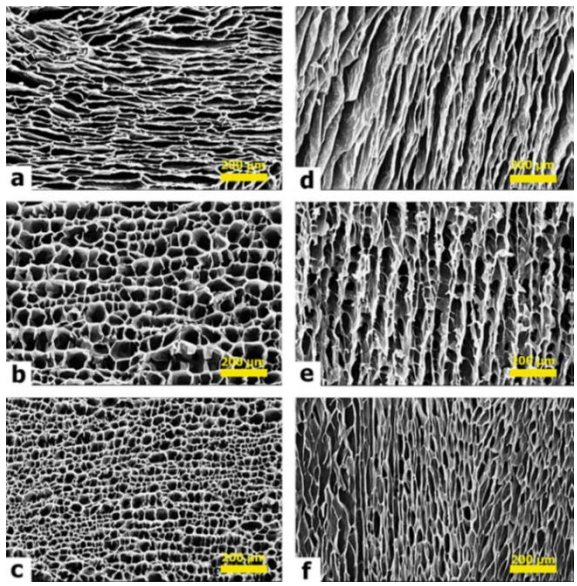

Figure 1.9 – SEM images of gelatin scaffold structure as function of the gelatin concentration at 1% (a-d), 3% (b-e) and 5% (c-f) at a constant cooling rate (3°C/min) parallel and perpendicular to the ice growth directions. All samples contain glutaraldehyde as cross-linker [79]

The effect of cooling rate is also important because in a 5% gelatin does not alter pores shape but modifies the diameters. Faster is the cooling step, smaller are the pore diameters (Figure 1.10).

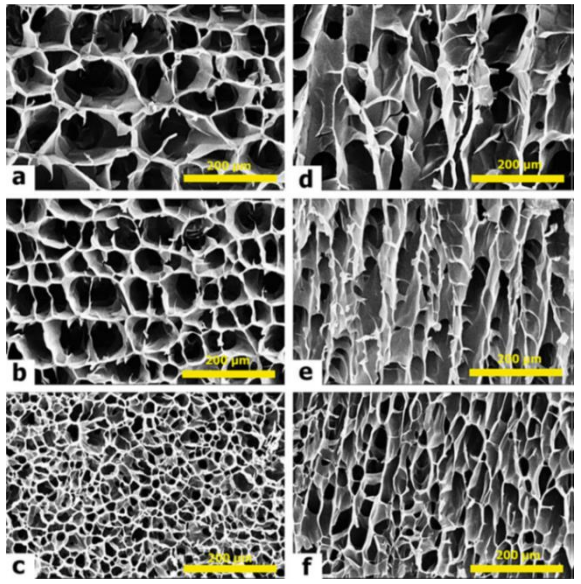

Figure 1.10 – Structure of 5% gelatin as function of the cooling rate of 1°C/min (a-d), 3°C/min (b-e) and 6°C/min (c-f) in direction parallel or perpendicular to the ice growth. All samples contain glutaraldehyde as cross-linker [79]

Although many aspects and properties of the gelatin have been widespread investigated, there are still gaps in the full understanding of its structure and structure-related mechanisms, which require further investigations.

1.3.1 Structure-related mechanisms: swelling effect

As already mentioned, the structure of the gelatin gel can be strongly influenced by several factors including gelatin concentration, temperature, pH and humidity. For this reason, the final structure can show great differences in the arrangement of the macromolecules, in the pore morphology, orientation, and average size, by changing the also final physico-mechanical properties.

Swelling is one of the main structure-related mechanisms involved in gelatin network modification. It is an osmotic phenomenon during which water tends to diffuse and intercalate in the interspaces of the material. In response, gelatin network reacts with an

elastic force reaching a balance at the equilibrium [80]. Swelling kinetics is generally described with a second-order equation [81, 82] controlled by diffusion of the solvent (water) and relaxation of the macromolecule chains [83]. However, also swelling process depends on various factors, in particular temperature [84, 85] salt concentration in the solvent [81, 86] pH and charge distribution [81]. When the stability of the system is improved by addition of cross-linkers, such as glutaraldehyde [87-89], interspaces are already filled, so that the water uptake is highly reduced [90]. It is interesting to note that swelling phenomenon is not uniform inside the sample, but there is the formation of a swelling front that progresses from edges to the center [91]. Molecular dynamics of water inside gelatin structure has been investigated by NMR, a non-invasive, powerful technique, which allowed to demonstrate the behavior of water into the network. Different states of water have been found and defined based on their distance from the gelatin network [92] and hence their mobility. For example, water molecules far from the network is defined as "free water" [93]. The presence of all these states are however related to the experimental conditions. In addition to NMR, generally used to study gel point [94] or the behavior of the solvent during gelation process [95], techniques such as microscopy imaging [77, 96, 97], dynamic light scattering or diffusion of labelled molecules of different sizes and molecular weights [98], have been proposed as valid tools to investigate structural modification of gelatin gels. These studies allowed to estimate pores size and pore connectivity but a complete overview on the gelatin structure modification in response to different mechanisms is still difficult to obtain.

1.4 Localization of molecules by immunofluorescence

In the last few years, it is increasingly common to have a multidisciplinary approach to complex problems, which had been previously tackled from different perspectives in individual disciplines. This approach allowed to obtain new and interesting results in several fields from biology to chemistry and engineering. A typical example is the possibility to use immunofluorescence technique for the visualization of specific molecules, with high spatial resolution, in not-biological samples, such as in complex systems, in particular emulsions.

The immunofluorescence is a well-established method of cell biology, generally used for the specific localization of molecules of interest visualized by fluorescence microscopy. To this aim, it requires the use of specific fluorescently labelled antibody, which recognize the molecule of interest, thus enabling the localization by confocal microscopy. Briefly, an antibody is an immune system-related protein composed of two heavy chains (F_c domain) and two light chains (F_{ab} domain) forming a Y-shape structure (Figure 1.11a). Final tip of F_{ab} domains are responsible for the antigen recognition and are defined as antigen-binding site [99, 100]. This unique property allows the detection by targeting antigens with a single fluorophore-labeled antibody (direct method), or through binding of a fluorophore-labeled secondary antibody raised against the F_c domain of an unlabelled primary antibody (indirect method) (Figure 1.11b).

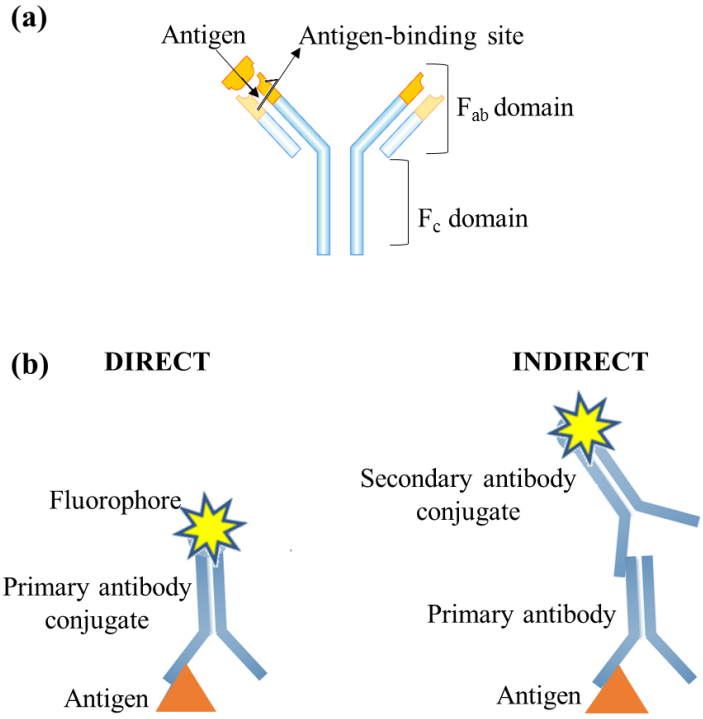

Figure 1.11 – Y-shape antibody structure (a) and methods of detection (b)

Antibodies are an important tool for demonstrating both the presence and the subcellular localization of an antigen. In some cases, staining may also be used to determine the approximate concentration of an antigen, especially by an image analyzer.

When used for molecule detection in biological samples, immunofluorescence protocol requires several specific steps, for example, definition of the antigen, permeabilization and fixation of the specimen (when possible) before the antibodies staining, choice of the incubation time of the antibody at specific temperature and washings with saline buffer in order to remove excess unbound antibody. If this technique is applied to a different field, some steps can be slightly modified based on specific requirements. For example, in the case of emulsions, or more in general liquid samples, washing step is not trivial. It could be possible to overcome the problem by gentle successive centrifugations, but making attention to avoid the precipitation of the materials of interest [101].

This approach could be proposed as innovative and multidisciplinary method for the successfully localization of molecules used as component in pharmaceutical emulsions, in particular, phospholipids.

1.4.1 Phosphatidylcholine: definition and applications

Phospholipids are amphipathic biomolecules composed of a polar head (phosphate group), which is the "water loving" region and two nonpolar fatty acid tails, which represent the "water fearing" region. A wide classification of phospholipids is possible based on the source and on the type of head group or aliphatic chains. The amphipathic property gives them the ability to assemble at the interface between polar and nonpolar phases.

The most common phospholipid is Phosphatidylcholine (PC), derived from lecithin of egg yolk or soybeans, and incorporate choline as head group. For years, it has been topic of many works due to its important applications. It is the major building block in eukaryotic cell membranes, acts as pulmonary surfactant [102], but its essential role has also been demonstrated as nutritional supplement [103] and for liver [104] and brain functions [102, 105, 106]. Being a natural components of cells, PC is highly biocompatible and is approved by the various pharmacopoeia as a natural surfactant with good emulsifying properties, which makes it suitable as a component of O/W emulsions, in food [107, 108], as well as in cosmetic and pharmaceutical products [109].

Often, in order to guarantee the stability of the emulsions over long time, phospholipids are mixed and combined with other components, in particular proteins or synthetic surfactants. In such complex cases, having each component a different behavior, it is more difficult to investigate the interaction and the resulting structure which can be formed [110],[111] in the bulk or directly at the interface between polar and non-polar phases. The presence of these complex structures can interfere with the detection techniques, making difficult to selectively localize the molecule of interest.

Many literature works have been focused on the understanding of proteins-phospholipids interaction at liquid-liquid interface or in form of monolayers [112-115], but further investigations are still at order.

1.4.2 Phosphatidylcholine localization: current problems

The experimental determination of the interfacial concentration of PC in O/W emulsions, in particular when used in combination with other surface-active ingredients, is still an ambitious task. So far, there are not yet any method able to localize and determine the concentration of phospholipids at the interface. However, the only identification is possible by the use of current techniques such as the pendant drop or shear rheology. Pendant drop tensiometry [116-118] allows to measure the expansion or compression of the surface of the drop, whose volume is increased or reduced. The surface tension, related to the molecules at the interface, can be then calculated as a function of the drop surface area [119]. In shear rheology [120], instead, the droplet interface is deformed while keeping the surface area constant. Direct and indirect methods allow to obtain important information about forces and deformations, as well as interfacial properties. Although these techniques give important parameters specific for the whole system, they are not useful for the quantification of molecules at the interface.

Microscopy could represent a powerful tool to obtain a general overview of the system morphology, but also to investigate chemical composition, and in particular to localize and quantify interfacial concentration of specific molecules. In particular, CLSM has been successfully used to investigate structure and lateral organization of molecules at the droplet interface [121, 122] by using fluorophores covalently labelled to the phospholipids, commercially available and known as phospholipid analogs [21, 123].

The choice of different fluorophores for each phospholipid and the possibility of a multi-channel CLSM acquisition could allow to visualize the single species in one time [124]. In this case, protocol requires the addition of phospholipid analogs to the final system, in which phospholipids are already present as component. Therefore, the main limit of this approach is the impossibility to estimate the concentration of phospholipids already present in the system, but only to understand their position and organization. Moreover, the use of phospholipid analogs could contribute to alter the interfacial microstructure inducing a local phase separation, if used at high concentration. In this case, phospholipid analogs can be considered as impurities and can disturb the structure of the system. For this reason, concentrations suggested are usually very low[125].

1.4.3 TEPC-15 for choline-based phospholipids localization

A valid alternative to the use of phospholipids analogs, for the localization of phospholipids, but in particular for PC, is the use of antibodies that specifically bind to PC. In some cases, custom-made antibodies, JE-1 and JE-8, have been developed [126], the first more specific for longer fatty chains and the second for short fatty acyl chains of PC. Both of them present the important property of no cross-reaction with other phospholipids such as phosphatidylethanolamine (PE) and phosphatidylserine (PS). However, the custom-made production is not suitable on a large scale.

A commercial anti-PC monoclonal antibody, TEPC-15, has been instead used for recognition of PC in plaques from subgingival and supragingival in patients with periodontal diseases [127]. Its specificity, tested by immunodiffusion, has been demonstrated for the hapten binding of lipids carrying phosphorylcholine [128]. Based on the arrangement of phospholipids in the system, the efficiency of TEPC-15 can vary, for example, it recognizes poorly PC in liposome or lipoproteins, but it is highly specific for lipid emulsions, cell membranes of some bacteria (e.g. *Streptococcus pneumococci*), oxidized phospholipids, and lipid monolayers [129-132].

1.5 Aim of the work

The absence of a complete comprehension of the penetration process through the skin and the lack of techniques able to give qualitative and quantitative information in one

time are the main motivations of the present work. In the light of these issues, the aim is to propose an experimental method, able one to observe molecules penetration and to understand their interaction with skin components. The possibility of a multidisciplinary approach to the problem, for example by using method proper of the cell biology to stain specific components of the formulation, is also another key factor of this work.

Moreover, the proposal of using soft materials to mimic skin morphology and properties, to overcome problems such as skin biopsies availability and high costs of commercial membranes, is the most innovative aspect.

As it was amply explained in the previous sections, this work can be fundamental in order to improve not only the experimental technique, but also the final product optimization, including its microstructure and carriers design.

In particular, this project of thesis aspires to set the basis for an innovative set-up that will be able to elucidate the entire pathway of drug through the skin, from application to the release site. Promising results will be compared and discussed.

2 Immunofluorescence applied to colloidal systems

In this chapter the immunofluorescence technique, generally used in the biology field, is presented as valid tool to localize specific molecules, in particular, phospholipids, in O/W emulsions. Major attention is focused on PC localization, being often one of the main components of cosmetic and pharmaceutical products. Experiments are carried out by using CLSM, and a specific antibody for choline-based phospholipids, TEPC-15, on two different cell lines (as control), on O/W emulsions and on phospholipids films. Materials and methods, as well as detailed immunofluorescence protocols are reported. Moreover, the effect about the addition of proteins on the staining procedure is also investigated for emulsions and films. The staining efficiency is demonstrated by CLSM images and related image analysis. Reported results are also content of a published peer-review paper in 2016 in RSC Advances [133].

2.1 Materials and methods

2.1.1 Cell culture

HaCaT cells, an immortalized non-cancerous human keratinocyte cell line, (Biobank, CEINGE, Italy), and NIH\3T3 mouse embryo fibroblast cell line (Biobank, CEINGE, Italy), were chosen as models for TEPC-15 specificity experiments, due to their plasmatic membrane, mainly composed of PC. Both cell lines were cultured in Dulbecco's modified Eagle's Medium (Lonza), supplemented with L-glutamine 200 mM (Lonza), 10% fetal bovine serum (Lonza) and the appropriate amount of penicillin/streptomycin (Lonza) in a humidified atmosphere containing 5% CO_2 in air. Cells were plated in a µ-Slide 8 Well (Ibidi) (Figure 2.1a) and fixed in 10% neutral buffered formalin, approximately 4% formaldehyde (05-K01009, Bio-optica) before immunofluorescence assay (Figure 2.1b). Mouse anti-PC antibody TEPC-15 at dilution of 1:50 was incubated overnight at 4°C (Figure 2.1c). Rabbit anti-Mouse IgG (H+L), Alexa Fluor® 488 conjugate (A-21204, Invitrogen) (Rb α-mouse 488) was added at dilution of 1:250 and incubated for 1 h at room temperature (RT) in the dark (Figure

2.1d). Successive washings with Phosphate Buffered Saline (PBS, Lonza), indicated with a star in Figure 2.1c-d, allowed removing excess unbound antibodies before and after incubation with the secondary antibody and before imaging (Figure 2.1e). A detailed schematization of the entire protocol is reported in Figure 2.1.

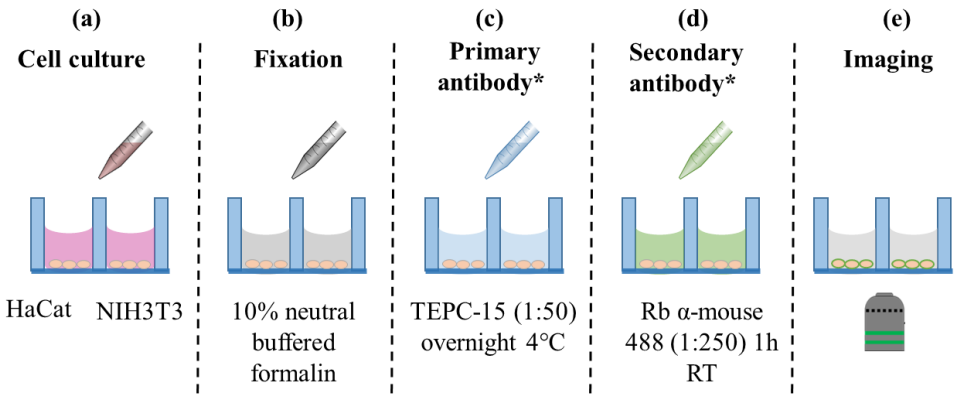

Figure 2.1 - Schematization of cell lines staining procedure. Stars in c-d indicate the necessity of washing steps. Taken from [133]

2.1.2 Emulsions preparation and staining

O/W emulsions were prepared with commercial sunflower oil and bi-distilled water, with the addition of phospholipids and/or proteins as natural surfactants. Emulsions, at a final volume of 100 ml were used to verify the specificity of TEPC-15 for choline-based phospholipids at the interface of the two phases. When phospholipids were used as stabilizing agents, 0.10 g of Egg Lipid Powder (ELP, with a content of 50% phospholipids, of which 72.5% PC, 17.5% PE and 10% others) was dissolved in 100 g of a bi-distilled water solution at 40°C. For emulsions stabilized with proteins, 5.63 g of Protein Mix Powder (PMP, with a content of 50% proteins, of which 60% whey proteins and 40% casein) was in 95 g of bi-distilled water at 40°C. When phospholipids and proteins were used together, both ELP and PMP at the concentrations reported above were added in 95 g of bi-distilled water at 40°C (Figure 2.2a). The complete powder dissolution was obtained leaving the sample for 1 h at 40°C under gentle stirring (magnetic flow). Then, the final O/W emulsions were obtained by adding 3.3 g of sunflower oil at 40°C (Figure 2.2b), and mixing using an Ultra-Turrax T18 digital homogenizer (IKA) for 1 minute at 16000 rpm (Figure 2.2c). Droplets dimension ranged

between 2 and 11 µm. Due to the instability of the final system, fresh emulsions were prepared shortly before each experiment. A withdrawal of 100 µl of the emulsion was incubated for 1 h at RT with TEPC-15 at a dilution ranging from 1:200 to 1:10 (Figure 2.2d). Then, the secondary antibody, Rb α-mouse 488 or Donkey anti-Mouse 488 IgG (H + L) (A-21202, Invitrogen) (Dk a-mouse 488) Alexa Fluor® 488 conjugate was added and incubated for another 1 h at RT in dark (Figure 2.2e). Samples were then imaged by CLSM (Figure 2.2f). In order to avoid excessive movement of the droplets, samples were mixed with a drop of agarose solution 0.5% (161-3101, Bio Rad). The washing steps were here omitted in order to prevent loss of interfacial materials, thus resulting in a lower signal to noise ratio and in a higher background signal from unbound excess antibody.

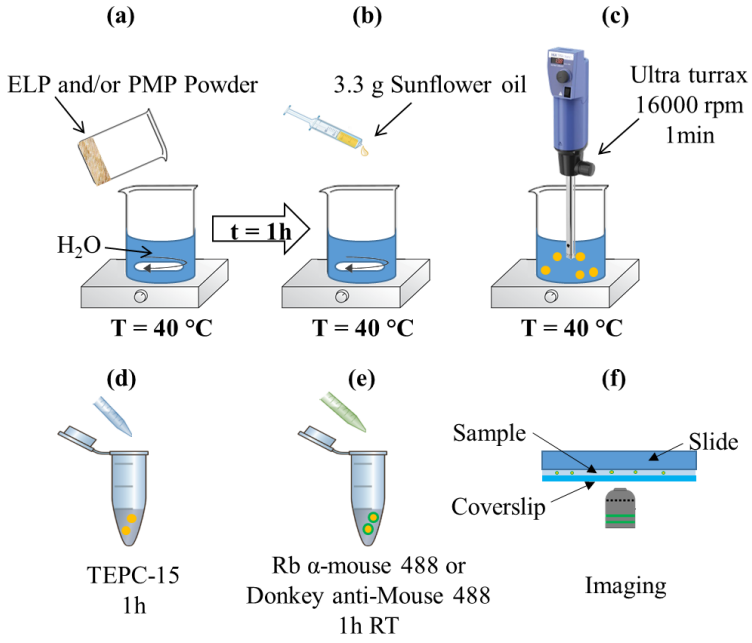

Figure 2.2 – Emulsions preparation and staining procedure. Taken from [133]

Double staining of the emulsion was achieved by using a fluorescent dye for neutral lipids, Nile red (9-diethylamino-5H-benzoalphaphenoxazine-5-one; Sigma-Aldrich), added to the oil phase at a concentration of 0.03 µg/ml before emulsification process, and fluorescently acyl chain labelled phospholipids 2-(6-(7-nitrobenz-2-oxa-1,3-diazol-4-yl)amino) hexanoyl-1-hexadecanoyl-sn-glycero-3-phosphocholine (NBD C6-HPC,

N-3786, Invitrogen) in the final emulsion at a concentration of 0.1 mg/ml, added just before images acquisition. Stock solution of Nile red was prepared by dissolving Nile red powder in ethanol by vortexing. The working solution was obtained by adding the proper amount of Nile red stock to sunflower oil at 40 °C for 1 h under magnetic stirring. After that, ethanol was let to evaporate under vacuum. Stock solution of NBD C6-HPC was obtained by dissolution of phospholipids in ethanol at a concentration of 1 mg/ml. Dilutions were then realized at the concentration desired directly in the final O/W emulsion.

2.1.3 PC coating

Purified egg L-α-phosphatidylcholine, (P3556, Sigma-Aldrich) was suspended in ethanol at a concentrations of 50 and 100 mg/ml at RT as suggested by the product datasheet. Then, 0.4 µl of the suspension was uniformly distributed, with a pipette, on the bottom of a µ-Slide 8 Well (Figure 2.3a). The PC coating was obtained after ethanol evaporation (Figure 2.3b-c). The staining protocol was the same as for the emulsions (Figure 2.3d-e). Washing steps were also in this case omitted to avoid loss of materials. In some cases, PMP solution was added to the PC coating to investigate the effect of the proteins on the staining efficiency (Figure 2.3f).

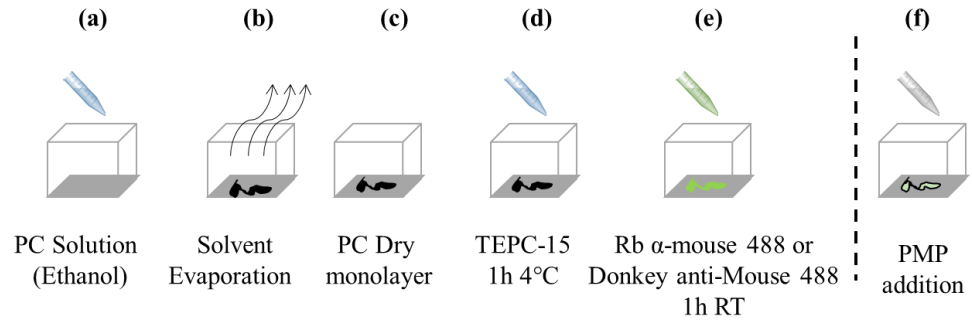

Figure 2.3 – Preparation and staining protocol of PC coating. Taken from [133]

2.1.4 Images acquisition and analysis

For each sample, images were acquired by using an inverted CLSM (Zeiss, LSM Pascal) using a 20x objective (Zeiss Plan-Neofluar, image size 449.12x449.12 nm) connected to a motorized focus system controlled by a dedicated software (Pascal), and two laser

excitations (He-Ne at a wavelength of 543 nm, or Ar at 488 nm). The apparatus is installed on an anti-vibration table that significantly increases the quality of produced images. The samples were observed both in bright field and in confocal mode. Images were then processed by a commercial software, Image Pro-Plus® 6.0 (Media Cybernetics, Silver Spring), in order to measure the Mean Green Level (MGL) corresponding to the intensity value of the fluorescent components, in case of emulsions, the phospholipids at the droplet interface. For the analysis, the droplet interface thickness was chosen equal to 0.5 µm (about 4 pixel) based on the diffraction limit of 0.2 µm, which suggests the impossibility to observe spots smaller than 0.2 µm. The MGL value was normalized with respect to the fluorescence intensity of the entire image (MGL Tot) and plotted as function of droplet size or of the percentage of proteins added to the sample.

In the case of PC coating, images were acquired at each step of the staining protocol in both brightfield and confocal mode. In addition, the effect of proteins on PC coating was investigated by acquiring images of the same field of view after the PC staining (t0), immediately after the addition of 150 µl of PMP solution (t1), 10 minutes (t2), and 25 minutes (t3) after the addition. Between consecutive acquisitions the sample was maintained in the dark to avoid photobleaching with a consequent alteration of the fluorescent signal.

2.2 Results

The specificity of TEPC-15 for choline-based phospholipids in HaCaT and NIH\3T3 cell lines has been tested to visualize phospholipids naturally present in the cell membrane. Here, phospholipids, aligned side-by-side, form a bilayer mixed with proteins to separate internal and external environment of the cell. Among all phospholipids, PC represents the main constituent. Results are reported in Figure 2.4. As expected, a fluorescent signal is located on cells membrane, while dark nuclei are visible in the center (yellow arrows). High signal to noise ratio has been obtained thanks to extensive washings of the samples with PBS, which allowed the removal of non-specific staining.

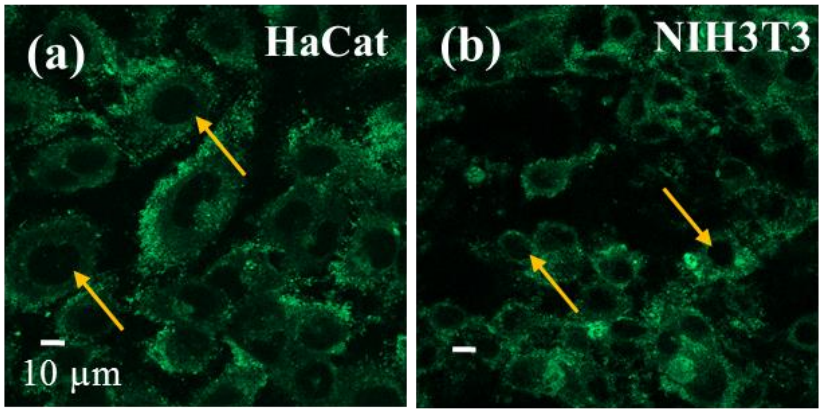

Figure 2.4 – TEPC-15 staining in HaCat and NIH/3T3 cell lines. Fluorescent signal corresponds to phospholipids on cell membranes. Yellow arrows indicate dark nuclei of the cells. Taken from [133]

Representative orthogonal images of the z–y and x–z planes of the confocal z-stack throughout the entire thickness of HaCaT cells is reported in Figure 2.5. It is evident that fluorescence signal follows the curvature of cells membrane, suggesting the specificity of the antibody for molecules on the outer cell membrane. Although molecules on cells membrane can be localized by several antibodies, such as those belonging to the anti-cadherin family [134], the specificity of TEPC-15 for PC, could be a valid alternative to quantify PC concentration and its interaction with other components or molecules.

After assessing the specificity of TEPC-15 for PC, in order to be sure of the presence of phospholipids at the interface of O/W emulsions, a first experimental campaign has been carried out by double staining oil phase with Nile red, and by adding NBD C6-HPC phospholipids as surfactant.

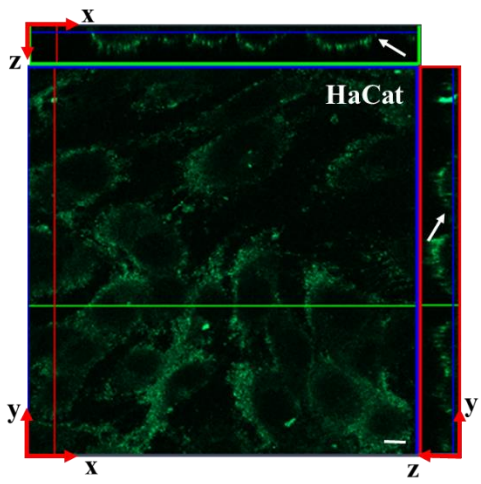

Figure 2.5 – Ortho-reconstruction of the z–y and x–z planes from the confocal z-stacks of HaCaT cells. White arrows indicate the curvature of cell membranes where fluorescence signal is located. Fluorescent curvature suggests the high specificity of the antibody. Scale bar is 10 µm. Taken from [133]

Corresponding result is reported in Figure 2.6a-b. As expected phospholipids are mainly arranged at the interface and the fluorescent signal is uniformly distributed on the droplet surface, as also well visible in the zoomed image in the inset of Figure 2.6a. Fluorescent spots are however detectable in the bulk phase, because of the lack of washing steps.

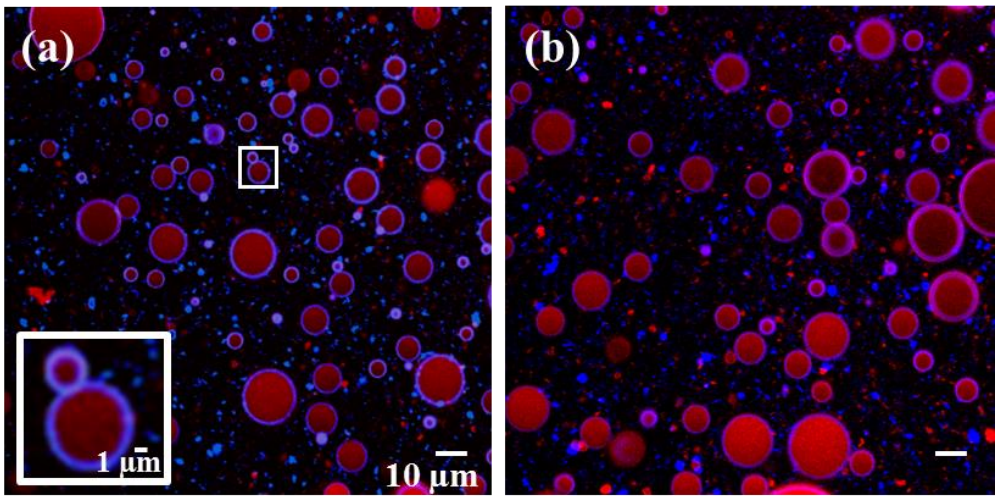

Figure 2.6 – Double staining of O/W emulsion. Oil phase is labeled with Nile red (red) and droplets interface with NBD-C6-HPC (blue). Images (a) [133] and (b) are two different fields of view of the same sample. Droplets in the inset suggest the uniform distribution of the phospholipid molecules at the interface

Once the presence of the phospholipids at the interface has been assessed, the experiments have been repeated by using TEPC-15 staining. As a rule, a negative control experiment has been carried out on an O/W emulsion stabilized with a different surfactant, in particular PMP. In Figure 2.7a it is possible to observe that if only proteins are present as stabilizing agents, no signal is detectable in a specific manner, but only a fluorescent background due to the randomly antibodies in the bulk phase (Figure 2.7a). Contrariwise, in the sample stabilized with phospholipids (Figure 2.7b), the fluorescence signal is again detectable at the interface. However, fluorescence pattern is not homogeneous as in the case of NBD C6-HPC, showing irregular spots and regions of the interface not stained at all (withe arrows, inset Figure 2.7b). This difference can be due to a non-homogeneous distribution of the phospholipids at the interface or to some interaction with other phospholipids present in the ELP which can interact and obstacle the antibody staining.

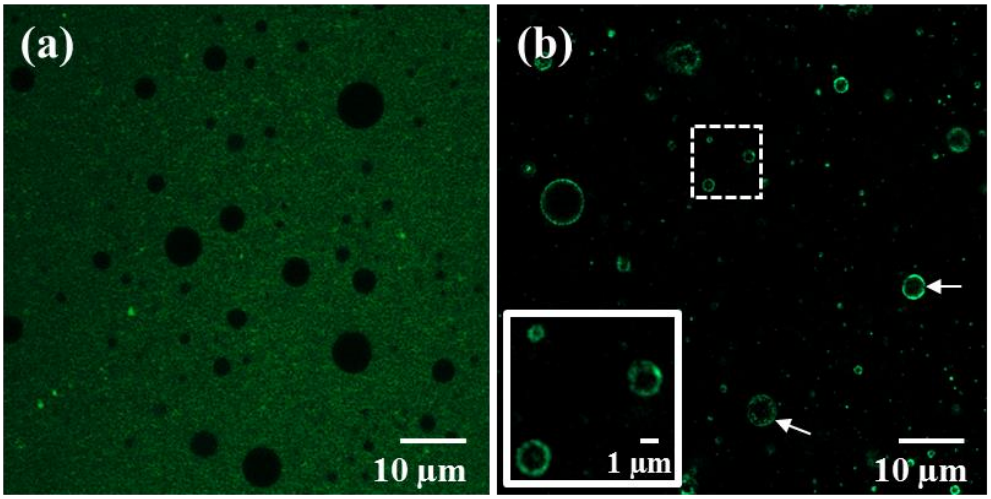

Figure 2.7 – O/W emulsions staining by TEPC-15. (a) Control experiment on emulsion stabilized with PMP. A diffused background signal is detectable while droplets interface are not stained. (b) O/W emulsion stabilized with ELP. Fluorescence signal is evident at the droplet interface. The pattern distribution is not uniform, as indicated by white arrows. Readapted from [133]

It is worth mentioning that in all experiments with emulsions, the lack of the washing step leads to a not negligible background signal which complicates the following quantification of the molecules at the interface. The presence of many bright spots in the bulk phase is an evident consequence of an excess of unbounded antibody or of a reduced

adsorption of phospholipids at the interface when dissolved in water phase, which can bring to the formation of suspended aggregates.

Staining procedure with TEPC-15 can be strongly influenced by the addition of other molecules in the emulsions, in particular proteins, as demonstrated in Figure 2.8. Four increasing concentrations of PMP powder, specifically 0%, 0.03%, 0.05%, 0.07% wt, added to final ELP emulsions have been let to homogenize for 10 min under gentle stirring before starting the immunofluorescence protocol. As visible from Figure 2.8 samples at 0% and 0.03% show a similar result, where droplets interfaces are completely stained, even if not homogenously. Sample at 0.05% of PMP starts to differentiate presenting an irregular staining and some droplets not stained at all. Finally, sample at 0.07% PMP shows all droplets unstained, suggesting a more complex interaction between phospholipids and proteins, which affect the staining procedure. In particular, it is known that phospholipids can form monolayer or multi-layers structure at the interface, while proteins rearrange their structure and unfold depending on the nature of the interface, in order to stabilize the system [135, 136]. It is difficult to define, in this case, what is the real interaction between the two molecules or with antibodies. It could be that proteins are able to hide the antibody, or unfold because of the presence of other emulsifying agents, bringing to a molecule displacement or to the formation of complex structure which do not allow the antibody to reach its epitope. The higher background signal in sample at 0.05% and 0.07% PMP is justified by the proximity of the glass support, which induces a slight reflection of the laser beam.

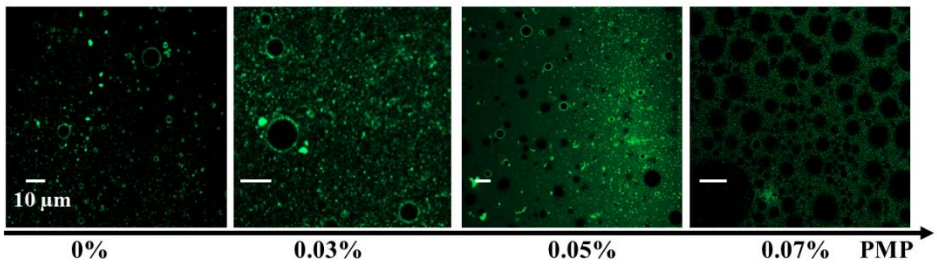

Figure 2.8 – TEPC-15 staining of O/W emulsions at different PMP concentrations. Staining starts to be compromised from 0.05% PMP, where fluorescence signal is altered. At 0.07% PMP droplets are completely unstained. Readapted from [133]

In order to quantify the amount of phospholipids at the interface, the normalized MGL of about 10 droplets per sample, with diameter in the range 2-11 µm has been measured as described in the methods, and reported in Figure 2.9 as function of droplet diameter and PMP concentration. It is possible to observe that MGL, that means the antibody staining efficiency, does not seem to be influenced by droplet diameter. It is higher for sample at 0% PMP and starts to decrease by increasing PMP concentration. Data trends indicated by the linear regression (solid line) suggest any dependence from droplet dimension and only a slight decrease is appreciated in the case of 0.05% PMP, probably due to the initial perturbation of the staining procedure close to a critical PMP value. Above this value staining is not possible. MGL as function of proteins concentration is reported in Figure 2.9b where a strong and exponential reduction of the fluorescence intensity is detectable, reaching a value of about zero for the sample at 0.07% PMP.

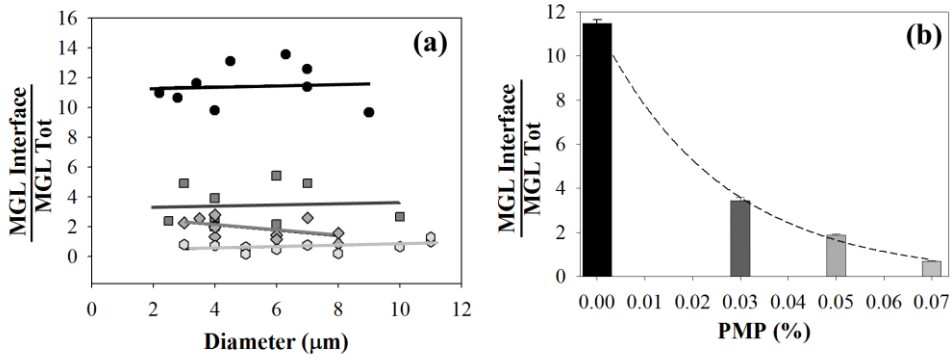

Figure 2.9 – (a) Normalized MGL of the droplets interface as function of droplets diameter and (b) of PMP concentration. Solid lines in (a) are a guide for the eye. (b) MGL as function of PMP%. An exponential decay is appreciable by increasing PMP concentration from 0% to 0.07%. Readapted from [133]

Further experiments with higher dilutions of secondary antibodies (1:100, 1:20, 1:10) (Figure 2.10a-c) have been carried out on emulsions in which ELP and PMP have been mixed together as describe in the methods. This approach did not allow to visualize PC as well, highlighting the strong influence of the proteins on the staining procedure.

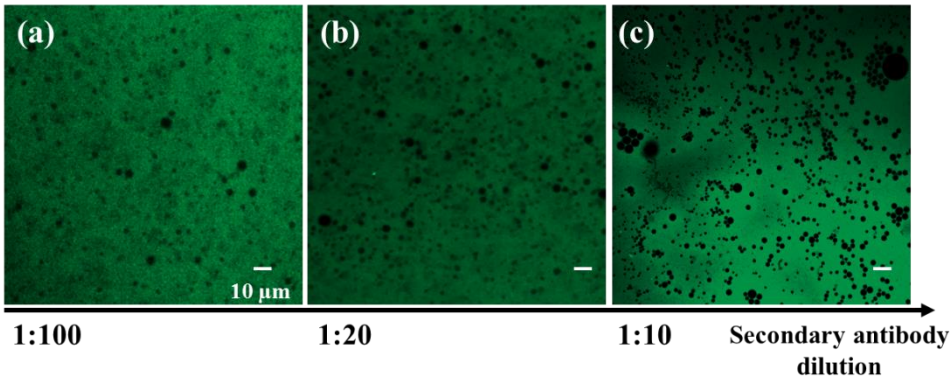

Figure 2.10 – O/W emulsions stained with increasing dilution of the secondary antibody. Only a background signal is visible in all cases. Taken from [133]

As in the previous case, Figure 2.10 shows only a high background signal, while droplets remain totally unstained. Therefore, the value of 0.07% PMP could be considered as indicative of a very low threshold suggesting a limited efficiency of the TEPC-15 staining. However, at the same time, this procedure show a high sensitivity, being able to detect also small changes in PMP concentration.

In order to overcome this poor efficiency, the staining protocol has been varied by changing the instant of PMP addition (before or after staining with antibodies) without significant results. For this reason, further experiments have been carried out on PC coating, since it is known that interaction between antibodies and antigens can be strongly dependent on the type of antigens and on the nature of antibody-surface interaction [131, 132]. In fact, antibody structure can be altered by lowering the recognition of the antigen. PC coating has been prepared on the bottom of a µ-slide. Images of the same field of view have been acquired in both, brightfield and confocal mode (Figure 2.11).

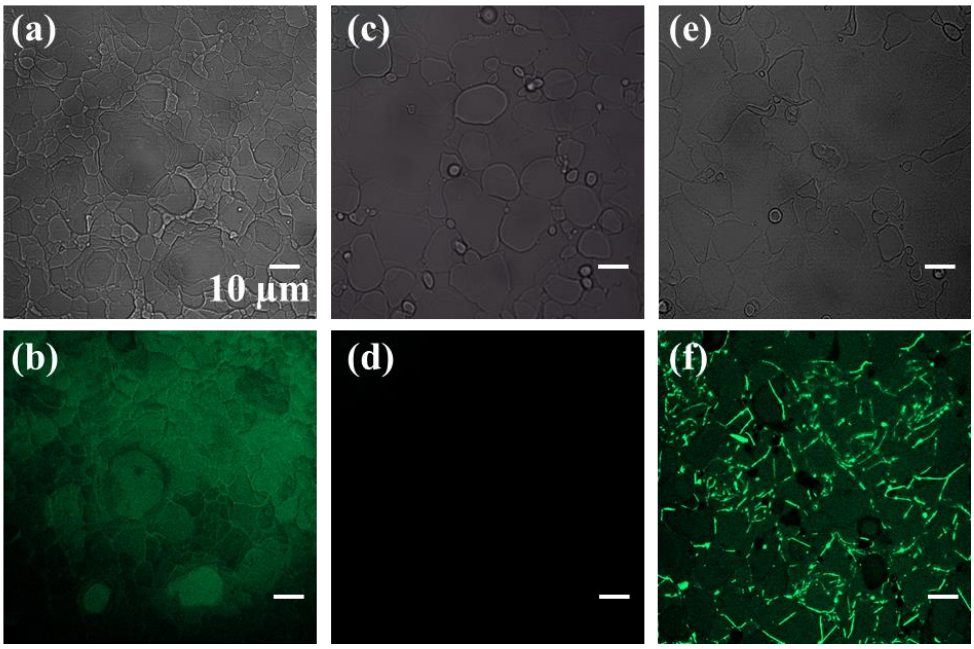

Figure 2.11 – PC coating in brightfield and confocal mode. (a-b) PC coating just prepared. PC does not form a uniform monolayer but stratified domains. (c-d) PC coating after TEPC-15 incubation. No signal is detectable. (e-f) PC coating at the end of the staining protocol. Fluorescence signal is detectable on the PC domains edges. Readapted from [133]

As in Figure 2.11a-b, PC does not form a homogenous monolayer, but it presents stratified domains, suggested from a different reflection of the laser beam on the glass bottom of the slide. After incubation with TEPC-15 (Figure 2.11c-d), no fluorescent signal is expected, resulting in an acquired dark image. It is interesting to note that after second incubation with secondary antibody (Rb α-mouse 488) the fluorescent signal is mainly located on the edges of the PC domains (Figure 2.11e-f). This result can be validated thanks to the correspondence with brightfield acquisition, where are still visible the PC domains even if slightly out of focus because of the dilution due to the aqueous buffer of the antibody.

In order to confirm the poor efficiency of the staining procedure in the presence of proteins, experiments on PC coating have been carried out and images of the same field of view have been acquired after staining with TEPC-15 (t_0), immediately after PMP addition (t_1), and 10 min (t_2) and 25 min (t_3) after the addition (Figure 2.12).

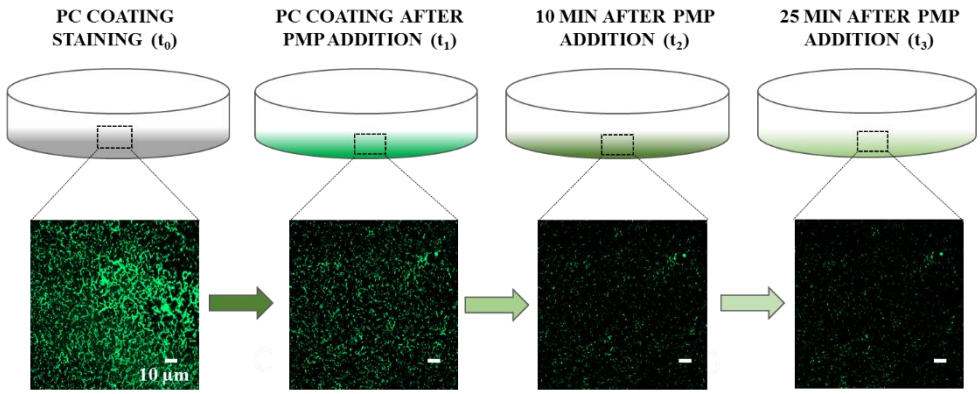

Figure 2.12 – PC coating after TEPC-15 staining (t_0), after PMP addition (t_1), 10 min (t_2) and after PMP addition (t_3). Signal decreases exponentially from t_0 to t_3. Readapted from [133]

As already demonstrated, immediately after the staining, the fluorescence signal is strong, showing some saturated pixels. After the addition of PMP, as in the case of emulsions, signal starts to decrease maybe due to a complex interaction between the two molecules. Fluorescent pixels are still visible even after 25 min from PMP addition (t_3). As also reported quantitatively in the histograms data in Figure 2.13a, the effect is more evident passing from t_0 to t_1, the number of fluorescent pixels decreases but in all cases a step up is present around 250 suggesting some saturated pixel, also visible in the images. MGL of images at each time instant is reported in Figure 2.13b. It is worth mentioning that only four images have been acquired, in order to avoid photobleaching.

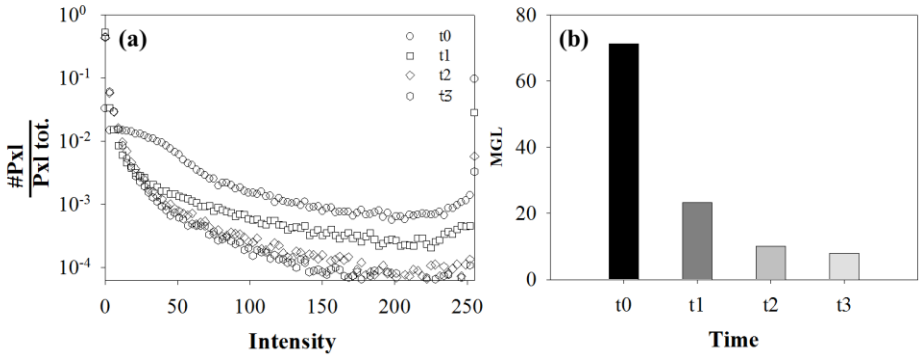

Figure 2.13 – (a) Data histograms of PC coating at all-time instants. Signal is lower after addition of PMP. (b) MGL of images in Figure 2.12 as function of time. Readapted from [133]

2.3 Conclusion

Localization and quantification of phospholipids in biological and colloidal systems is still an ambitious task. Immunofluorescence technique is here presented as innovative tool to localize and quantify specific molecules by CLSM not only in biological samples but also in colloidal systems. However, this technique requires an appropriate tuning of the protocol by choosing specific antibodies and incubation times, based on the investigated system and on the molecule of interest. Localization of more molecules in the same sample, at the same time is also possible. TEPC-15 has been here used as primary antibody to localize choline-based phospholipids, in particular, phosphatidylcholine, PC, in cells, O/W emulsions and PC coating. The specificity of TEPC-15 has been first successfully tested on two different cell lines, then the protocol has been adapted for the use in emulsions and PC coating. Where PC is used as component, even in presence of other phospholipids, the staining efficiency remains high. However, if different molecules interact with PC in the emulsion, such as proteins, complex structures can form influencing the antibody staining at droplet interface. In particular, it has been demonstrated that the staining efficiency is affected when the percentage of proteins exceeds the 0.07% causing no detection of the molecule of interest. It is clear that proteins affect staining procedure probably hiding the antigen-bounding site of PC. On this aspect further investigations are needed. Similar results have been obtained on PC coating where the fluorescence intensity of the antibody starts to decrease after addition of proteins.

Here, for the first time, the immunohistochemistry has been applied to emulsions, but more in general it can be used for different colloidal systems. Given the wide diffusion of micro-structured fluids, this result could be of relevant interest in different industrial applications from food to cosmetic and pharmaceutical industries.

3 Diffusion through the skin

In this chapter the development and the validation of an innovative experimental set-up based on CLSM and image analysis, for penetration studies through the skin is reported in detail. Preparation and staining protocols of solutions and emulsions used for successive diffusion experiments are described as well as the CLSM details for images acquisition. Preliminary diffusion experiments on skin biopsies are also reported. Results of diffusion experiments are finally presented and discussed. Main results reported in this chapter are also the subject of a published peer-review paper in 2017 in The Canadian Journal of Chemical Engineering [137].

3.1 Materials and methods

3.1.1 Agarose gel

A 2% agarose gel was prepared by adding the appropriate amount of agarose powder to distilled water. The suspension obtained was heated at 90°C until complete dissolution of agarose and then slowly cooled at RT. Prior to gelation, the viscous solution of agarose was distributed on a glass slide in order to obtain a film of gel thickness of about 1 mm. As better explained in the results paragraph, agarose gel has been used only for the developing of the experimental set-up without any correlation with skin architecture and properties.

3.1.2 O/W emulsion

O/W emulsions were prepared at a final volume of 10 ml with purified water and sunflower seed oil. Water/oil ratio is 80/20. As surfactant, a commercial lecithin based emulsifier [138], Biophilic H™ (Lucas Meyer Cosmetics) at a final concentration of 5% wt was added to the oil phase under gentle stirring for 30 min at 80°C. Biophilic H™ is a phospholipids-based emulsifier combined with other fatty acids and fatty alcohols able to improve the emulsifying properties. It forms a monolayer around oil droplets and progressively a bilayer network is formed in the aqueous phase to create a lamellar O/W

emulsion (which is also able to entrap active ingredients). Water was then gradually added under stirring for 8 min at the same temperature until a coarse emulsion is formed. The sample was then processed with a high shear mixer (Ultra-Turrax, IKA) at 16000 rpm at 70°C for 1 min. The emulsion was then cooled for about 30 min under stirring and at RT. Oil/water ratio as well as percentage of surfactant were chosen in order to guarantee a good stability of the emulsion. To this aim, different emulsions, whose compositions are reported in Table 1 were stored in some test tubes for several weeks and optically inspectioned. In order to follow eventual separation phenomena, images of the samples were acquired with a high definition camera (Canon EOS 60-D) at different times: just prepared (t0), after 2 (t2h) and 24 (t24h) hours and after a month (t1). After this time, situation is not changed anymore.

Table 1 - Emulsions identification and composition for stability study

Sample	Oil [%]	Water [%]	Biophilic H™ % [w/w]
A1	20	80	5
A2	20	80	1
A3	20	80	0,1
A4	20	80	0,01
A5	10	90	5
A6	5	95	0,1
A7	5	95	0,01

Images of samples from A1-A4 at three different times are reported in Figure 3.1 where it is possible to observe that only a surfactant concentration of 5% guarantees a stability over 1 month. Morphology of the latter is also reported in fluorescence mode where oil is stained with Nile red always at the concentration reported in 3.1.3. Other samples start to show a separation phase immediately or after 24h. Sample A5 have shown a stability similar to A1, while A6-A7 are unstable.

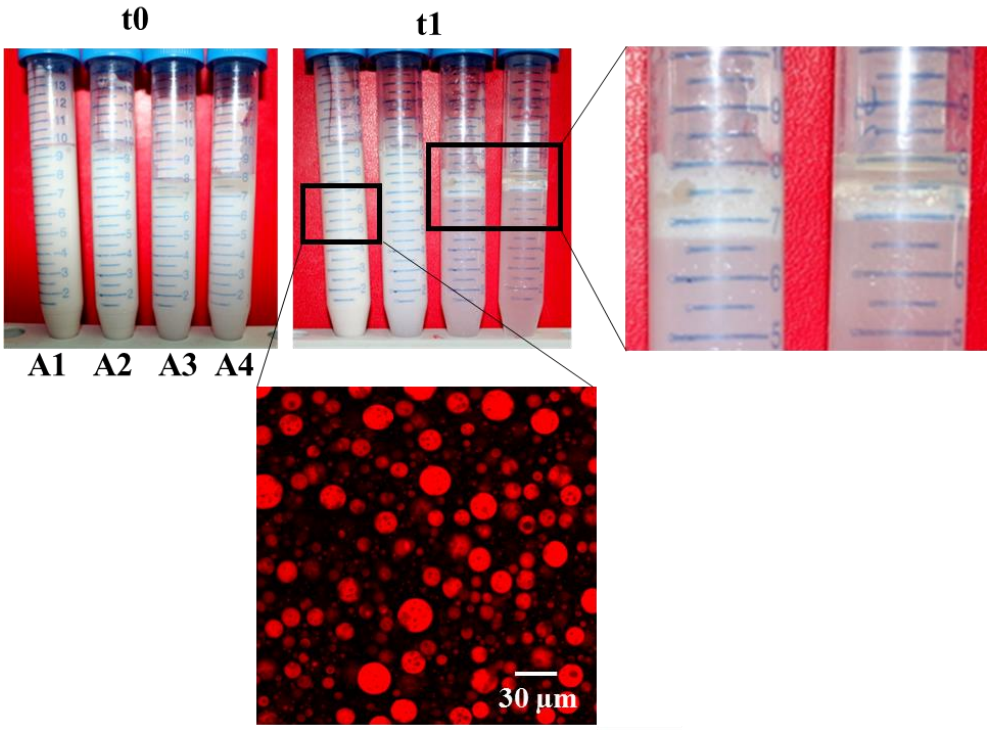

Figure 3.1 – Stability study of O/W emulsion at different oil/water ratios and different Biophilic H™ concentration. CLSM image shows the internal microstructure of the emulsion stained with Nile red. Specification of all samples are reported in Table 1

3.1.3 Solutions and emulsions staining

Distilled water and commercial sunflower seed oil were labeled by adding specific dyes for polar and non-polar phase, respectively Rhodamine B (Sigma-Aldrich) and Nile red (Sigma-Aldrich), at a concentration of 0.01 mg/ml. Stock solution of Nile red was obtained as reported in 2.1.2. For Rhodamine B, powder was directly added to water at RT and left under gentle stirring until complete dissolution. The concentration value of 0.01 mg/ml was chosen after a calibration of the two dyes, carried out in order to assure a linear relationship between measured fluorescence intensity and concentration of diffusing molecule. Starting from stock solutions, successive dilutions were prepared at concentrations gradually decreasing, specifically at 0.1, 0.05, 0.01 and 0.001 mg/ml. The fluorescence intensity of each dilution was then plotted as a function of the respective known concentration value. After dye addition, solutions were left to stand for 30 minutes under gentle stirring in order to achieve a complete homogenization. For

emulsions staining, Nile red was previously added to the oil phase before emulsification process.

3.1.4 Skin biopsies

Human skin biopsies were obtained from healthy volunteers, subject to cosmetic surgery on different donor sites, thanks to a collaboration with Prof. Pasquale Abete from the Medical School of the University of Napoli Federico II. Morphology of skin was investigated on untreated samples by using auto-fluorescence signal of skin components. For diffusion experiments, biopsies were stored in 10% neutral buffered formalin (Sigma-Aldrich) for at least 12 h in order to cancel out auto-fluorescence signal of sme skin components, such as keratin, collagen and elastin.

3.1.5 Diffusion experiments

A schematic representation of the experimental set-up is reported in Figure 3.2. A little reservoir was obtained inserting a coverslide in an O-ring, thanks to appropriate spacers (SunJin Lab) of 200 µm thickness, in which allocate solutions or emulsions. The agarose gel film or skin biopsies slice, prepared as above, were placed in contact with the reservoir by placing them on the edges of the spacres. The O-ring edges were filled with water and covered during the experiment in order to avoid water evaporation from emulsion or solution in the reservoir. The system was then closed with another coverslide and put on the stage of a confocal microscope (Zeiss LSM Pascal, see 2.1.4).

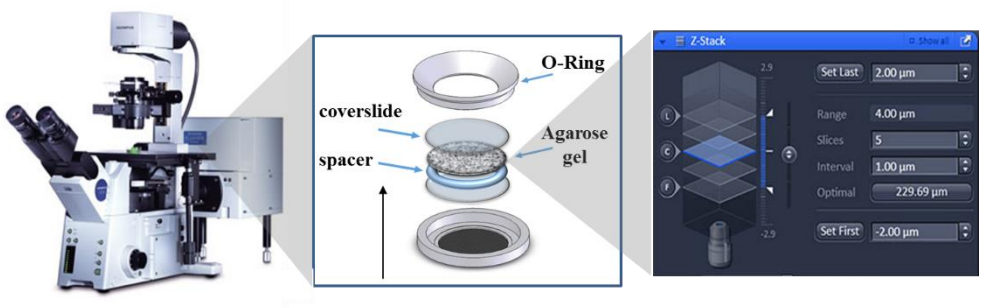

Figure 3.2 – Schematization of the CLSM experimental set-up and acquisition images procedure. Taken from [137]

Images were acquired with a 20x (Plan-Neofluar) objective and excitation was provided by a He-Ne laser at a wavelength of 543 nm. Sample were identified in the fluorescence mode because of an intrinsically auto-fluorescence signal, as in the case of skin components, or through an induced fluorescence due to the use of dyes or fluorochromes, molecules which absorb photons at a specific wavelength, and emit fluorescence at a higher wavelength. The recorded fluorescence intensity was measured as described in the following paragraph by the use of images analysis software.

Furthermore, microscope is equipped with a manual focus system, which allows to select the field of view within the sample. The diffusion of the labelled fluid was observed by iterating every two minutes the acquisition of a z-stack images along a thickness of about 300 µm with a slice distance of 5 µm. The experiment length was 120 min. Diffusion experiments were carried out with labelled water and oil solutions and with an O/W emulsion prepared as described above.

Preliminary studies on diffusion of a pure oil solution stained with Nile red was also carried out by substituting agarose gel with skin biopsies. The experimental conditions and parameters set were the same than in the previous case, except for the penetration depth, that, due to the high thickness of the sample and its turbidity is only 30 µm.

3.1.6 Image analysis and data processing

Images obtained at the end of the diffusion experiments were analyzed with a commercial software, Image Pro Plus® 6.0 by calculating the mean fluorescence intensity of each image at different times and depths. It is worth mentioning that a main limitation of CLSM resides in the depth-addiction of the image quality, because the agarose gel acts as a quencher of the laser beam. A correction of intensity data is hence necessary. Attenuation constant K was estimated from data fitting with Lambert Beer law ($I = I_0 e^{-Kz}$) after a steady state condition in the sample was reached. It relates the light intensity I_0, emitted from a plane at a given depth z in the sample to the value I measured. To this aim a small sample of agarose gel was completely soaked in the solution (or emulsion) for at least 24 h. After this time a z-stack in the sample was recorded and the corresponding data fitted.

Although the estimation of diffusion constant *D* is generally obtained by fitting data with Equation 7, where the reservoir is considered as infinite, this approach does not consider complex interaction that can occur between external molecules and skin during penetration. For this reason, a more realistic approach is to consider the reservoir as stock of a finite amount of solution. Considering *h* as the half- depth of the reservoir, and C_0 always the initial reservoir concentration, the solution of differential equation becomes:

$$C = \frac{1}{2} C_0 \left\{ erf \frac{(h-z)}{2\sqrt{Dt}} + erf \frac{(h+z)}{2\sqrt{Dt}} \right\} \qquad \textit{Equation 9}$$

This solution is valid for a semi-infinite slab and a finite reservoir. However, it is also possible to consider the case of finite slab and finite reservoir with the corresponding solution [57]:

$$C = \frac{1}{2} C_0 \sum_{n=-\infty}^{\infty} \left\{ erf \frac{h + 2nl - z}{\sqrt{4Dt}} + erf \frac{h - 2nl + z}{\sqrt{4Dt}} \right\} \qquad \textit{Equation 10}$$

In order to define the rightest model, Equation 7, Equation 9 and Equation 10 were reported in Matlab for selected parameters (*2h* = 200 µm, *l* = 1 mm) at a given time (Figure 3.3). The script is reported in the Appendix A with relative comments.

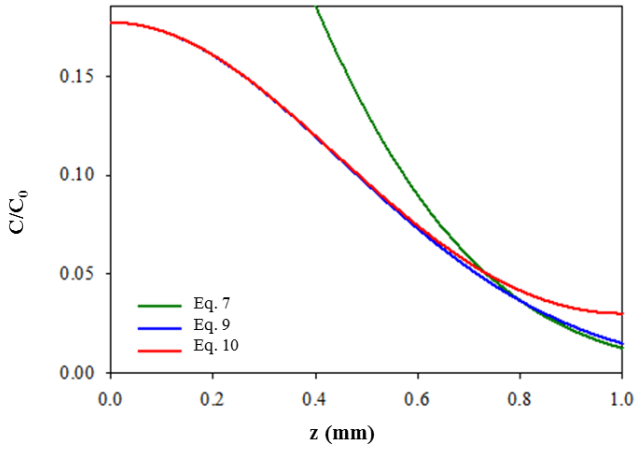

Figure 3.3 – Matlab plots of Equation 7 (green), Equation 9 (blue) and Equation 10 (red) for h=200 µm, l=1 mm and t=83min. Readapted from [137]

As visible from the plot, Equation 7 presents a totally different trend compared to the other two cases. On the contrary, Equation 9 and Equation 10 start to deviate each other

far from the interface. Being the region explored in the sample only 300 µm, Equation 9 was chosen for the data fitting and resulting *D* estimated. Fit was made for each independent time step acquisition and the final value of the diffusion coefficient was calculated as the mean value of independent calculations.

3.2 Results

Calibration of the two dyes, Rhodamine B (Figure 3.4a) and Nile red (Figure 3.4b), has been carried out in order to easily convert intensity data in concentration data. Known values of concentration have been plotted as function of the corresponding intensity, measured with CLSM and images analysis. A linear regression has confirmed a direct relationship between the two variables in the tested range of concentrations, which allow an easy switch from one measurement to the other.

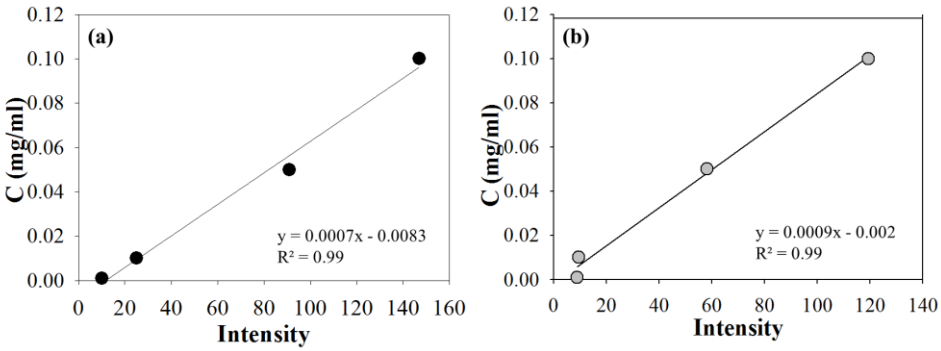

Figure 3.4 – Calibration of Rhodamine B (a) and Nile red (b). Linear regression (solid lines) confirm a direct relationship between concentration of molecules and fluorescence intensity in the tested concentration range

Once defined the dye concentration, 0.01 mg/ml, and in order to follow fluorescent molecules diffusion by CLSM, successive experiments have been carried out to stain one phase of the O/W emulsion. An example of an O/W emulsion prepared as described in 3.1.2 in which the oil phase has been stained with Nile red is shown Figure 3.5a, while the case of a stained aqueous phase with Rhodamine B is reported in Figure 3.5b.

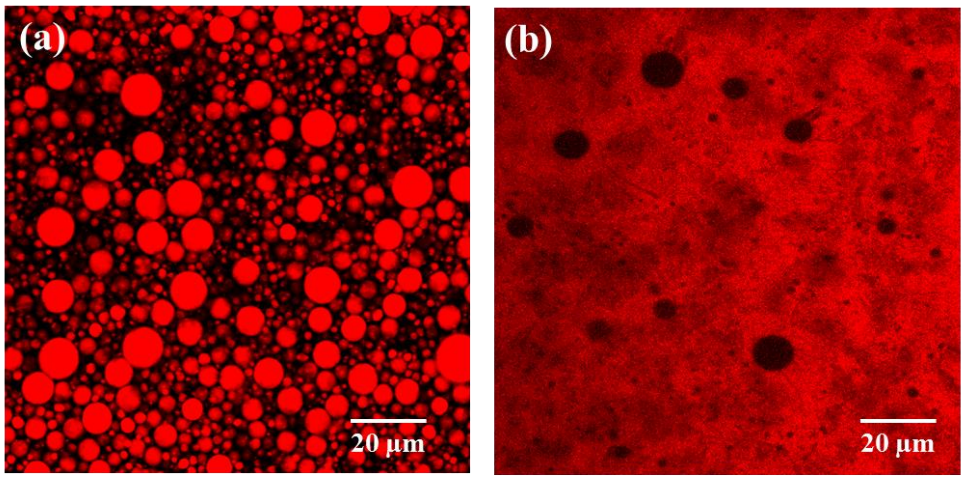

Figure 3.5 – Staining of an O/W emulsion. Oil phase stained with Nile red (a) and water matrix stained with Rhodamine B (b). In the case of Rhodamine B staining, a lower number of droplets is visible due to a quite solubility of the dye in all vegetable oils. In the other case, solubility of Nile red in water is less than 0.1 µg/ml. Readapted from [137]

As visible from Figure 3.5a-b, in the case of stained oil phase, red droplets are easily distinguishable and in contrast with the black aqueous matrix, in which Nile red solubility is less than 1 µg/ml. In the other case, instead, black droplets are dispersed in the stained matrix. It should be noted that in the latter case the number of droplets is clearly lower than in the previous case, although the volumetric fraction of the oil phase is the same. This effect is explained by the fact that the Rhodamine B once dissolved in water, is easily soluble in all vegetable oils, such as that used in the current formulation. For this reason a higher signal is detected with a greater difficulty in the visualization of the droplets.

It is important to assert that, as explained in the introduction, emulsions used for cosmetic or pharmaceutical applications present a droplet dimension in the range of few nanometers, different from this case where the range is about 1-10 µm. For this reason a further tuning of the microstructure of the emulsion could help to optimize results about successive penetration process.

Water, oil and O/W emulsion, properly stained, have been in fact used for diffusion experiments in a model system based on agarose gel. The latter has been chosen only for the developing of the experimental set-up taking into account that it does not mimic at

all the skin structure. Furthermore, it is a handy system to investigate behaviors of solutions and emulsions based on their intrinsic properties, and their affinity with it.

A qualitative and quantitative comparison on diffusion of all formulations is reported in Figure 3.6. From images analysis, fluorescence intensity data have been converted in concentration values, corrected according to Lambert Beer's law, normalized respect to the initial concentration $C_{0,}$ and plotted as function of the penetration depth. Comparison is after 120 min of experiment.

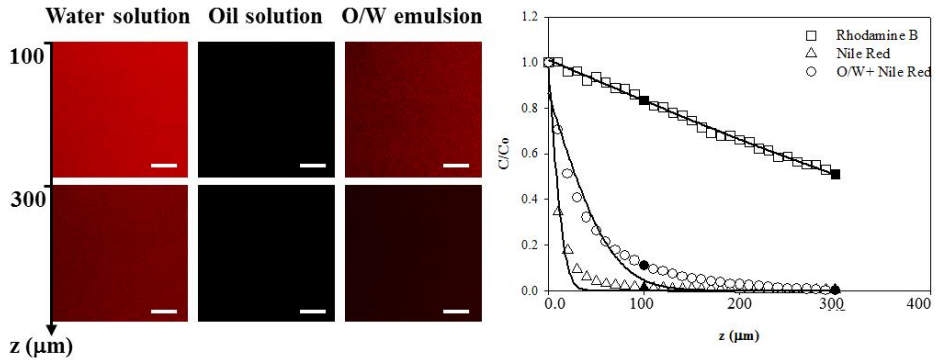

Figure 3.6 – Fluorescence intensity at 100 µm and 300 µm depth in the agarose gel, after 2 h diffusion for water solution (left) stained with Rhodamine B, oil solution (center) stained with Nile Red, and O/W emulsion (right) stained with Nile Red. Scale bar is 10 µm. Normalized concentration of Rhodamine B in water (squares), Nile Red in oil (triangle) and Nile Red in O/W emulsion (circles) as function of the penetration depth in the agarose gel is reported in the diagram. Full symbols corresponds to the images reported. Solid lines represent fitting of data with Equation 9. Taken from [137]

As noticeable, in the case of water solution (squares), the concentration becomes approximately half of the initial value after 120 min but the signal is still high. This behavior is in agreement with the high affinity of the agarose gel with water (hydrophilicity). In fact, corresponding images show a uniform and strong fluorescent signal. The oil solution (triangles), with lower affinity for agarose, presents a decreasing trend reaching a zero value at about 100 µm depth. The different affinity of the water and oil solutions with the agarose gel is confirmed by a three order of magnitude difference in the diffusion coefficients estimated by data fitting (solid lines) with Equation 9, and respectively $2.18*10^{-6}$ and $2.6*10^{-9}$ cm^2/s. The non-perfect overlap of analytical curves with the experimental data may be due to an incorrect discrimination of the interface between the reservoir and the gel, which corresponds to the start point

(first slice) of the z-stack. On the other hand, when the same oil and water solutions are used in the form of an O/W emulsion, oil droplets diffuse better than the pure solution, reaching a penetration depth of about 150 µm, with a diffusion coefficient of $2.06*10^{-8}$ cm^2/s. This result is also visible from images, where the fluorescence signal of O/W emulsion at the same depth is higher compared to the oil solution. It is clear that a finer dimension of the droplets, as well as an optimization of the surfactants combination, could further improve this enhancer effect.

In addition, these results suggest that, based on their own properties, carriers such as droplets in the emulsions, can chose a preferential route to penetrate the medium. In the case of skin, for example, lipid vesicles or oil droplets, seem to prefer lipid bilayers between corneocytes as principal pathway [41, 139]. It is hence important to highlight that fluid microstructure plays a key role in the penetration process. Therefore, further investigations on the role of the formulation microstructure are necessary in order to understand the real interaction of the formulations with skin components together with the reason of the improved efficiency.

Preliminary studies on skin biopsies have been carried out one to visualize skin morphology and to test the ability of diffusion of a pure oil solution stained with Nile red. For morphology studies, images have been acquired with CLSM, by exploiting auto-fluorescence signal of skin components such as collagen, keratin and elastin (Figure 3.7a). As visible from Figure 3.7a auto-fluorescence signal is strong enough to distinguish single cells and eventual wrinkles on the skin surface (white arrows). Moreover, such a packing of cells suggests the possibility that during treatment and storage of skin biopsies, SC may have been easily damaged, exposing first layers of SG, where cells are more densely packed. It is worth mentioning that working on skin biopsies is very difficult due to the high variability and dependency of skin structure by body site, sex and age. Diffusion of oil solution stained with Nile red has been monitored with the same previous set-up in an arm skin biopsy for 2 h by acquiring z-stack images at time intervals of 2 min and by measuring the mean fluorescence intensity at different depths and times (Figure 3.7b). In this case auto-fluorescence signal has been cancel-out with formalin treatment in order to assure only dyes signal. As visible from Figure 3.7b-

c, Nile red penetrates the whole SC up to a depth of 30 µm, following a lipid route around corneocytes. From the reconstruction at the initial times and after 90 min, it is clear how the fluorescence intensity, at a given depth, increases over time. Due to the limited penetration power of the laser in such turbid medium, it is impossible to reach a depth higher than about 50µm. The use of clarifying agents has not been successful to improve penetration depth. Quantification of the intensity data has been obtained from data fitting (solid lines) with Equation 9 (Figure 3.7c) with a resulting diffusion coefficient in the order of 10^{-9} cm^2/s, in good agreement with literature data [44].

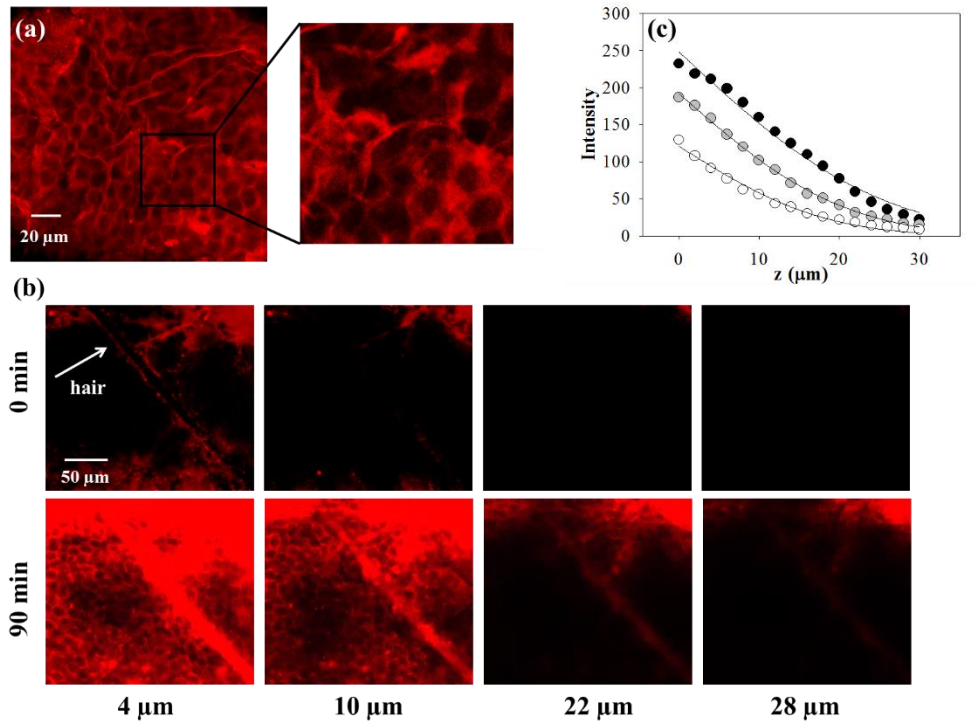

Figure 3.7 - (a) Auto-fluorescence signal of skin arm biopsy before incubation in formalin buffer. Single cells are well distinguishable. (b) Reconstruction of diffusion of oil stained with Nile red in skin biopsy for 2 h, at different depths in the sample at initial and final times. (c) Intensity data as function of penetration depth at 1 h (black), 1.3 0 h (grey) and 2 h (white). Solid lines correspond to the fit with Equation 9

3.3 Conclusions

In this chapter, an innovative experimental set-up based on CLSM and image analysis has been presented for the investigation of penetration process of fluorescent molecules

for TDD applications. To this aim, studies have been performed in a model system based on agarose gel by following the diffusion of water and oil solutions as well as O/W emulsion, properly stained with specific dyes. In the case of emulsions, stability was guaranteed by choosing the right oil/water ratio and percentage of surfactants. Only sample that guarantees a stability over 1 month has been chosen for successive diffusion tests. Results of diffusion in agarose gel have demonstrated that fluid microstructure as well as formulation own properties play a key role in the penetration process. O/W emulsion, in fact, shows a diffusion coefficient of one order of magnitude higher than the pure oil solution. On the other hand, as expected, water solution presents the highest diffusion due to their strong affinity with the agarose gel. Diffusion of red-colored oil has also been carried out in skin biopsies suggesting the role of the intercellular route as the main penetration pathway for lipophilic molecules, with results in agreement with literature.

The proposed method can provide useful information for a fine tuning of the formulation and optimization of TDD efficiency by exploiting an easy and reliable tool.

4 Model systems

Due to the poor availability of skin biopsies and the difficulty of the treatment, the possibility to use soft materials to mimic skin properties and/or morphology is not to exclude. In this chapter, Bicontinuous Emulsion Gels (BEGs) composed of gelatin gel as hydrophilic phase and crosslinked oil as hydrophobic phase are presented as good model to to mimic SC properties. Protocols for BEGs formulations, with different surfactants and/or cross-linkers are reported in detail. Images of the resulting morphology are then presented and compared. Together with previous results in chapter 3, the main results of this chapter are also subject of a published peer-review paper in The Canadian Journal of Chemical Engineering [137].

4.1 Materials and methods

4.1.1 BEGs formulation

Type A gelatin from Extraco Gelatin under the trade name of Geltec (UG-719- H) derived from collagenous tissue by acid treatment was supplied in powder form. Gelatin powder at 30% wt was used as hydrophilic component of BEG and prepared by gradually adding gelatin powder to distilled water at 50°C under gentle stirring until the solution becomes transparent. As hydrophobic phase, sunflower oil was used in combination with surfactants and/or crosslinkers in order to obtain a gel-like consistency which contribute to the easily hand of the final system. The first part of the research was focused on the choice of surfactants (or mixture of surfactants) able to produce a stable W/O emulsion. To this aim, the HLB (Hydrophile-Lipophile Balance) of the surfactant was used as reference to understand, *a-priori*, the possibility to obtain the desired system. This value varies between 0 and 18 indicating the simultaneous attraction of the surfactant for water and/or to the oil. Based on these information, Sorbitan monooleate (Span 80, HLB=4.3) or the combination of Span 80 with Sorbitan Monolaurate (Tween 20, HLB=16.7) were used to obtain stable emulsions. The combination of Span 80 and Tween 20 is preferred since one is soluble in the oil and the other in the water, so the respective lipophilic and

hydrophilic portions arrange at the two sides of the droplet interface generating a dense interfacial film. Another surfactant is the Polyglycerol polyricinoleate (PGPR, Palsgaard) that although presents characteristics similar to Span 80, it has molecular groups which dispose differently at the interface. Biophilic H™ and Myverol™ 18-04K (Kerry), instead, are used as crosslinkers, the latter of which is composed of monoglycerides of saturated fatty acids which help to obtain a more waxy oil phase. Obviously, based on their properties, crosslinkers are added before emulsification in the phase where they are more soluble.

BEGs were prepared at a final volume of 10 ml. After preparation of the gelatin, it was added to the oil phase and immediately emulsified with an Ultra-turrax at 70°C and 24000 rpm for 1 min. Systems were left to cool at RT for at least 1 h.

In Table 2 are reported the details about the compositions of the BEGs with more promising results.

Table 2 – Composition of BEGs

Sample	Gelatin %	Oil %	PGPR %	Span 80 %	Tween 20 %	Biophilic H %	Myverol %
A	40	60	3				
B	40	60	5				
C	40	60		3			
D	40	60		3		1	
E	45	55		3	3		10

In order to investigate morphology of these systems, gelatin phase or oil phase were stained, as previously, by adding Rhodamine B or Nile red at a concentration of 0.01 mg/ml, the first for samples A and B and the second for the other samples. Images of each sample were then acquired by CLSM at different magnification by exciting molecules with a He-Ne laser at a wavelength of 543 nm, in brightfield and in confocal mode (see 2.1.4). Only for sample E, a mosaic of images with a 2.5x objective was reconstructed in order to observe a larger field of view and to better define morphology

of the system. Qualitative image analysis was carried out by only considering dimensions of gelatin or oil droplets (or network) compared to the SC structure. Hydrophilicity and hydrophobicity of SC components are guaranteed by the intrinsic properties of the gelatin and the oil.

4.2 Results

As already mentioned in the introduction, SC can be schematized in a simplistic way as a “bricks and mortar model". In order to make possible a deep investigation about the penetration process avoiding the high request of skin biopsies, the use of soft material properly tuned to mimic hydrophilicity of skin cells embedded in the hydrophobic lipid bilayers could be a good alternative.

BEGs have been formulated by changing type of surfactants or crosslinkers, allowing the system, previously prepared at high temperature, to gel. Morphology of the sample A and B are quite similar and reported in Figure 4.1. Either after the emulsification or after cooling, the internal structure appears monophasic on a macroscopic scale. Only in brightfield a tiny dispersion of small droplets in appreciable. By confocal inspection, it is possible to note tiny oil islands (black) in a gelatin matrix (red-colored). After cooling, structure is still present although the oil phase appears more finely dispersed. Two problems are evident in these samples, the consistency, too smooth to the purpose, and the impossibility to mimic SC structure since the presented BEG shows completely the reverse case of the desired structure, maybe due to a phase inversion verified during emulsification process.

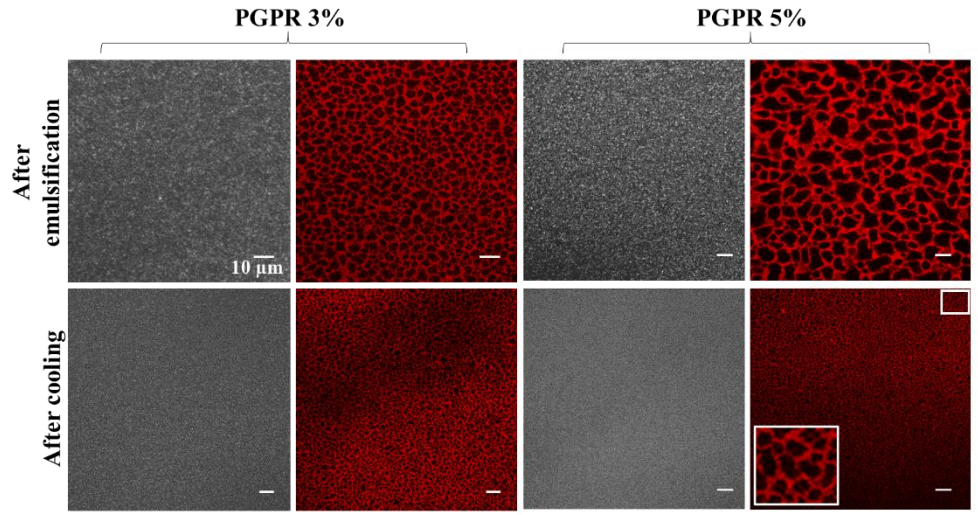

Figure 4.1 – CLSM images of samples A and B (Table 2) in brightfield and confocal mode, immediately after emulsification and after cooling. Gelatin phase is stained with Rhodamine B and forms a network around black oil islands, which become highly dispersed after cooling. Readapted from [137]

A different result is obtained by evaluating BEG morphology obtained for sample C (Figure 4.2).

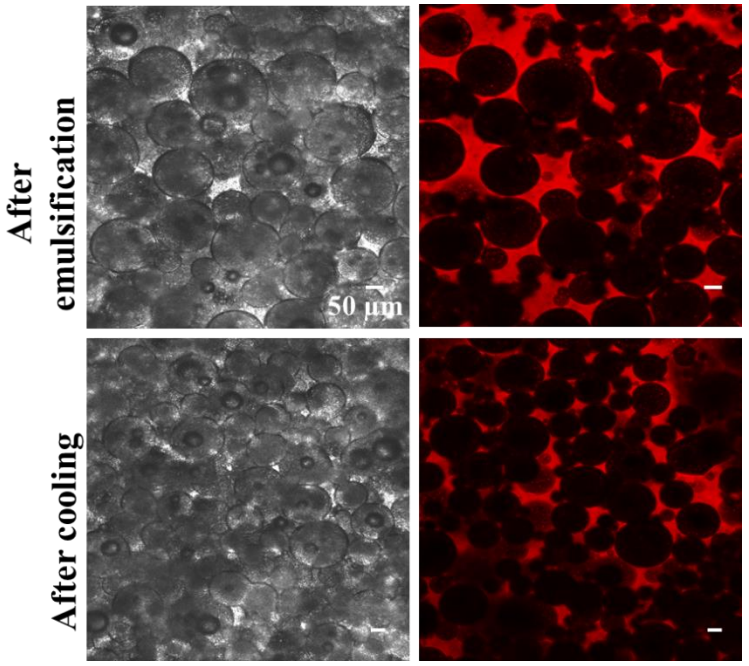

Figure 4.2 – CLSM images of internal morphology of sample C (Table 2) in brightfield and confocal mode. Oil phase is stained with Nile red. Gelatin droplets form a dense structure after cooling with a granular consistency

After emulsification, a high number of gelatin droplets are visible in the oil matrix. Dimension of droplets are however in the range of hundreds of micrometers, that is far from real cellular dimension in the range of tens of micrometers. After cooling gelatin droplets tend to aggregate forming a more dense structure reducing interspaces of the external oil matrix between droplets. This aspect is promising considering that in the SC, lipid matrix is only the 4% wt of the total volume. The consistency of the final system is not easy to handle remaining a bit granular even after the emulsification. Moreover, over time a separation between the two phases is clear due to a strong coalescence of the gelatin droplets.

In order to improve the stability of the previous system, the same formulation has been prepared by adding a 1% wt of Biophilic H™ as crosslinker for the oil phase. Results after emulsification is not so different from the previous BEG, where densely packed gelatin droplet are immersed in the oil matrix (stained with Nile red). Nevertheless, combination of a surfactant and a crosslinker seems to reduce or to slow down the coalescence phenomenon, which however occurs at longer times (Figure 4.3). Great gelatin clusters are visible in the images after cooling, where oil phase is still present contributing to reduce consistency of the system. Further experiments have been carried out by increasing Biophilic H™ concentration in order to improve consistency of the oil phase, but no significant difference have been highlighted.

The experimental campaign has been continued by slightly increasing gelatin/oil ratio (sample E, Table 2) and by adding a couple of surfactants, Tween 20 and Span 80, respectively in the gelatin and in the oil phase. Mixed together, these surfactants improve BEG stability due to a synergistic effect, which is the result of compact interfacial packing due to an enhanced mutual compatibility between water and oil, and favourable molecular interactions between the different surfactants [140].

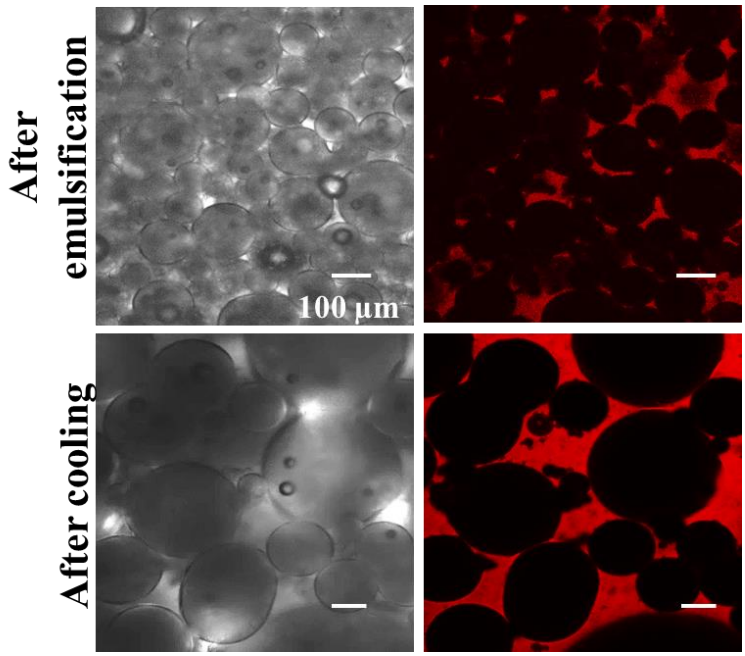

Figure 4.3 - CLSM images of internal morphology of sample D (Table 2) in brightfield and confocal mode. Oil phase is stained with Nile red. Coalescence phenomenon of gelatin is only reduced by the addition of a cross-linker in the oil phase but not avoided. Taken from [137]

In addition, the crosslinker Myverol 18-04K at a concentration of 10% wt has been added to the oil phase in order to give a gel-like consistency to the final system. For a visual inspection, Nile red has been always used to stain lipophilic phase. As visible from Figure 4.4, immediately after the emulsification gelatin clusters, are in turn composed of a high number of droplets not packed. This situation is not well appreciable in confocal image where a net separation between the two phases is visible. After cooling the system presents a gel-like consistency (Figure 4.4a), easy to handle and quite elastic. However, by analyzing the internal microstructure, droplet-like emulsion microstructure is replaced by a bicontinuous morphology, visible in both images, but better detectable in the confocal one. A broader view into the system is possible by reconstructing a mosaic of images with a lower magnification, which allow to better visualize the bicontinuous structure (Figure 4.4b).

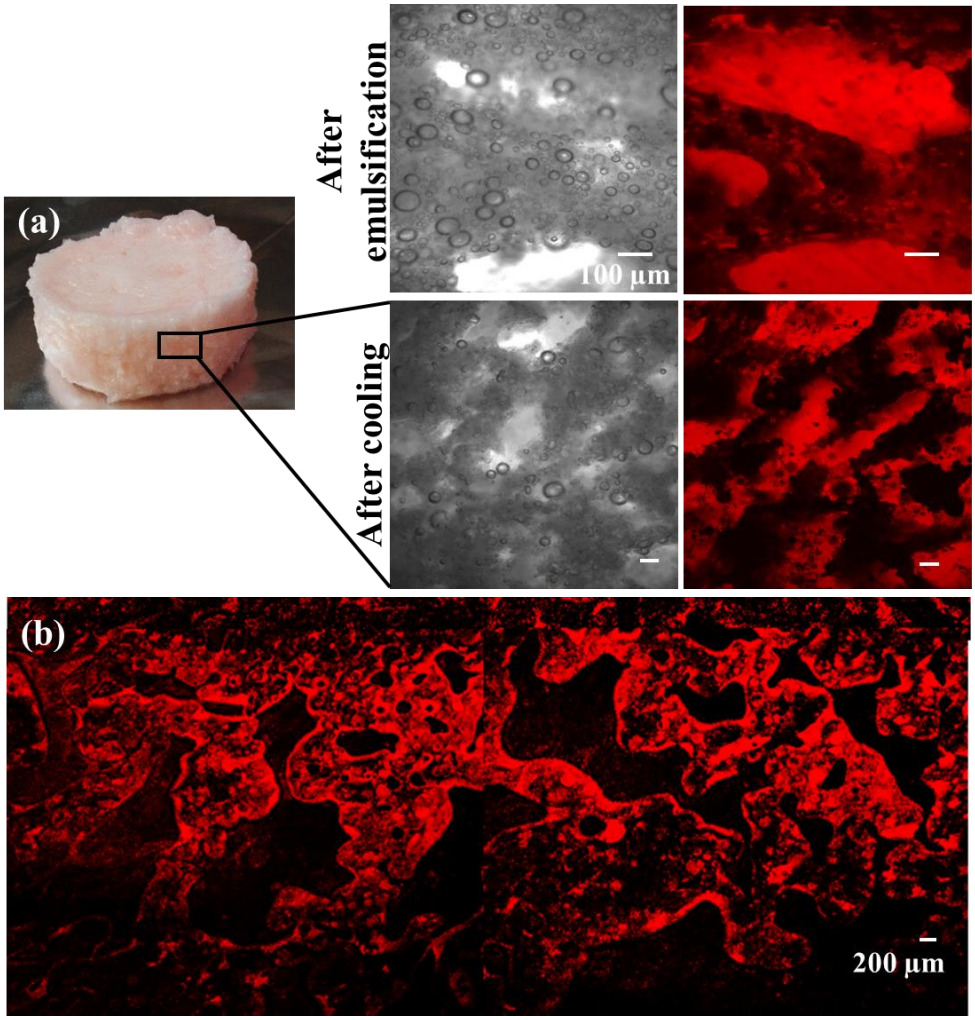

Figure 4.4 – (a) Photograph of the sample E (Table 2) after cooling at RT. CLSM images of the system in brightfield and confocal mode after emulsification and after cooling. (b) Mosaic of images of the internal bicontinuous structure of the system. Oil phase is red-colored with Nile red. Readapted from [137]

This last BEG represents the best formulation to the purpose of mimicking SC structure. Although a further tuning is necessary, in particular regarding the amounts of surfactants which guarantee a better stability, and the gelatin/oil ratio, still far for the real system, the obtained bicontinuous morphology could be a valid result for the mimicking of the tortuous pathway through the skin cells. Moreover, detailed rheological characterization of these soft materials could be also helpful to compare texture of BEGs to the desired properties.

4.3 Conclusions

BEGs, obtained from emulsification process, have been proposed as soft materials to mimic skin morphology and/or properties. Gelatin gel has been used as water phase to mimic skin cell hydrophilicity, while sunflower oil, with the addition of crosslinkers, has been used as lipophilic phase. Gelatin/oil ratio has been set at 40/60% wt/wt. Then, surfactants and/or crosslinkers have been added to the phase in which they are more soluble. Different formulations have been presented and the morphology investigated by CLSM after staining one of the two phases with Rhodamine B or Nile red. Among all the formulations tested, only one (sample E) has allowed to obtain a good stability and a morphology similar to the SC. However, amounts of ingredients and gelatin/oil ratio require further tuning to optimize the formulation and the morphology, whose dimensions are still far from the real system. Other tested formulations have been rejected due to the too smooth consistency or to a strong instability which brings to a fast gelatin droplets coalescence.

These systems, if properly tuned, could represent a suitable and low cost method which could result in an innovative methodology, biopsy-less, to test different kind of formulations. Moreover, the interaction between formulation and the two main component of the skin, cells and lipid matrix could be deeper understood.

5 Gelatin gels

In order to mimic corneocytes hydrophilicity in SC, gelatin gel is chosen as reference model and properly characterized. Its properties, in particular porosity, related to initial polymer concentration, and the corresponding ability to swell are investigated by NMR and CLSM. NMR measurements are the results of a collaboration with Dr. Carmine D'Agostino from University of Cambridge. In this chapter, protocols about gelatin preparation at different concentrations and successive studies in absence and during swelling are reported. Information about changes in gelatin structure during swelling are also obtained by CLSM visualization during permeation of solid polystyrene particles, with diameter larger than gelatin pores. Effect of swelling in combination with diffusion of a fluorescent molecule is also determined by following permeation of Rhodamine B. Finally, a qualitative description about the tension distribution inside the gelatin network during swelling is also described using birefringence images acquisition and time-lapse experiments. All corresponding results are following reported. In particular, CLSM and NMR results are also content of a peer-review paper in 2017 in Soft Matter [141].

5.1 Materials and methods

5.1.1 Gelatin solution

Gelatin powder, type A, was purchased from Extraco Gelatin under the trade name of Geltec (UG-719- H), derived from collagenous tissue by acid treatment. Powder was added to hot water (40-50°C) at the desired concentration under gentle stirring until solution became transparent.

5.1.2 Rhodamine B diffusion

For diffusion experiment in gelatin gel at 30% wt, gelatin was left to cool at RT in the Ibidi µ-slide well (9.4×10.7×6.8 mm). After gelation, half sample was removed with a knife, and replaced with Rhodamine B solution (200 µl) at a concentration of 0.01 mg/ml. Sample was kept sealed in order to prevent water evaporation, and positioned

under the confocal microscopy (Zeiss, LSM Pascal). Images inside the gel (starting from the interface with water solution) were acquired at time intervals of 1 min for 1 h with a 20x objective and with an excitation by a He-Ne laser at 543 nm. With the same procedure two experiments were carried out, one to observe and measure swelling of the interface due to the Rhodamine B solution and another to follow diffusion of the fluorescent molecule in the gelatin network. Images were then analyzed with Image Pro Plus® 6.0 in order to measure swelling and molecule concentration.

For swelling measurements, the increasing distance of the interface from the initial position was measured and swelling defined in percentage as ratio between final and initial position (L_t/L_0).

For diffusion measurements, after 1 h, consecutive images in the gelatin sample were manually acquired until fluorescent signal was almost zero. Resulting intensity data were fitted with Equation 9 and the diffusion coefficient estimated as mean of a triplicate of experiments.

5.1.3 Swelling ratio

Gelatin solutions at different concentrations, specifically at 10, 15, 20 and 30% wt were prepared as previously described. Solutions were then transferred in a glass mold (25×15×1 mm) until complete gelation. Being the gelation time dependent on the polymer concentration, a conservative time of 1 h was waited for all samples. The mold was used to assure the same dimensions of the specimens. All samples were then completely soaked in aqueous buffer for 72 h. A thin layer of mineral oil (Sigma-Aldrich) was applied on the bottom of the reservoir in order to avoid gel sticking. At different time intervals, samples were collected and weighted. A filter paper was used before each weight in order to remove the excess water. SR was estimated by the following formula:

$$SR\% = \left(\frac{W_t - W_0}{W_0}\right) \times 100 \qquad \textit{Equation 11}$$

where W_t is the weight of the swollen gel at time t and W_0 is the initial weight of the sample. SR for all samples of gelatin was then plotted as function of the time.

5.1.4 NMR measurements

For NMR investigations about the role of polymer concentration, gelatin solutions at different concentrations in the range 10-30% wt were directly injected in the NMR tube (4 mm) and allowed to gel, avoiding formation of air bubbles. To study the swelling effect, instead, small cylinder punches with 2 mm diameter and 3 cm length of a 30% gelatin were allowed to swell in an aqueous buffer. Samples were collected at different swelling times, specifically after 2, 5, 8, 21, 24, 48, and 72 h, and gently inserted in the NMR tubes.

All the NMR experiments were performed at RT on a Bruker Biospin DMX 300 operating at a ^{1}H frequency of 300.13 MHz using a Bruker Biospin Diff-30 diffusion probe capable of producing magnetic field gradient pulses up to 11.76 T m^{-1}. NMR T_1 relaxation times were measured using the standard inversion recovery pulse sequence [142]. The T_1 relaxation time constant was obtained by fitting the experimental data on the NMR signal intensity as a function of the time delay, $S(t)$, to the equation [142]:

$$S(t) = S_0 \left[1 - 2\exp\left(-\frac{t}{T_1}\right)\right] \qquad \textit{Equation 12}$$

^{1}H PFG NMR diffusion measurements were performed using the alternating pulsed gradient stimulated echo (APGSTE) sequence [143] in order to minimize the effects of background magnetic field gradients. The measurements were carried out holding the gradient pulse duration, δ, constant and varying the magnetic field gradient strength, g. The gradient pulse duration, δ, was set to 1 ms. For each sample, the observation time, Δ, was varied from 20 to 1600 ms. Values of the diffusion coefficient, D, were obtained by fitting the PFG NMR experimental data to the expression [144]:

$$\frac{E(g)}{E_0} = exp[-D\gamma^2 g^2 \delta^2 (\Delta - \delta/3)] \qquad \textit{Equation 13}$$

where $E(g)$ and E_0 are the NMR echo signal intensity in the presence and absence of magnetic field gradient, respectively.

5.1.5 Effect of solid particles diffusion

In order to investigate possible changes in gelatin structure due to the penetration of solid particles, gelatin samples were probed by CLSM and NMR.

For CLSM experiments, fluorescent polystyrene particles of 0.1 μm (Polyscience) and 1 μm (Sigma-Aldrich) were suspended at 1% in aqueous buffer and used to this aim. Gelatin at 30% wt was allowed to gel directly in an Ibidi μ-slide multi-well (9.4×10.7×6.8 mm). As for Rhodamine B diffusion experiment, after gelation, half sample was removed and replaced with particles solution. Samples were kept sealed in order to prevent water evaporation from the solution and drying of the gel. After 24 h images were acquired with a 63x oil immersion objective along the entire gel sample by an inverted Leica TCS SP5 CLSM. Image analysis was carried out using the commercial software Image Pro Plus® 6.0. The density of particles inside the gel were measured by counting manually all particles in the image and dividing this number by the image area in μm^2. This operation was repeated for 11 images at different depths in the sample and the mean density was estimated.

On the other hand, polystyrene particles with diameter of 0.1 μm (Sigma-Aldrich) and 1 μm (Bangs Laboratories, Inc.) were suspended in aqueous buffer at a solid concentration of 1% and subsequently used for NMR experiments. For this purpose, gelatin at 30% wt was prepared directly into the NMR tubes as previously described. After gelation, 200 μL of particles solution was added on the top of the gel and samples were then sealed and kept at RT for 24 h. After this time, excessive solution was removed and the sample analyzed by NMR.

5.1.6 Tension inside gelatin gels during swelling

Possible changes in the tensional state inside gelatin network during swelling were investigated by carrying out two experiments. In the first case, the same experimental set-up presented in 5.1.2 for diffusion experiment was used by acquiring five consecutive images, starting from the interface, each 10 min for a total experiment length of 90 min, under polarized light during water diffusion. To this aim, a system of two polarizing filters aligned parallel to the light beam (45°) was used to have a maximum light

intensity. Once defined polarizing filter position, gelatin sample was rotated of a specific angle until the anisotropy structure was well detectable. A greater mosaic of images was reconstructed after 5 h to have an overview of a bigger field of view inside the sample. Reconstruction of the images was performed with Image Pro-Plus 6.0®. Only qualitative measure of the birefringence signal was conducted by comparing colored-images with the standard Michel-Levy Birefringence Chart, which allows the estimation of the birefringence for sample with a thickness up to 0.06 mm.

In a second experiment, gelatin solution was prepared as described but with a higher stirring, which brought to the formation of air bubbles entrapped in the gelatin network, once gelled. The experimental set-up was always the same. Three bubbles were chosen at increasing distance from the interface with water solution. An inverted optical microscope (Zeiss Axiovert 200) mounted on an anti-vibration table, was used in order to follow bubbles behavior for 24 h. The microscope is provided with a sample table and of a focusing system with both stepper motors, which allow to automatically choose the field of view within the sample. Images were acquired using a monochrome CCD camera (Hamamatsu Orca AG) and sent to a personal computer via Firewire interface. The digital image is made up of a matrix of 1344x1024 pixels. The entire workstation is governed by a controller (Objective Imaging) via computer through a Time-Lapse software that works in Labview environment. Such software enables the periodic scanning of desired areas of one or more samples. As input data a manually selection of the fields of view within the sample were set and the time interval between two consecutive scans chosen. Once started, the program stores the coordinates of the selected fields of view and controls the motorized table in order to acquire and store all data. After each scan, the program remains stopped until the next iteration. Scanned images are saved on the hard disk into separate directories for each selected area. After the experiment, for each field of view, a series of images can be processed to create a sequence which allows to observe the qualitative evolution of the sample over time. In the case of experiments on bubbles behavior during swelling, acquisitions of the three bubbles were made every 5 min. Due to the swelling, it was impossible to determine the distance of the bubbles from the interface with water, so the closest one was chosen as

reference. The remaining two were chosen at a distance of 193 and 2470 μm from it. At the end of the experiment, dissolving time of the bubbles and their areas, always measured with Image Pro-Plus 6.0®, normalized with respect to their initial dimension, were plotted as function of the time and compared in order to relate their behavior with the tensional state inside the gelatin network.

5.2 Results

Diffusion of Rhodamine B solution in a gelatin gel at 30% has been carried out to have a general overview about swelling of the gelatin when in contact with water solutions. At the same time, estimation of the diffusion coefficient of the fluorescent molecule could be a valid reference in order to choose a concentration of the gelatin which better answer to the purpose of BEGs formulation (see chapter 4).

In Figure 5.1 are reported images of the two experiments where different fields of view, one in the Rhodamine B solution (to observe swelling front, Figure 5.1a) and another in the gel (to observe Rhodamine B diffusion, Figure 5.1b) have been acquired for 1 h at time intervals of 1 min.

As visible in Figure 5.1a gelatin front progresses over time suggesting a significant water uptake, which is penetrating in the gelatin network causing its enlargement. Total swelling, estimated in percentage by the ratio between final and initial position (L_t/L_0) , is about 7%. This value is in good agreement with the total swelling of skin cells along the z direction. At the same time, when the attention is focused inside the gelatin network, a fluorescent gradient is clearly visible (Figure 5.1b). After 1 h, consecutive images in the sample have been acquired from the interface till no fluorescence signal is visible (Figure 5.1c). The corresponding intensity profile has been measured, plotted as function of the penetration depth in the gelatin gel and fitted with Equation 9 (Figure 5.1d). The diffusion coefficient obtained as mean of a triplicate of experiments is 1.26×10^{-7} cm^2/s.

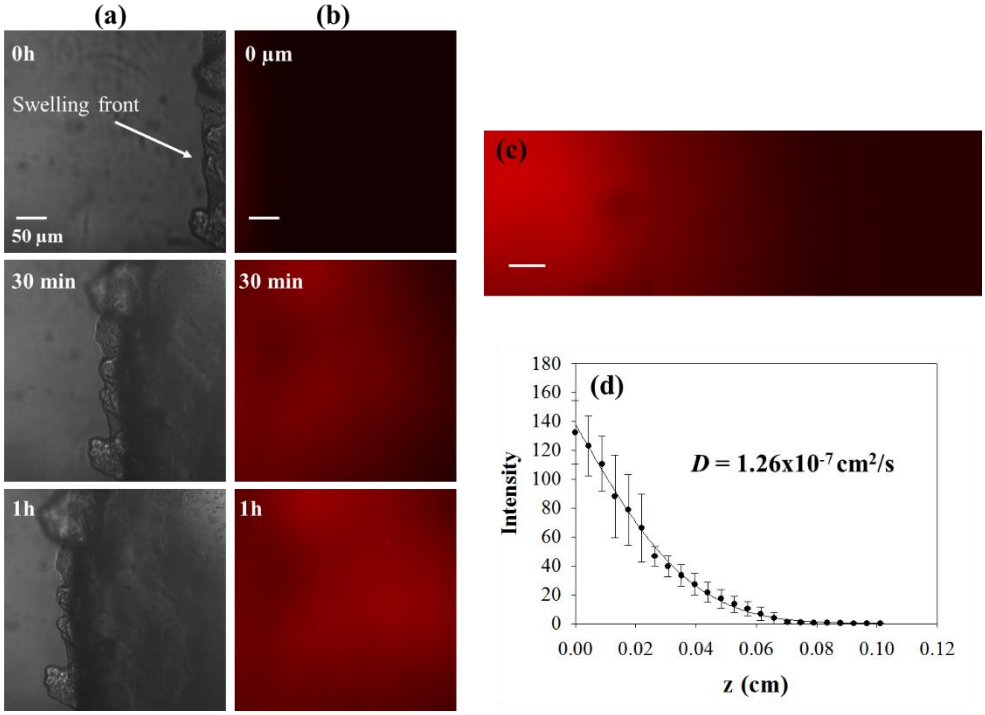

Figure 5.1 – (a) Swelling front of the gelatin interface at the beginning of the experiment, after 30 min and after 1 h.(b) Increasing fluorescent signal of Rhodamine B in the gelatin at fixed z depth at different times. (c) Reconstruction of the fluorescence profile of Rhodamine B in the gelatin at the end of the experiment. (d) Intensity profile as function of the penetration depth in the sample. Experiments have been repeated in triplicate

Unfortunately, the field of view during the experiment is fixed and it is impossible to know how the fluorescent profile evolves at different depths over time. Moreover, it is now clear that simultaneously to the diffusion, gelatin front is moving due to the swelling, in the opposite direction, so the position at $z=0$ as starting point of the diffusion is not properly correct. However, once measured at the equilibrium the swelling of the interface, or by acquiring images as in Figure 5.1c, it could be possible a correction of the diffusion data. This approach could be an efficient alternative to the proposed experimental set-up presented in 3.1.5. to follow molecules during their diffusion in a system, which could be tuned as desired. It is obvious that this set-up is favorable in the case of samples which can be prepared directly in the well, guaranteeing a perfect adhesion to the well walls and avoiding later diffusion of the solution. BEGs samples,

for example, are instead more suitable candidates for the previous set-up since they are inserted in the O-ring after gelation is completed.

The SR of gelatin gels at concentration in the range 10-30% has been reported in Figure 5.2. Results indicate that gel at lower concentrations adsorb more water compared to samples where polymer concentration is higher. Moreover, it is clear that at short times, above 2 h, swelling rate is very fast, then it slows until reaching the equilibrium. It is interesting to note that for all samples there is a slight drop down of the SR, more pronounced for 10% and 15% gelatin around 24 h. For higher concentrations, the same behavior is observed at longer times.

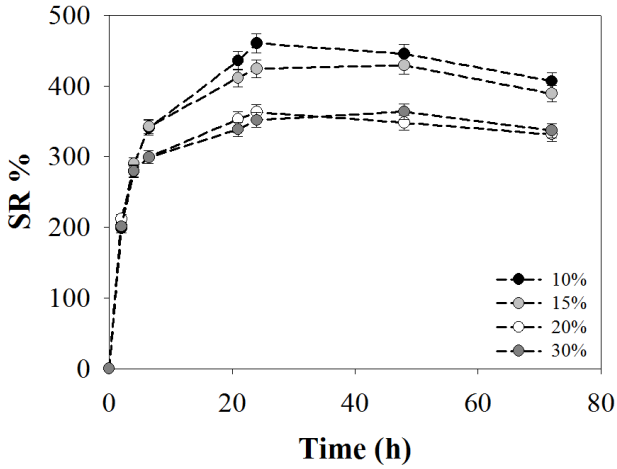

Figure 5.2 – SR of gelatin gels at different concentrations. After a first initial increase, a slow down is visible until a plateau. A slight decrease from the plateau value is detectable for all samples at different times. Taken from [141]

Figure 5.3 shows typical T_1 inversion recovery (Figure 5.3a) and PFG log attenuation plots (Figure 5.3b) of water in the presence of different gelatin concentrations. The plots clearly show significant changes of relaxation and diffusion properties of water as the gelatin concentration increases.

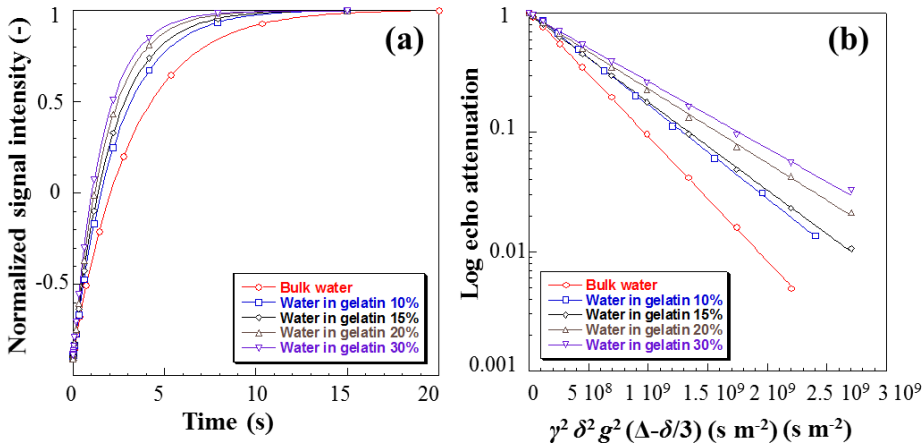

Figure 5.3 - (a) T_1 inversion recovery and (b) PFG log attenuation plots of water in the presence of different gelatin concentrations. Solid lines are fitting to: (a) Equation 12 and (b) Equation 13. Taken from [141]

From the data in Figure 5.3 it is possible to evaluate the values of the T_1 relaxation time and self-diffusion coefficient, D, of water as a function of gelatin concentration, which are reported in Figure 5.4. It is clear that by increasing polymer concentration, both the T_1 and D values decrease, suggesting a reduced rotational and translational dynamics of water molecules as more gel is added.

More in detail, T_1 can be written as:

$$\frac{1}{T_1} = \frac{1}{T_{1,bulk}} + \frac{S}{V}\rho_1 \qquad \textit{Equation 14}$$

where $T_{1,bulk}$ is the relaxation rate of the bulk fluid and is a constant at fixed temperature, ρ_1 is the surface relaxivity, depending on the material and in this case can be assumed to be constant, and S/V is the surface-to-volume ratio of the gelatin structure. Therefore, a decrease in T_1, that is, an increase of the $1/T_1$ relaxation rate, implies an increase of S/V.

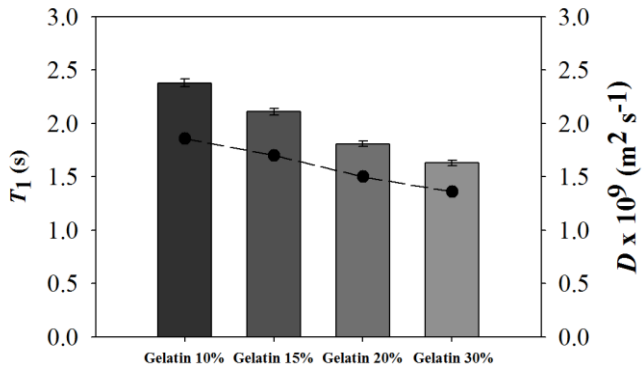

Figure 5.4 - T_1 relaxation time (columns) and self-diffusion coefficient D (circles) of water inside gelatin with different polymer concentration. Dashed line is a guide to the eye. Taken from [141]

Behavior of water inside the gelatin structure has been investigated at different observation times, in particular at 20, 200, 800 and 1600 ms. Already after 20 ms water molecules experience the presence of the gelatin network, for all gelatin concentrations, showing a self- diffusion coefficient from 1.89×10^{-9} m^2 s^{-1} for 10% gelatin to 1.4×10^{-9} m^2 s^{-1} for 30% gelatin, values lower than the bulk water, which is 2.35×10^{-9} m^2 s^{-1}. For this independence from the observation times, for all other analysis, *D* values at 200 ms have been considered.

In order to better investigate the role of gelatin concentration on its internal structure, two other parameters have been defined:

$$\eta = \frac{T_{1,bulk}}{T_{1,pore}} \qquad \textit{Equation 15}$$

$$\xi = \frac{D_{bulk}}{D_{pore}} \qquad \textit{Equation 16}$$

The η parameter is representative of the reduction of the rotational dynamics of molecules within the pore network compared to the bulk [145]. The parameter ξ is the so-called PFG interaction parameters [145, 146] which indicates the extent to which translational dynamics of molecules within the pore network is reduced relative to the

bulk and can be considered a measure of the apparent tortuosity experienced by water molecules diffusing within the pore network. These parameters are equal to one, when fluid molecules behave such in the bulk, while increase when slower molecular dynamics are present. Values of these parameters for gelatin samples at four different concentrations are reported in Figure 5.5.

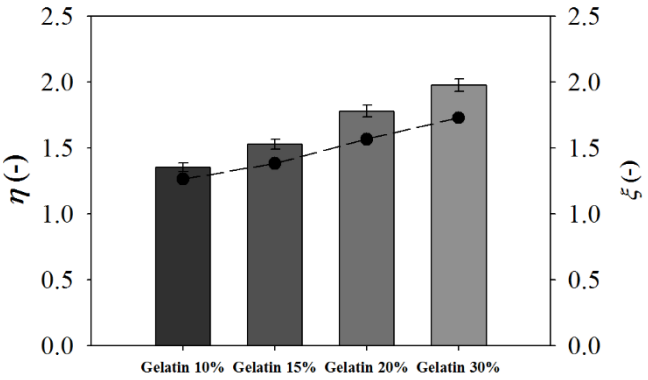

Figure 5.5 - Values of η (columns) and ξ (circles) parameters of water in gelatin with different polymer concentrations. Taken from [141]

The increase of both parameters relative to bulk water, suggests a reduced rotational dynamics of water inside the gelatin due to an increase to surface-to-volume ratio in the pore or to a possible reduction of pore dimension in consequence of an increased polymer concentration. Moreover, the increasing value of ξ suggests a higher tortuosity that is a more complex connection of the pores.

Once investigated the role of the polymer concentration it is interesting to evaluate possible changes in molecular dynamics of the water inside the gelatin at different swelling times. To this aim the gelatin sample at 30% has been used. Results of T_1 and D are reported in Figure 5.6a. Similar to the trend observed for the SR both, T_1 and D, show a rapid increase during the first 5 h, reaching a value almost constant between 20 and 40 h, before to drop slightly. As explained for the SR, these results suggest a possible increase in the average pores size with a reduction of S/V showing a molecular dynamics closer to that of the bulk water (T_1 = 3.22 s and $D = 2.35\times10^{-9}$ m^2 s^{-1}). This behavior is also confirmed by the trends of η and ξ in Figure 5.6b that decrease quickly

approaching to one, which corresponds to the free bulk water value. It is possible to note that towards the end of the experiment values tend to increase again, suggesting the possible relaxation of the gelatin network due to an excess swelling.

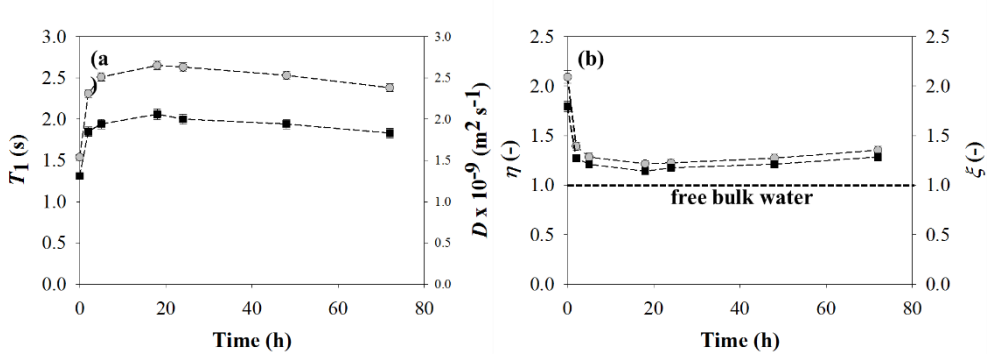

Figure 5.6 – (a) T_1 relaxation time (grey) and self-diffusion coefficient D (black) of water inside gelatin at 30% wt at different swelling times. (b) Values of η (grey) and ξ (black) parameters of water in gelatin at different swelling times. Taken from [141]

It is interesting to note a good agreement between macroscopic studies (SR) and microscopic investigations (NMR) on the same gelatin sample, but even on samples prepared in different batches with a good reproducibility of the results.

Since gelatin gel is one of the most common ingredients used in biomedical applications, and also for our purpose to mimic the SC, hence interacting with external formulations it could be interesting to investigate possible structural changes when the system enters in contact with external polymeric particles. A similar approach can be useful to mimic the behaviour of polymeric particles when used as carriers for active principles during drug-loaded gels and delivery, the latter dependent on the degree and rate of swelling as well as on gelatin concentration and gelatin-particles interaction.

To this aim NMR and CLSM investigations have been carried out on gelatin gel at 30% after 24 h of polystyrene particles diffusion. The objective has been to understand how the gelatin network responds to the penetration of particles with diameters much larger than its pores. The results for T_1 relaxation times and self-diffusion coefficients, D, of water and the corresponding η and ξ parameters measured by NMR after particles (no-fluorescent) diffusion are reported in Figure 5.7a-b.

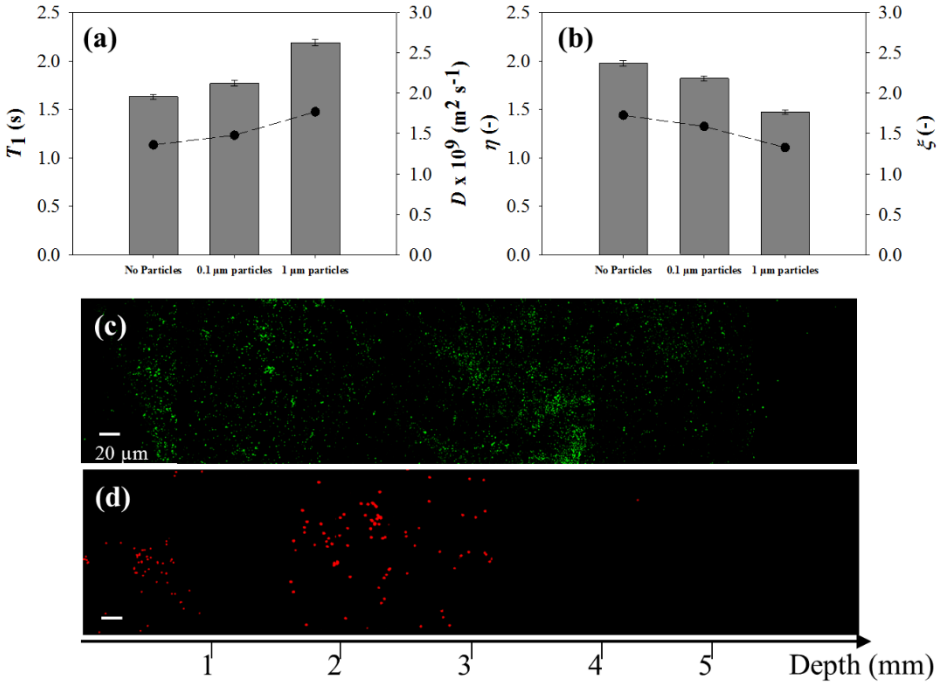

Figure 5.7 – T_1 relaxation time (columns) and self-diffusion coefficient D (circles) (a) and η (columns) and ξ (circles) parameters (b) of water inside gelatin after 24 h penetration of polystyrene particles of 0.1 and 1 µm diameters. (c) CLSM reconstruction of the penetration path of 0.1 µm particles (green) and 1 µm particles (red) in gelatin gel 30% after 24 h. Taken from [141]

It is evident from the histograms that both particles have a strong effect on the gelatin network compared to the sample without particles. In particular, larger particles show higher values of T_1 and D closer to that of bulk water. Consequently, decreasing values of η and ξ tend to approach to one. This results suggest that larger particles can pass through larger pores in the network, which is highly dis-homogeneous, or that particles affect more the gelatin structure, probably improving pores connectivity. It is indeed conceivable that larger particles cause significant alteration in the network, as also demonstrated by CLSM images. A complete reconstruction of the penetration paths of particles after 24 h of penetration, shows a difference between 0.1 and 1 µm particles behavior. More in detail, 0.1 µm particles are able to penetrate through the entire gel sample up to a distance from the interface of about 5-6 mm. The distribution of the particles in not uniform and in certain points it seems to accumulate in large number.

Contrariwise, 1 μm particles do not reach the second interface of the sample, and stop their penetration almost soon. It is possible that they can exploit larger pores create as consequence of the gel swelling, but at the equilibrium they do not have enough force to continue their penetration. Moreover, a possible creation of a stress around them due to the convective transport in water during the swelling can also contribute to further modification in the structure. Here, again the distribution is not uniform. Density is very different between the two samples, being 0.04 and 0.01 for 0.1 μm and 1 μm particles. It is worth mentioning that these results could suggest a helpful method to improve the drug-loaded and delivery of particles from gelatin, where one of the main problem is the formation of aggregates able to affect the stability of the whole systems. Here, as also reported in Figure 5.7 no clusters or aggregates formation is highlighted in either NMR or CLSM experiments. Anyhow, this does not represent the main goal of the present work.

In order to complete the characterization of the gelatin structure modification, the average pore size has been estimated for different gelatin concentrations and for different swelling times by assuming pores of cylindrical shape and by using the Equation 14 modified in the following formula:

$$\frac{1}{T_1} = \frac{1}{T_{1,bulk}} + \frac{4}{d}\rho_1 \qquad \textit{Equation 17}$$

where d is the average pore diameter. It has been possible to estimate the surface relaxivity ρ_1 from *Equation 17* by using T_1 value, estimated experimentally, and the pore diameter for a 10% gelatin of 20 nm, known from literature [97]. Results gives a $\rho_1 \approx 5.5\text{x}10^{-4}$ μm s^{-1}. Once known the surface relativity it has been easy to estimate the average pore size for samples at different concentrations of gelatin and for a 30% gelatin at different swelling times (Figure 5.8a-b).

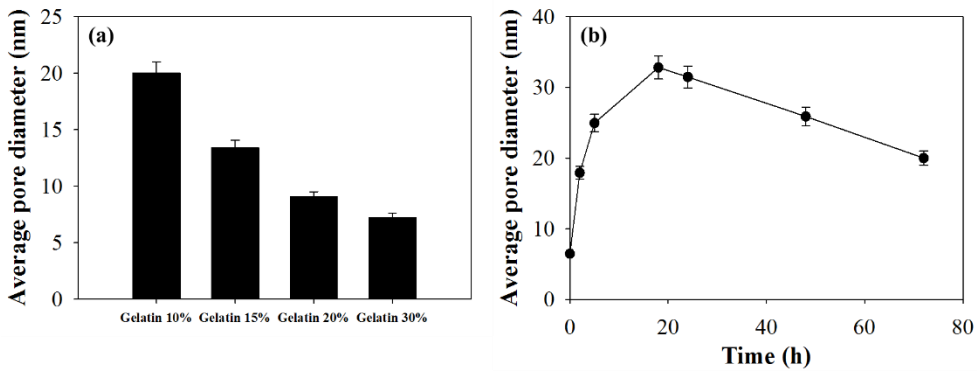

Figure 5.8 – Average pore diameter as function of gelatin concentration (a) and for gelatin 30% wt as function of the swelling times (b). Taken from [141]

It is clear that to an increase in the polymer concentration corresponds a strong reduction in the pore dimension, reaching a value of about 7 nm for a 30% gelatin. The values are in good agreement with results from literature for similar samples which range from tens of nm down to a few nm [147] [148]. In Figure 5.8b it is evident an increase of the pore dimension as the swelling proceeds reaching a maximum of 32 nm after 24 h, then a net decrease starts reaching 20 nm after 72 h. Indeed, it is interesting to note that this behavior is consistent with the trend observed for the SR and other NMR investigations, which underlines the importance of this possible relaxation of the network which cause a reduction of the pore size. Moreover, this aspect, to our knowledge, has never been reported yet in literature. For this reason further analysis may be needed to validate the result.

Another important aspect to consider is the distribution of the tensions inside the gelatin network. In particular, considering the deep study carried out on the alteration of the structure due to the swelling, the distribution of the tension inside the gelatin during water uptake results of significant importance. To this aim, an experiment with the same set-up presented in 5.1.2 has been carried out, acquiring images under polarized light during water diffusion. The experiment length was 1.30 h with acquisitions at time intervals of 10 min. As visible from Figure 5.9, when water is not yet in contact with gelatin, at 0 min, the sample shows a slight birefringence only in close proximity of the interface.

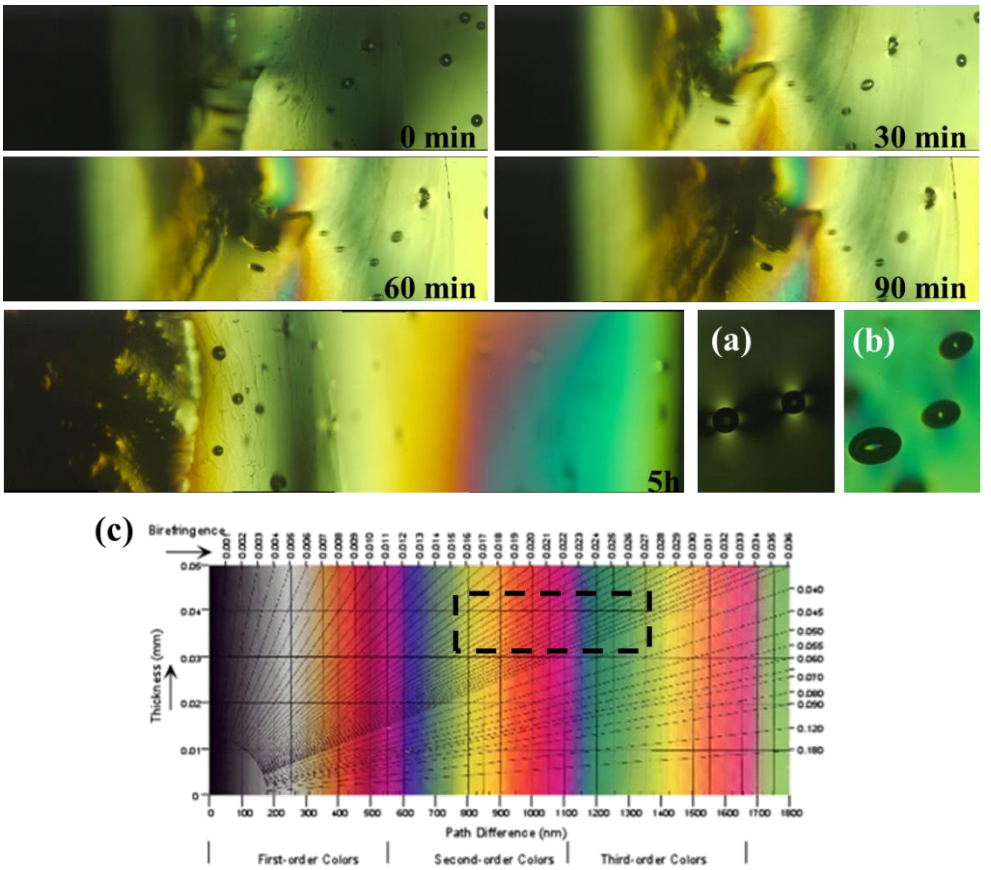

Figure 5.9 – Birefringence images of gelatin gel at 30% wt during swelling at different times. Mosaic images show the whole birefringence distribution in the gelatin after 5 h. Birefringence around air bubbles interface before swelling (a) and after 5 h (b). Michel-Levy Birefringence Chart (c). The birefringence trend in the dotted square is the same in the gelatin gel after 5 h

Already after 30 min, it is possible to note that different birefringence signal, to which corresponds a different and brighter color, is detectable, starting from the interface toward the inner gel. This situation continues and increases at 60 and 90 min showing a more pronounced signal. After 5 h a mosaic of images of the gel has been reconstructed to have an overview of the situation. Here, it is clear that a distribution of the tensional state, that is, a color distribution from grey to green is well defined. As qualitative measure, a comparison with the Michel-Levy Birefringence Chart (Figure 5.9c) allows to identify the same color distribution. However, value of birefringence obtainable from the chart are only for sample thickness up to 0.06 mm, while gelatin sample has a thickness of about 50 mm. Although this difference, a perfect overlap of the

birefringence distribution, is clear. This result suggests, as also demonstrated by NMR measures that the swelling induces a change not only of the structure (pores dimension, tortuosity, etc.) but also of the tension in the gelatin network. All these aspects have to be considered if gelatin has to be used as model system to mimic desired properties.

It is also interesting to note what happens when air bubbles are present in the gel. They can be easily formed during stirring of the gelatin solution. Microscopically, around them, it is possible to observe a birefringence signal, probably due to the curvature, where a change in the tensional state of the gelatin network is localized (Figure 5.9a). During swelling, birefringence around bubbles changes, as visible form the change in color in Figure 5.9b, which becomes more uniform, while bubbles deform in the direction of swelling.

In order to better understand the role of the tension in the gelatin sample, three bubbles have been followed with a Time-Lapse microscope, which allows to choose different fields of view and to record them over time in an automated way. Bubbles with a similar area have been chosen at different distances from the interface and followed for 24 h with acquisition every 5 min. A schematic representation of the experiment is reported in Figure 5.10.

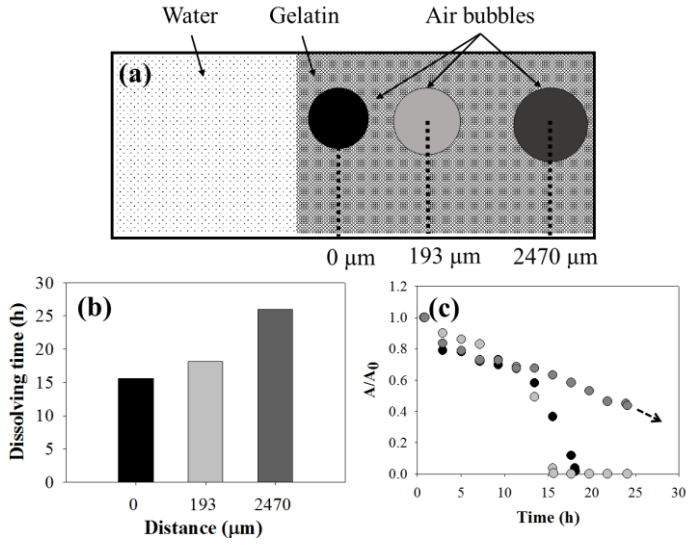

Figure 5.10 – (a) Schematization of the experimental set-up, (b) Dissolving time of air bubbles as function of the distance from the interface. The air bubble closest to the interface is the reference point to measure distance of other bubbles. (c) Normalized area of air bubbles as function of the time. Bubble far from the gelatin interface does not dissolve in 24 h

Sequences created by all acquired images suggest that, depending on the distance from the interface, air bubbles are initially pushed in the opposite direction of the swelling, probably due to the advancing water front, and then start to deform and move in the swelling direction. Deformation continues until a change in the tension, related to the external and/or internal pressure, leads to a dissolution of the bubbles. This could also be due to the enlargement of the network which reduces the tension on the bubble interface. The time necessary for bubble dissolution in reported in the histogram (Figure 5.10b) where it is clear that bubble far from the interface dissolves later compared to the closest one. As consequence, the bubbles area, normalized compared to their initial dimension, plotted as function of the time, show that only the bubble at a distance of 2470 μm, after 24 h has not still dissolved, requiring more time. The other bubbles tend to zero already after 10 h (Figure 5.10c). This behavior seems to be directly related to the tensional state, which changes during water adsorption affecting the entire network. This aspect results once again of significant interest, for example, when gelatin is used to encapsulate drugs, which could be affected by possible internal structure changes during swelling once introduced in the organism.

5.3 Conclusions

Despite the large applications of gelatin gel in many different fields, a complete overview on its structure and the related mechanisms that can be cause of its alteration is not totally elucidated. A combination of NMR, CLSM and birefringence studies can highlight new insights in the modification of gelatin structure induced by swelling or solid particles penetration. SR measurements revealed for all the concentrations evaluated, a rapid water uptake in the first hours before to reach a plateau value, which then slightly drops maybe due to a relaxation of the network caused by an excess water. Moreover, lower is the polymer concentration, faster and higher is the SR. Changes in the gelatin network have been also confirmed by NMR on gelatin samples at concentrations in the range 10-30%. In particular, at higher concentrations relaxation time T_1 and self-diffusion coefficient of water, D, have been far from values of the free bulk water suggesting that water molecules are strongly affected by the hindrance of the network. An increase in the tortuosity and a reduction of the pore size can also be

possible explanation of this result. Concerning the effect of the swelling times on gelatin at 30% it has been interesting to observe that the water uptake causes an enlargement of the pores which corresponds to a T_1 and a D that increase approaching the values of the bulk water. An improved pores connectivity has been also assessed. However, at longer times the shrinkage of the structure is confirmed by a slight increase of the investigated parameters, in agreement with SR measurements. Further structure alterations have been demonstrated by NMR and CLSM by analyzing 30% gelatin sample after 24 h of solid particles penetration of 0.1 and 1 μm. Results suggest that larger particles alter more the gelatin network improving pores connectivity. Although the gelatin structure is highly heterogeneous the number of pores with diameter comparable to that of larger particles are few, justifying the low density of 1 μm particles compared to 0.1 μm particles. Finally, the average pore size has been estimated in the range of 7-21 nm for gelatin samples at a concentration from 10% to 30%, in agreement with similar systems in literature. In addition, qualitative evaluation of a tension distribution in the gelatin sample carried out by birefringence has demonstrated a clear distribution of the tension during the swelling. As expected, the closer is the interface with water, higher is the tensional state, as also shown by experiments with air bubbles. Such knowledge can be of importance for many applications where gelatin is involved, but in particular it can represent the base on which to define the optimal gelatin parameters for BEGs formulations and successive good skin mimicking.

6 Conclusions and future works

In this work, transdermal drug delivery has been presented as one of the main routes of administration for cosmetic and pharmaceutic active principles, and as a valid alternative to the traditional routes of drug administration such as oral or parenteral delivery. However, one of the main problems when active principles are released through the skin is to overcome the skin barrier. Skin, in fact, is a highly complex stratified structure, whose morphology can vary depending on the body site, aging and sex. The outer layer of the skin, the *stratum corneum*, SC, represents the main barrier to the penetration of the external compounds. A general overview about the standard methods or techniques used so far for the investigation of penetration process through the skin, as well as the optimization of the carriers to improve drug penetration, have highlighted several limits such as the impossibility to have both qualitative and quantitative information in one time as well as the lack of a deep comprehension about the interaction between skin components and formulation ingredients.

Here, an innovative experimental set-up based on CLSM and images analysis has been presented aimed to the investigation of the penetration process through the skin. Before the validation of the experimental set-up, a wide study on the possibility to use immunofluorescence technique to localize specific molecules in O/W emulsions has been carried out. A specific antibody, TEPC-15 has been chosen to localize, phosphatidylcholine, PC, commonly used as natural surfactant in cosmetic of pharmaceutical formulations. Protocols have been adapted to the requirements. Staining efficiency has been tested on two cell lines and in presence of other phospholipids. The presence of other molecules, in particular proteins, can induce the formation of complex molecular interactions at the interface of oil droplets which can seriously affect the antibody staining. A threshold equal to 0.07% wt of proteins has been identified to affect the staining procedure. Similar results have been obtained on PC coating. To our knowledge, this is the first time that immunofluorescence is applied to colloidal systems. This approach can be helpful in the staining of specific molecules whose penetration

through the skin can be followed, by allowing a better understanding about pathways and interactions with skin components.

Validation of the set-up has been carried out by diffusion experiments of fluorescent molecules, Rhodamine B and Nile red, in solution or in O/W emulsions, in a model system based on agarose gel. The latter has been chosen only for the easy preparation and low cost, while the two dyes have been chosen for the different properties of hydrophilicity and hydrophobicity in order to mimic properties of different drugs. In such a way, it has been possible to understand the different diffusion behaviour of the molecules depending on their own properties and the affinity with the medium in which they diffuse. Results of the diffusion experiments have been obtained after 2 h of z-stack images acquisitions inside the agarose sample, and from successive images analysis and data fitting with a particular solution of Fick's law based on our experimental conditions. It has been found that the diffusion coefficient of Rhodamine B and Nile red differ from three order of magnitude, due to their different properties. However, the O/W emulsion has shown an enhancer effect compared to the pure oil solution, suggesting an important role of the formulation microstructure, which is not totally clear from literature. Preliminary diffusion experiments in skin biopsies have also been reported. In this case the affinity between diffusing oil solution and lipid matrix in the SC have shown the intercellular route as main path for the penetration of hydrophobic molecules. It is worth mentioning the difficulties to work with biological samples which requires great attention for manage them and for their maintenance.

Moreover, in order to overcome the problem of skin biopsies availability or the high costs of synthetic membranes, Bicontinuous Emulsion Gels (BEGs) have been presented as model system based on a tuneable soft material to mimic SC structure and/or properties. To this aim, gelatin gel and sunflower oil (with the addition of surfactants or cross-linkers) have been used respectively as hydrophilic and hydrophobic phases to mimic skin cells and lipid matrix of the SC. Contrary to agarose gel, gelatin undergoes a fast swelling when in contact with water, as happens for skin cells. Different formulations have been tested and corresponding morphologies investigated by CLSM, by staining one of the two phases. Among all the samples prepared, only the sample with

a gelatin/oil ratio of 45/55 and a combination of two surfactants, Tween 20 and Span 80, together with a cross-linker, Myverol 18-04K is able to produce an internal bicontinuous structure, similar to that of SC. However, gelatin/oil ratio is still far from the real case and the stability of the system requires further investigations due to the continuative evolution of the gelatin, which tends to coalesce, even after gelation is completed.

For this reason a deep investigation about the behaviour of gelatin gel and its structure-related mechanisms, in particular during the swelling, has been carried out by CLSM, NMR and optical birefringence. The SR has been calculated from a wide range of gelatin concentrations, showing a higher swelling effect for lower concentrations. Equilibrium value drops down slightly for all samples, suggesting a possible weakness of the gelatin structure maybe due to an excess of water. NMR investigations on the molecular dynamics of water molecules in the sample, have confirmed that by increasing gelatin concentration, water molecules experience the network hindrance causing a subsequent increase in the porosity and tortuosity of the network. On the other hand, when gelatin sample in affected by swelling, water mass transfer is facilitated approaching to a free bulk water behaviour. Therefore, a dis-homogenous structure is expected as demonstrated by NMR and CLSM investigation on gelatin sample at 30% after particles diffusion with diameters much larger than pores size. 1 μm particles are able to penetrate remodelling the network by forming larger pores or by exploring existing great ones, which are fewer compared to 0.1 μm particles able to penetrate the whole gel. Finally, a possible tension distribution in the gelatin network during swelling has been qualitatively demonstrated by birefringence images. Different colours distribution, that is a tensions distribution, is clear starting from the interface between gelatin and water solution toward the inner core of the gel, where the effect of the swelling is delayed.

Future works will be oriented to the improvement of the BEGs formulation, in order to tune properties and to improve similarity with skin structure. To this aim, rheological and mechanical tests could be also very helpful. By this way, diffusion experiments in BEGs will be performed and compared with results in synthetic membranes or skin biopsies. The easy preparation and the low cost of the BEGs could represent a real improvement in the investigation about the interaction between formulations and skin

components. By this way, it will be also possible to optimize formulation, or drug carriers, improving the whole penetration efficiency.

Appendix A

In this appendix, a Matlab macro with comments to the code is listed. The macro can be run in the Matlab "Command Window".

```
D= 2e-7; %Diffusion coefficient value in cm^2/s
x=linspace (0,0.06,100); %Distance in cm, range of interest
0.06 cm, step 10 µm(10^-3 cm)
t=5000; % Time in seconds
h=0.01; % half-depth of the reservoir in cm
l=0.1 % gel thickness in cm

for j = 1:length(x)
     c2(j)=0.5*(erf((x(j)+h)/(2*(D*t)^0.5))+erf((-
x(j)+h)/(2*(D*t)^0.5)));
     end;

c3=zeros(1,length(x));

for n = 0:100 % number of iterations
 for k = 1:length(x)
 c3(k)=c3(k)+0.5*(erf((-
x(k)+h+2*n*l)/(2*(D*t)^0.5))+erf((x(k)+h-
2*n*l)/(2*(D*t)^0.5)));
 end
end

for i=1:length(x)
    s(i)=(c3(i)-c2(i))^2;
end
s2=(sum(s)/length(x))^0.5 % mean square error

plot (x,c2); %plot of the equation(7)

hold on

plot (x,c3,'r') % plot of the equation(9)

hold on
plot (x,c4,'r') % plot of the equation(10)
```

Bibliography

[1] R. Liuzzi, A. Carciati, S. Guido, S. Caserta, Transport efficiency in transdermal drug delivery: What is the role of fluid microstructure?, Colloids and Surfaces B: Biointerfaces, 139 (2016) 294-305.
[2] B. Wang, L. Hu, T.J. Siahaan, Drug delivery: principles and applications, John Wiley & Sons, (2016).
[3] A. Kogan, N. Garti, Microemulsions as transdermal drug delivery vehicles, Advances in colloid and interface science, 123 (2006) 369-385.
[4] M.R. Prausnitz, R. Langer, Transdermal drug delivery, Nature biotechnology, 26 (2008) 1261-1268.
[5] H. Marwah, T. Garg, A.K. Goyal, G. Rath, Permeation enhancer strategies in transdermal drug delivery, Drug delivery, 23 (2016) 564-578.
[6] R. Gupta, Transdermal Drug Delivery System, 3 (2014) 375-394.
[7] M.R. Prausnitz, Microneedles for transdermal drug delivery, Advanced drug delivery reviews, 56 (2004) 581-587.
[8] M. Foldvari, Non-invasive administration of drugs through the skin: challenges in delivery system design, Pharmaceutical science & technology today, 3 (2000) 417-425.
[9] Z. Ya-Xian, T. Suetake, H. Tagami, Number of cell layers of the stratum corneum in normal skin–relationship to the anatomical location on the body, age, sex and physical parameters, Archives of dermatological research, 291 (1999) 555-559.
[10] S. Mine, N.O. Fortunel, H. Pageon, D. Asselineau, Aging alters functionally human dermal papillary fibroblasts but not reticular fibroblasts: a new view of skin morphogenesis and aging, PLoS One, 3 (2008) e4066.
[11] M. Förster, M.A. Bolzinger, H. Fessi, S. Briançon, Topical delivery of cosmetics and drugs. Molecular aspects of percutaneous absorption and delivery, European Journal of Dermatology, 19 (2009) 309-323.
[12] M.R. Prausnitz, S. Mitragotri, R. Langer, Current status and future potential of transdermal drug delivery, Nature Reviews Drug Discovery, 3 (2004) 115-124.
[13] N. Monteiro, A. Martins, R.L. Reis, N.M. Neves, Liposomes in tissue engineering and regenerative medicine, Journal of The Royal Society Interface, 11 (2014) 20140459.
[14] S.S. Dudhamal, V. Khadkutkar, M. Bhange, An Advanced Nanotechnology for cancer therapy: a review, World Journal of Pharmaceutical Research , 4 (2015) 668-686.
[15] Y. Zhai, R. Xu, Y. Wang, J. Liu, Z. Wang, G. Zhai, Ethosomes for skin delivery of ropivacaine: preparation, characterization and ex vivo penetration properties, Journal of liposome research, 25.4 (2015) 316-324.
[16] Z. Zhang, Y. Wo, Y. Zhang, D. Wang, R. He, H. Chen, D. Cui, In vitro study of ethosome penetration in human skin and hypertrophic scar tissue, Nanomedicine: Nanotechnology, Biology and Medicine, 8 (2012) 1026-1033.
[17] H. Schreier, J. Bouwstra, Liposomes and niosomes as topical drug carriers: dermal and transdermal drug delivery, Journal of controlled release, 30 (1994) 1-15.
[18] V. Mohanraj, Y. Chen, Nanoparticles–a review, Tropical Journal of Pharmaceutical Research, 5 (2006) 561-573.
[19] A. Patzelt, J. Lademann, The Increasing Importance of the Hair Follicle Route in Dermal and Transdermal Drug Delivery, in: Percutaneous Penetration Enhancers Chemical Methods in Penetration Enhancement, Springer, (2015), 43-53.
[20] F. Knorr, J. Lademann, A. Patzelt, W. Sterry, U. Blume-Peytavi, A. Vogt, Follicular transport route–research progress and future perspectives, European Journal of Pharmaceutics and Biopharmaceutics, 71 (2009) 173-180.
[21] M. Kreilgaard, Influence of microemulsions on cutaneous drug delivery, Advanced Drug Delivery Reviews, 54 (2002) S77-S98.
[22] J. Zhang, B. Michniak-Kohn, Investigation of microemulsion microstructures and their relationship to transdermal permeation of model drugs: ketoprofen, lidocaine, and caffeine, International journal of pharmaceutics, 421 (2011) 34-44.

[23] Y. Zheng, W.Q. Ouyang, Y.P. Wei, S.F. Syed, C.S. Hao, B.Z. Wang, Y.H. Shang, effects of carbopol® 934 proportion on nanoemulsion gel for topical and transdermal drug delivery: a skin permeation study, International Journal of Nanomedicine, 11 (2016) 5971.
[24] O.A. Bamisaye, O.C. Eromosele, E. Dare, Development of Oil In Water Nanoemulsion Formulations for Spontaneous Transdermal Delivery of Drugs, (2016).
[25] A.C. Williams, B.W. Barry, Penetration enhancers, Advanced drug delivery reviews, 64 (2012) 128-137.
[26] L.B. Lopes, Overcoming the cutaneous barrier with microemulsions, Pharmaceutics, 6 (2014) 52-77.
[27] K.R. Pawar, R.J. Babu, Lipid Materials for Topical and Transdermal Delivery of Nanoemulsions, 31 (2014) 429-458.
[28] M.E. Lane, Skin penetration enhancers, International journal of pharmaceutics, 447 (2013) 12-21.
[29] M. Manconi, C. Caddeo, C. Sinico, D. Valenti, M. Mostallino, S. Lampis, M. Monduzzi, A. Fadda, Penetration enhancer-containing vesicles: composition dependence of structural features and skin penetration ability, European Journal of Pharmaceutics and Biopharmaceutics, 82 (2012) 352-359.
[30] OECD, in: Guideline for the Testing of Chemicals, Guideline 428, OECD, Paris (2004).
[31] OECD, in: Guideline for the Testing of Chemicals, Guideline 427, OECD, Paris (2004).
[32] F. Netzlaff, C.M. Lehr, P. Wertz, U. Schaefer, The human epidermis models EpiSkin®, SkinEthic® and EpiDerm®: an evaluation of morphology and their suitability for testing phototoxicity, irritancy, corrosivity, and substance transport, European Journal of Pharmaceutics and Biopharmaceutics, 60 (2005) 167-178.
[33] F. Netzlaff, M. Kaca, U. Bock, E. Haltner-Ukomadu, P. Meiers, C.M. Lehr, U.F. Schaefer, Permeability of the reconstructed human epidermis model Episkin® in comparison to various human skin preparations, European Journal of Pharmaceutics and Biopharmaceutics, 66 (2007) 127-134.
[34] T. Uchida, W.R. Kadhum, S. Kanai, H. Todo, T. Oshizaka, K. Sugibayashi, Prediction of skin permeation by chemical compounds using the artificial membrane, Strat-M™, European Journal of Pharmaceutical Sciences, 67 (2015) 113-118.
[35] D. Karadzovska, J.E. Riviere, Assessing vehicle effects on skin absorption using artificial membrane assays, European Journal of Pharmaceutical Sciences, 50 (2013) 569-576.
[36] S.A. Imran, U. Anand, R. Agu, Human Skin Substitute (Strat-M®) as an Alternative for Testing Transdermal Delivery of Levothyroxine, in: Endocrine Society's 96th Annual Meeting and Expo (2014).
[37] A. Simon, M.I. Amaro, A.M. Healy, L.M. Cabral, V.P. de Sousa, Comparative evaluation of rivastigmine permeation from a transdermal system in the Franz cell using synthetic membranes and pig ear skin with in vivo-in vitro correlation, International Journal of Pharmaceutics, 512 (2016) 234-241.
[38] T.J. Franz, Percutaneous absorption. On the relevance of in vitro data, Journal of Investigative Dermatology, 64 (1975) 190-195.
[39] H. Nakazawa, N. Ohta, I. Hatta, A possible regulation mechanism of water content in human stratum corneum via intercellular lipid matrix, Chemistry and physics of lipids, 165 (2012) 238-243.
[40] L. Norlén, A. Emilson, B. Forslind, Stratum corneum swelling. Biophysical and computer assisted quantitative assessments, Archives of dermatological research, 289 (1997) 506-513.
[41] R. Rastogi, S. Anand, V. Koul, Flexible polymerosomes-An alternative vehicle for topical delivery, Colloids and Surfaces B: Biointerfaces, 72 (2009) 161-166.
[42] T.W. Prow, J.E. Grice, L.L. Lin, R. Faye, M. Butler, W. Becker, E.M. Wurm, C. Yoong, T.A. Robertson, H.P. Soyer, Nanoparticles and microparticles for skin drug delivery, Advanced drug delivery reviews, 63 (2011) 470-491.
[43] Z. Teixeira, B. Zanchetta, B.A. Melo, L.L. Oliveira, M.H. Santana, E.J. Paredes-Gamero, G.Z. Justo, H.B. Nader, S.S. Guterres, N. Durán, Retinyl palmitate flexible polymeric nanocapsules: characterization and permeation studies, Colloids and Surfaces B: Biointerfaces, 81 (2010) 374-380.
[44] R.M. Hathout, S. Mansour, A.S. Geneidi, N.D. Mortada, Visualization, dermatopharmacokinetic analysis and monitoring the conformational effects of a microemulsion formulation in the skin stratum corneum, Journal of colloid and interface science, 354 (2011) 124-130.
[45] W. Naoui, M.A. Bolzinger, B. Fenet, J. Pelletier, J.-P. Valour, R. Kalfat, Y. Chevalier, Microemulsion microstructure influences the skin delivery of an hydrophilic drug, Pharmaceutical research, 28 (2011) 1683-1695.
[46] S. Ge, Y. Lin, H. Lu, Q. Li, J. He, B. Chen, C. Wu, Y. Xu, Percutaneous delivery of econazole using microemulsion as vehicle: formulation, evaluation and vesicle-skin interaction, International journal of pharmaceutics, 465 (2014) 120-131.

[47] P.J. Lee, R. Langer, V.P. Shastri, Novel microemulsion enhancer formulation for simultaneous transdermal delivery of hydrophilic and hydrophobic drugs, Pharmaceutical research, 20 (2003) 264-269.
[48] M.A. Bolzinger, S. Briançon, J. Pelletier, H. Fessi, Y. Chevalier, Percutaneous release of caffeine from microemulsion, emulsion and gel dosage forms, European Journal of Pharmaceutics and Biopharmaceutics, 68 (2008) 446-451.
[49] A.C. Sintov, S. Botner, Transdermal drug delivery using microemulsion and aqueous systems: influence of skin storage conditions on the in vitro permeability of diclofenac from aqueous vehicle systems, International Journal of Pharmaceutics, 311 (2006) 55-62.
[50] D.S. Mahrhauser, H. Kählig, E. Partyka-Jankowska, H. Peterlik, L. Binder, K. Kwizda, C. Valenta, Investigation of microemulsion microstructure and its impact on skin delivery of flufenamic acid, International Journal of Pharmaceutics, 490, Issues 1-2 (2015) 292-297.
[51] S. Guido, Shear-induced droplet deformation: Effects of confined geometry and viscoelasticity, Current Opinion in Colloid & Interface Science, 16 (2011) 61-70.
[52] C.W. Pouton, Formulation of self-emulsifying drug delivery systems, Advanced Drug Delivery Reviews, 25 (1997) 47-58.
[53] S. Caserta, M. Simeone, S. Guido, Evolution of drop size distribution of polymer blends under shear flow by optical sectioning, Rheologica acta, 43 (2004) 491-501.
[54] S. Caserta, L. Sabetta, M. Simeone, S. Guido, Shear-induced coalescence in aqueous biopolymer mixtures, Chemical engineering science, 60 (2005) 1019-1027.
[55] A. Pommella, S. Caserta, S. Guido, Dynamic flow behaviour of surfactant vesicles under shear flow: role of a multilamellar microstructure, Soft Matter, 9 (2013) 7545-7552.
[56] P. Caspers, G. Lucassen, G. Puppels, Combined in vivo confocal Raman spectroscopy and confocal microscopy of human skin, Biophysical journal, 85 (2003) 572-580.
[57] J. Crank, The mathematics of diffusion, Second edition, Clarendon Press Oxford (1975).
[58] S. Aland, J. Lowengrub, A. Voigt, Particles at fluid-fluid interfaces: A new Navier-Stokes-Cahn-Hilliard surface-phase-field-crystal model, Physical Review E, 86 (2012) 046321.
[59] F. Thivilliers, N. Drelon, V. Schmitt, F. Leal-Calderon, Bicontinuous emulsion gels induced by partial coalescence: Kinetics and mechanism, Europhysics Letters, 76 (2006) 332.
[60] E.M. Herzig, Bijel-a novel composite material from colloids on liquid-liquid interfaces, (2008).
[61] M.E. Cates, P.S. Clegg, Bijels: a new class of soft materials, Soft Matter, 4 (2008) 2132-2138.
[62] E. Herzig, K. White, A. Schofield, W. Poon, P. Clegg, Bicontinuous emulsions stabilized solely by colloidal particles, Nature materials, 6 (2007) 966-971.
[63] S. Fransson, O. Peleg, N. Lorén, A. M. Hermansson, M. Kröger, Modelling and confocal microscopy of biopolymer mixtures in confined geometries, Soft Matter, 6 (2010) 2713-2722.
[64] M. Gómez-Guillén, J. Turnay, M. Fernández-Dıaz, N. Ulmo, M. Lizarbe, P. Montero, Structural and physical properties of gelatin extracted from different marine species: a comparative study, Food Hydrocolloids, 16 (2002) 25-34.
[65] M. Simeone, V. Sibillo, M. Tassieri, S. Guido, Shear-induced clustering of gelling droplets in aqueous biphasic mixtures of gelatin and dextran, Journal of Rheology, 46 (2002) 1263-1278.
[66] L. Ghasemi-Mobarakeh, M.P. Prabhakaran, M. Morshed, M.-H. Nasr-Esfahani, S. Ramakrishna, Electrospun poly (ε-caprolactone)/gelatin nanofibrous scaffolds for nerve tissue engineering, Biomaterials, 29 (2008) 4532-4539.
[67] B. Loppinet, E. Stiakakis, D. Vlassopoulos, G. Fytas, J. Roovers, Reversible thermal gelation in star polymers: an alternative route to jamming of soft matter, Macromolecules, 34 (2001) 8216-8223.
[68] S.M. Tosh, A.G. Marangoni, F.R. Hallett, I.J. Britt, Aging dynamics in gelatin gel microstructure, Food Hydrocolloids, 17 (2003) 503-513.
[69] A. Duconseille, T. Astruc, N. Quintana, F. Meersman, V. Sante-Lhoutellier, Gelatin structure and composition linked to hard capsule dissolution: a review, Food Hydrocolloids, 43 (2015) 360-376.
[70] A. Karim, R. Bhat, Gelatin alternatives for the food industry: recent developments, challenges and prospects, Trends in food science & technology, 19 (2008) 644-656.
[71] A. Karim, R. Bhat, Fish gelatin: properties, challenges, and prospects as an alternative to mammalian gelatins, Food hydrocolloids, 23 (2009) 563-576.
[72] S. Singh, K.R. Rao, K. Venugopal, R. Manikandan, Alteration in dissolution characteristics of gelatin-containing formulations, Pharmaceutical technology, 26 (2002) 36-54.

[73] K.B. Djagny, Z. Wang, S. Xu, Gelatin: a valuable protein for food and pharmaceutical industries: review, Critical reviews in food science and nutrition, 41 (2001) 481-492.
[74] M. Rogowska, K. Iwaniak, A. Polski, K. Slawinska, K. Sobotka-Polska, J. Modrzewska, E. Poleszak, Influence of different excipients on the properties of hard gelatin capsules with metamizole sodium, Current Issues in Pharmacy and Medical Sciences, 29 (2016) 114-117.
[75] K. Dvořáčková, M. Rabišková, J. Muselík, J. Gajdziok, M. Bajerová, Coated hard capsules as the pH-dependent drug transport systems to ileo-colonic compartment, Drug Development and Industrial Pharmacy, 37 (2011) 1131-1140.
[76] M. Kreiner, N. Thayne, D. Harkins, K. Rae, G. Halbert, Liquid-filled hard gelatin capsules: excipient/capsule compatibility studies, in: 7th APS International Pharmaceutical Science Conference, (2016).
[77] H.W. Kang, Y. Tabata, Y. Ikada, Fabrication of porous gelatin scaffolds for tissue engineering, Biomaterials, 20 (1999) 1339-1344.
[78] S.M. Choi, D. Singh, D. Singh, S.S. Han, Surfactant role in modifying architecture of functional polymeric gelatin scaffolds, International Journal of Polymeric Materials and Polymeric Biomaterials, 63 (2014) 951-956.
[79] N. Arabi, A. Zamanian, Effect of cooling rate and gelatin concentration on the microstructural and mechanical properties of ice template gelatin scaffolds, Biotechnology and applied biochemistry, 60 (2013) 573-579.
[80] M. Kunitz, Syneresis and swelling of gelatin, The journal of general physiology, 12 (1928) 289-312.
[81] C. Qiao, X. Cao, Swelling behavior of physically cross-linked gelatin gels in varied salt solutions, Journal of Macromolecular Science, Part B, 53 (2014) 1609-1620.
[82] M.M. Welz, C.M. Ofner, Examination of self-crosslinked gelatin as a hydrogel for controlled release, Journal of Pharmaceutical Sciences, 81 (1992) 85-90.
[83] H. Schott, Swelling kinetics of polymers, Journal of Macromolecular Science, Part B: Physics, 31 (1992) 1-9.
[84] S.E. Kudaibergenov, V.B. Sigitov, Swelling, shrinking, deformation, and oscillation of polyampholyte gels based on vinyl 2-aminoethyl ether and sodium acrylate, Langmuir, 15 (1999) 4230-4235.
[85] Y. Takeoka, A.N. Berker, R. Du, T. Enoki, A. Grosberg, M. Kardar, T. Oya, K. Tanaka, G. Wang, X. Yu, First order phase transition and evidence for frustrations in polyampholytic gels, Physical Review Letters, 82 (1999) 4863.
[86] C.H. Lee, Y.C. Bae, Effect of Salt on Swelling Behaviors of Thermosensitive Hydrogels: Applicability of the Nonrandom Contact Model, Macromolecules, 48 (2015) 4063-4072.
[87] M. Azami, M. Rabiee, F. Moztarzadeh, Glutaraldehyde crosslinked gelatin/hydroxyapatite nanocomposite scaffold, engineered via compound techniques, Polymer Composites, 31 (2010) 2112-2120.
[88] V. Rattanaruengsrikul, N. Pimpha, P. Supaphol, Development of gelatin hydrogel pads as antibacterial wound dressings, Macromolecular Bioscience, 9 (2009) 1004-1015.
[89] J. Zhao, Y. Zhao, Q. Guan, G. Tang, Y. Zhao, X. Yuan, K. Yao, Crosslinking of electrospun fibrous gelatin scaffolds for apatite mineralization, Journal of Applied Polymer Science, 119 (2011) 786-793.
[90] X. Lou, T.V. Chirila, Swelling behavior and mechanical properties of chemically cross-linked gelatin gels for biomedical use, Journal of Biomaterials Applications, 14 (1999) 184-191.
[91] R.H. Pritchard, E.M. Terentjev, Swelling and de-swelling of gels under external elastic deformation, Polymer, 54 (2013) 6954-6960.
[92] P. Belton, NMR and the mobility of water in polysaccharide gels, International journal of biological macromolecules, 21 (1997) 81-88.
[93] A.S. Hoffman, Hydrogels for biomedical applications, Advanced drug delivery reviews, 64 (2012) 18-23.
[94] T. Brand, S. Richter, S. Berger, Diffusion NMR as a new method for the determination of the gel point of gelatin, The Journal of Physical Chemistry B, 110 (2006) 15853-15857.
[95] J. Maquet, H. Theveneau, M. Djabourov, J. Leblond, P. Papon, State of water in gelatin solutions and gels: An 1H nmr investigation, Polymer, 27 (1986) 1103-1110.
[96] X. Liu, P.X. Ma, Phase separation, pore structure, and properties of nanofibrous gelatin scaffolds, Biomaterials, 30 (2009) 4094-4103.

[97] S. Ma, M. Natoli, X. Liu, M.P. Neubauer, F.M. Watt, A. Fery, W.T. Huck, Monodisperse collagen–gelatin beads as potential platforms for 3D cell culturing, Journal of Materials Chemistry B, 1 (2013) 5128-5136.
[98] L.C. Dong, A.S. Hoffman, Q. Yan, Dextran permeation through poly (N-isopropylacrylamide) hydrogels, Journal of Biomaterials Science, Polymer Edition, 5 (1994) 473-484.
[99] I.D. Odell, D. Cook, Immunofluorescence techniques, The Journal of investigative dermatology, 133 (2013) e4-e4.
[100] J.A. Ramos-Vara, Technical aspects of immunohistochemistry, Veterinary Pathology, 42 (2005) 405-426.
[101] D. J. Asai, Immunofluorescence Microscopy, in: Current Protocols Essential Laboratory Techniques, John Wiley & Sons, Inc., (2008).
[102] R. Veldhuizen, K. Nag, S. Orgeig, F. Possmayer, The role of lipids in pulmonary surfactant, Biochimica et Biophysica Acta (BBA)-Molecular Basis of Disease, 1408 (1998) 90-108.
[103] C. Washington, The stability of intravenous fat emulsions in total parenteral nutrition mixtures, International Journal of Pharmaceutics, 66 (1990) 1-21.
[104] P.M. Kidd, Phosphatidylcholine, a superior protectant against liver damage, Alternative Medicine Review, 1 (1996) 258-274.
[105] S.H. Zeisel, Choline: an important nutrient in brain development, liver function and carcinogenesis, Journal of the American College of Nutrition, 11 (1992) 473-481.
[106] P. van Hoogevest, A. Wendel, The use of natural and synthetic phospholipids as pharmaceutical excipients, European Journal of Lipid Science and Technology, 116 (2014) 1088-1107.
[107] C.V. Nikiforidis, A. Matsakidou, V. Kiosseoglou, Composition, properties and potential food applications of natural emulsions and cream materials based on oil bodies, RSC Advances, 4 (2014) 25067-25078.
[108] D.J. McClements, Food emulsions: principles, practices, and techniques, CRC press, (2015).
[109] M. Trotta, F. Pattarino, T. Ignoni, Stability of drug-carrier emulsions containing phosphatidylcholine mixtures, European Journal of Pharmaceutics and Biopharmaceutics, 53 (2002) 203-208.
[110] Y.A. Shchipunov, P. Schmiedel, Phase behavior of lecithin at the oil/water interface, Langmuir, 12 (1996) 6443-6445.
[111] S. Shin, J.T. Ault, H.A. Stone, Flow-Driven Rapid Vesicle Fusion via Vortex Trapping, Langmuir, 31 (2015) 7178-7182.
[112] Q. He, Y. Zhang, G. Lu, R. Miller, H. Mohwald, J. Li, Dynamic adsorption and characterization of phospholipid and mixed phospholipid/protein layers at liquid/liquid interfaces, Advances in Colloid and Interface Science, 140 (2008) 67-76.
[113] J. Wu, J. Li, J. Zhao, R. Miller, Dynamic characterization of phospholipid/protein competitive adsorption at the aqueous solution/chloroform interface, Colloids and Surfaces A: Physicochemical and Engineering Aspects, 175 (2000) 113-120.
[114] J.M.R.g. Patino, J.M.N. García, M.R.R.g. Niño, Protein–lipid interactions at the oil–water interface, Colloids and Surfaces B: Biointerfaces, 21 (2001) 207-216.
[115] H. Mohwald, Phospholipid and phospholipid-protein monolayers at air-water interface, Annual Review of Physical Chemistry, 41 (1990) 441-476.
[116] D.S. Ambwani, T. Fort Jr, Pendant drop technique for measuring liquid boundary tensions, in: Surface and Colloid Science, Springer, (1979) 93-119.
[117] F. Hansen, G. Rødsrud, Surface tension by pendant drop: I. A fast standard instrument using computer image analysis, Journal of Colloid and Interface Science, 141 (1991) 1-9.
[118] J. Li, R. Miller, D. Vollhardt, G. Weidemann, H. Möhwald, Isotherms of phospholipid monolayers measured by a pendant drop technique, Colloid and Polymer Science, 274 (1996) 995-999.
[119] P. Cheng, D. Li, L. Boruvka, Y. Rotenberg, A.W. Neumann, Automation of axisymmetric drop shape-analysis for measurement of interfacial-tension and contact angles, Colloids and Surfaces, 43 (1990) 151-167.
[120] J. Kragel, S. Derkatch, Interfacial shear rheology, Current Opinion in Colloid & Interface Science, 15 (2010) 246-255.
[121] C. Lopez, M.N. Madec, R. Jimenez-Flores, Lipid rafts in the bovine milk fat globule membrane revealed by the lateral segregation of phospholipids and heterogeneous distribution of glycoproteins, Food Chemistry, 120 (2010) 22-33.

[122] J.M. Evers, The milkfat globule membrane-Methodologies for measuring milkfat globule (membrane) damage, International Dairy Journal, 14 (2004) 747-760.
[123] S. Gallier, D. Gragson, R. Jimenez-Flores, D. Everett, Using Confocal Laser Scanning Microscopy To Probe the Milk Fat Globule Membrane and Associated Proteins, Journal of Agricultural and Food Chemistry, 58 (2010) 4250-4257.
[124] R. Walder, A. Honciuc, D. Schwartz, Phospholipid Diffusion at the Oil-Water Interface, Journal of Physical Chemistry B, 114 (2010) 11484-11488.
[125] H. Mohwald, Phospholipid monolayers, Handbook of biological physics, 1 (1995) 187.
[126] K.S. Nam, K. Igarashi, M. Umeda, K. Inoue, Production and characterization of monoclonal-antibodies that specifically bind to phosphatidylcholine, Biochimica Et Biophysica Acta, 1046 (1990) 89-96.
[127] H. Schenkein, J. Gunsolley, A. Best, M. Harrison, C. Hahn, J. Wu, J. Tew, Antiphosphorylcholine antibody levels are elevated in humans with periodontal diseases, Infection and Immunity, 67 (1999) 4814-4818.
[128] B. Niedieck, U. Kuck, H. Gardemin, On the immune precipitation of phosphorylcholine lipids with tepc 15 mouse myeloma protein and with anti-lecithin sera from guinea pigs, Immunochemistry, 15 (1978) 471-475.
[129] A.C. Allison, Y. Nawata, Cytokines Mediating the Proliferation and Differentiation of B-1 Lymphocytes and Their Role in Ontogeny and Phylogeny, Annals of the New York Academy of Sciences, 651 (1992) 200-219.
[130] P.X. Shaw, L. Zhang, M. Zhang, H. Du, L. Zhao, C. Lee, S. Grob, S.L. Lim, G. Hughes, J. Lee, Complement factor H genotypes impact risk of age-related macular degeneration by interaction with oxidized phospholipids, Proceedings of the National Academy of Sciences, 109 (2012) 13757-13762.
[131] M.A. Urbaneja, G.D. Fidelio, J.A. Lucy, D. Chapman, The interaction of an anti-lipid antibody (TEPC 15) with a model biomembrane system (monolayer), Biochimica et Biophysica Acta (BBA)-Biomembranes, 898 (1987) 253-256.
[132] D.R. Blanco, C.I. Champion, A. Dooley, D.L. Cox, J.P. Whitelegge, K. Faull, M.A. Lovett, A monoclonal antibody that conveys in vitro killing and partial protection in experimental syphilis binds a phosphorylcholine surface epitope of Treponema pallidum, Infection and immunity, 73 (2005) 3083-3095.
[133] R. Liuzzi, S. Gallier, S. Ringler, S. Caserta, S. Guido, Visualization of choline-based phospholipids at the interface of Oil/Water emulsions with TEPC-15 antibody. Immunofluorescence applied to colloidal systems, RSC Advances, 6 (2016) 109960- 109968.
[134] A. Luciani, V.R. Villella, S. Esposito, M. Gavina, I. Russo, M. Silano, S. Guido, M. Pettoello-Mantovani, R. Carnuccio, B. Scholte, Targeting autophagy as a novel strategy for facilitating the therapeutic action of potentiators on ΔF508 cystic fibrosis transmembrane conductance regulator, Autophagy, 8 (2012) 1657-1672.
[135] D. Möbius, R. Miller, Proteins at liquid interfaces, Elsevier, (1998).
[136] H. Singh, A. Ye, D. Horne, Structuring food emulsions in the gastrointestinal tract to modify lipid digestion, Progress in Lipid Research, 48 (2009) 92-100.
[137] R. Liuzzi, Preziosi, V., Caserta, S. and Guido, S., Development of model systems for in vitro investigation of transdermal transport pathways, Accepted Manuscript, Canadian Journal of chemical Engineering, (2017).
[138] F. Zhang, A. Proctor, Rheology and stability of phospholipid-stabilized emulsions, Journal of the American Oil Chemists' Society, 74 (1997) 869-874.
[139] M. Manconi, C. Caddeo, C. Sinico, D. Valenti, M.C. Mostallino, G. Biggio, A.M. Fadda, Ex vivo skin delivery of diclofenac by transcutol containing liposomes and suggested mechanism of vesicle–skin interaction, European Journal of Pharmaceutics and Biopharmaceutics, 78 (2011) 27-35.
[140] P. Posocco, A. Perazzo, V. Preziosi, E. Laurini, S. Pricl, S. Guido, Interfacial tension of oil/water emulsions with mixed non-ionic surfactants: comparison between experiments and molecular simulations, RSC Advances, 6 (2016) 4723-4729.
[141] C. D'Agostino, R. Liuzzi, L.F. Gladden, S. Guido, Swelling-induced structural changes and microparticle uptake of gelatin gels probed by NMR and CLSM, Accepted in Soft Matter, (2017).
[142] E. Fukushima, Roeder, S.W., Experimental pulse NMR, Addison-Weslkey, Reading, US, (1981).

[143] R.M. Cotts, M.J.R. Hoch, T. Sun, J.T. Markert, Pulsed field gradient stimulated echo methods for improved NMR diffusion measurements in heterogeneous systems, Journal of Magnetic Resonance, 83 (1989) 252-266.
[144] J.E. Tanner, Use of stimulated echo in NMR diffusion studies, Journal of Chemical Physics, 52 (1970) 2523-2526.
[145] C. D'Agostino, J. Mitchell, L.F. Gladden, M.D. Mantle, Hydrogen bonding network disruption in mesoporous catalyst supports probed by PFG-NMR diffusometry and NMR relaxometry, The Journal of Physical Chemistry C, 116 (2012) 8975-8982.
[146] M.D. Mantle, D.I. Enache, E. Nowicka, S.P. Davies, J.K. Edwards, C. D'Agostino, D.P. Mascarenhas, L. Durham, M. Sankar, D.W. Knight, L.F. Gladden, S.H. Taylor, G.J. Hutchings, Pulsed-field gradient NMR spectroscopic studies of alcohols in supported gold catalysts The Journal of Physical Chemistry C, 115 (2011) 1073-1079.
[147] W.M. Saltzman, M.L. Radomsky, K.J. Whaley, R.A. Cone, Antibody diffusion in human cervical mucus, Biophysical Journal, 66 (1994) 508.
[148] S.M. Russell, G. Carta, Mesh size of charged polyacrylamide hydrogels from partitioning measurements, Industrial & Engineering Chemistry Research, 44 (2005) 8213-8217.

Appendix B

Publications

- **Liuzzi, R**., et al. "Interactions between microstructured fluids and stratum corneum: pharmaceutical and cosmetic applications." International Journal of Cosmetic Science 37.1 (2015): 156-157.
- **Liuzzi, R**., et al. "Transport efficiency in transdermal drug delivery: What is the role of fluid microstructure?." Colloids and Surfaces B: Biointerfaces 139 (2016): 294-305.
- **Liuzzi, R**., et al. "Visualization of choline-based phospholipids at the interface of oil/water emulsions with TEPC-15 antibody. Immunofluorescence applied to colloidal systems." RSC Advances 6.111 (2016): 109960-109968.
- **Liuzzi, R**. et al. "Development of Model Systems for in Vitro Investigation of Transdermal Transport Pathways", The Canadian Journal of Chemical Engineering, Accepted Author Manuscript, (2017), doi:10.1002/cjce.22835.
- D'Agostino C. and **Liuzzi R. (co-first author)** et al., "Swelling-induced structural changes and microparticle uptake of gelatin gels probed by NMR and CLSM".Soft Matter (2017).

Experiences in foreign laboratories

Visiting student research collaborator (VSRC) at University of Cambridge, Cavendish Laboratories (Prof. Pietro Cicuta). *Interaction between micro-structured fluids and biological systems for bioengineering applications,* (04/08/2016 – 08/11/2016).

Conferences

- Cosminnov_ Cosmetic Innovation Days – Orlèans (FR) – 8-9/10/2013
- XII National Convention of the Italian Rheology Society (SIR) – Brescia (IT) – 7-10/09/2014
- Stratum Corneum VIII – Cardiff (UK) – 17-19/09/2014
- National Convention of the Italian Gereontology and Geriatrics (SIGG) – Bologna (IT) – 26-29/11/2014
- Smart & Green Interfaces Conference, SGIC – COST ACTION MP1106 – Belgrade (SRB) – 30-01/04/2015
- 15th European Colloid Student Conference (ECIS) – Krakow (PL) – 8-11/06/2015

- Smart & Green Interfaces Conference, SGIC– COST ACTION MP1106 – Athens (GR) – 4-6/05/2016
- GRICU Meeting – Anacapri – 12-14/09/2016